

SOT

STRIPE FILTERS ON MULTISPECTRAL LINEAR ARRAYS

FINAL REPORT

CONTRACT NO. NAS 5-25622

15 MAY 1982

(NASA-CR-175305) STRIPE FILTERS ON
MULTISPECTRAL LINEAR ARRAYS Final Report
(Westinghouse Defense and Electronic
Systems) 118 p HC A06/MP A01

NE5-32252

CSCI 09C

Unclas
G3/33 25375

PRESENTED TO

NATIONAL AERONAUTICS AND SPACE ADMINISTRATION
GODDARD SPACE FLIGHT CENTER
GREENBELT, MARYLAND

BY

WESTINGHOUSE DEFENSE AND ELECTRONIC SYSTEMS CENTER
ADVANCED TECHNOLOGY DIVISION
ADVANCED TECHNOLOGY LABORATORY
BALTIMORE, MARYLAND



STRIPE FILTERS ON MULTISPECTRAL LINEAR ARRAYS

FINAL REPORT

CONTRACT NO. NAS5-25622

FOR

NASA GODDARD SPACE FLIGHT CENTER

GREENBELT, MARYLAND

COVERING THE PERIOD:

15 APRIL 1981 to 16 MARCH 1982

Authors:

J. H. Hall, F. C. Blaha, B. R. Frias, J. Halvis, E. Hubbard

WESTINGHOUSE DEFENSE AND ELECTRONIC SYSTEMS CENTER

SYSTEMS DEVELOPMENT DIVISION

ADVANCED TECHNOLOGY LABORATORIES

BALTIMORE, MARYLAND 21203

TABLE OF CONTENTS

SECTION		PAGE
1.0	BACKGROUND AND INTRODUCTION	1-1
2.0	FILTER TECHNOLOGY AND CCD OPERATION	2-1
3.0	MEASURED RESULTS - FILTER CHARACTERISTICS	3-1
4.0	ELECTRICAL AND OPTICAL CHARACTERIZATION	4-1
5.0	MEASURED RESULTS - FILTERS ON CCD CHIPS	5-1
6.0	PROBLEMS ENCOUNTERED IN FABRICATION	6-1
7.0	OPERATIONAL ENVIRONMENT TOLERANCE	7-1
8.0	CONCLUSIONS	8-1

(1083A/kaz/1712G/5/82)

1.0 BACKGROUND AND INTRODUCTION

This report is a summary of the results of work under contract NAS 5-25622 performed by the Westinghouse Systems Development Division, Advanced Technology Laboratories, for NASA-Goddard Space Flight Center in Greenbelt, Maryland.

The purpose of the program titled as "Stripe Filters on Multispectral Linear Arrays" was to design, fabricate and evaluate dielectric interference filters deposited directly on top of existing 200-element charge coupled device linear imaging arrays.

1.1 BACKGROUND

The Westinghouse ATD laboratories have been involved in previous NASA sensor programs. In one earlier program, photodiode chips butted together to form a 1728 element linear array produced high quality imagery of aerial photographs in a laboratory scanner. In another program, CCD chips with semitransparent gates were developed to demonstrate how time delay and integration (TDI) would extend effective exposure time to realize the signal to noise ratio performance needed for multispectral line array systems when using narrow band filters.

On independent research and development it was also demonstrated how narrow band filters can be used with TDI CCD chips to provide multispectral image sensing. In an early version, dye filters, actually the emulsion dyes

of a film intended for color microscopy, were exposed and developed to provide a pattern of red, blue, and green color stripes which could be placed over and in registry with the 15um wide TDI columns of the silicon CCD chip. When measurements showed that neither the color separation nor the resolving power of the blue and red emulsions was adequate for Landsat type applications, the filter approach was shifted to use interference filters deposited on glass. Chromium on glass patterns were made using the same pattern generator used for the plates for the CCD chips to assure accurate registry, and these patterns were used by Optoline, an external optics company, to form a red-green-blue-green stripe filter pattern on thin glass substrates. These were diced at Westinghouse and a set of stripe filters was placed over the sensing TDI columns of a CCD chip, of course with the filter stripes nearest the silicon. The filter assemblies could be accurately registered with the silicon, although accomplishing this registry was a time consuming hand operation, and trichromatic imagery was produced.

Several results were obtained from these experiments, which led to this program:

- o First, the transitions between filter elements were abrupt. There was no visible overlap when they were observed under the microscope, and in fact a narrow dark line appeared at each transition which acted as a guard band to provide for about 1 um misalignment tolerance.

o Second, although the filter transitions were sharp and optical registry was good, the signal separation between colors was not perfect. This was soon related to the basic physics of the silicon CCD chip. For longer wavelength photons, especially for band 4, silicon is relatively more transparent so that some of the photons are absorbed deep in the silicon beyond the depletion regions formed by the CCD gates. The resulting charge carriers (holes) diffuse through the field free bulk silicon until they recombine or until they reach a CCD well. For a chip used for heterochromatic imagery this effect appears as decreasing geometric resolving power (MTF) for longer wavelength light. Here it appeared as a loss of spectral separation. Table 1.1 shows the relative signals collected by first and second neighbor columns in a 15um chip for 5 wavelengths of narrow band filtered light. The data shows that for bands 1, 2, and 3, the second neighbor signal is essentially negligible.

Another resolving power/spectral separation limiting effect appears even for the shorter wavelength photons of bands 1 and 2. The TDI columns of the chips used in the experiment are separated by "channel stops", narrow stripes of highly (n+) doped, high conductivity material, into which the electric field from the CCD gates penetrates almost not at all. These stripes are essentially at the bulk silicon potential, hence act as barriers to prevent lateral motion of the holes collecting in the more negative CCD wells. However, photons absorbed in these stripes, which were 1 to 1.5um wide in this 15um

CCD chip, are again in a field free region and diffuse randomly until they enter either neighboring CCD column. Thus for any light absorbed in the channel stops there was an uncertainty about which element would collect the resulting signal, and 5 or 10% of the expected signal appears in the nearest neighbor. Eliminating these two effects is a goal of this sensor chip design investigation. A design layout which will accomplish this is shown in Figure 1.1. It was described in more detail in a recent MLA Instrument Definition Study Report by Eastman Kodak and Westinghouse. One of the goals of this program was to establish the adequacy of that chip/filter design or create a basis for revising it.

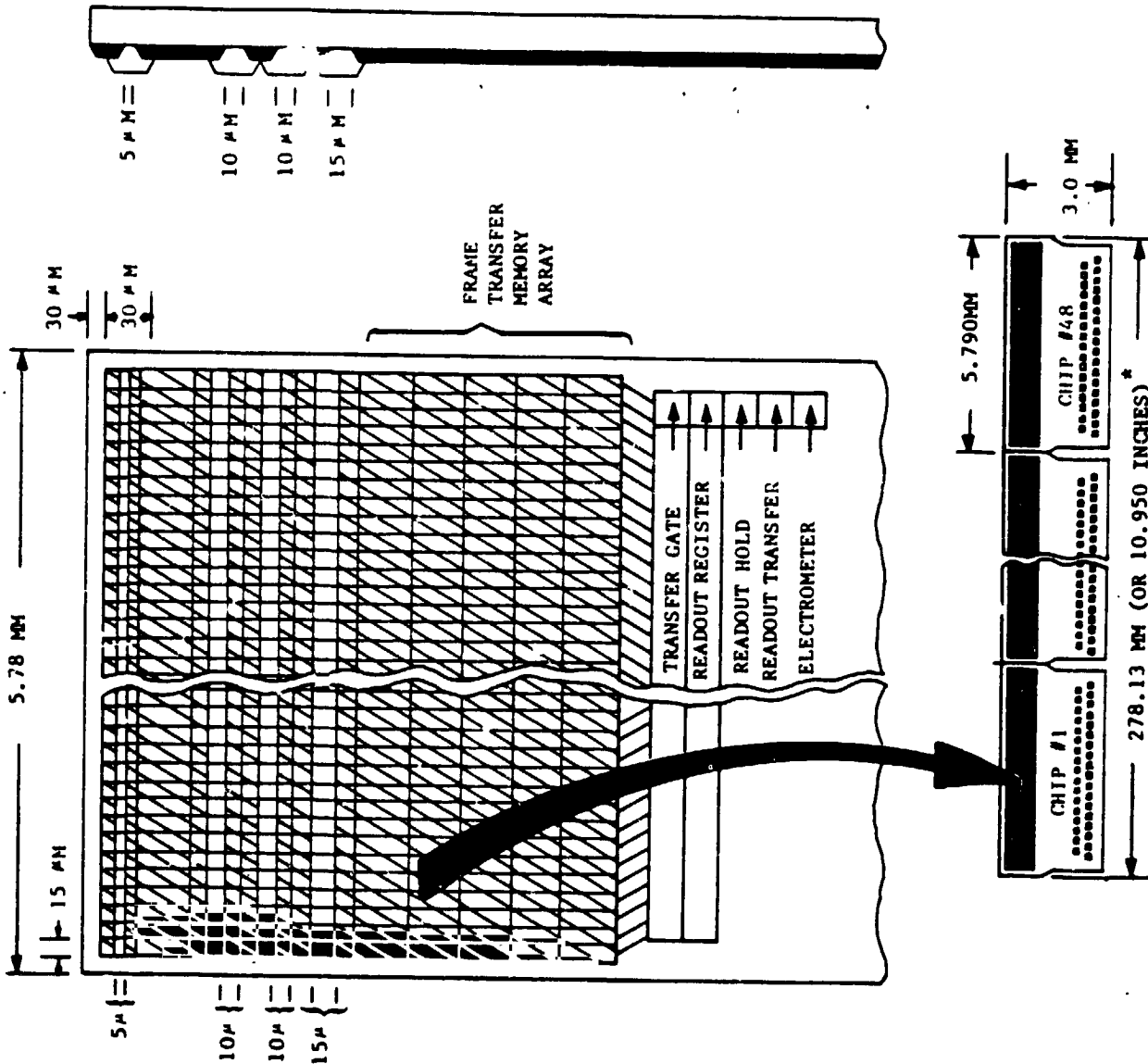
1.2 PROGRAM GOALS

The four bands of interest in remote sensing applications are:

BAND #	WAVELENGTH	COLOR
1	450 - 520	Blue-Green
2	520 - 600	Green
3	630 - 690	Red
4	760 - 900	near Infrared

It was an option of this program to choose any two of these for evaluation; Bands 2 and 3 were chosen.

FIGURE 1-1
Baseline Visible Chip



ORIGINAL PART
OF POOR QUALITY

A primary goal of the program as mentioned above was to verify the optical performance of the filters with regard to cross talk between adjacent detector elements. Additional goals were:

- 1) The filters should have an average in-band transmittance greater than 80% and a total out of band transmittance of less than 5%, with a recipe developed to the desired bandwidth.
- 2) Filter stability must be adequate for operation in a space environment, i.e., be insensitive to vacuum and have less than 1% variation when operated over the temperature range from 260⁰K to 320⁰K.
- 3) Filter elements should be defineable in 12 to 25 micron element size compatible with existing silicon detectors.
- 4) These types of measurements should be made:
 - a) Spectral transmission of the filter as deposited on witness plates
 - b) Spectral response of the silicon sensing device
 - c) Any optical interaction between the filter and sensing device affecting the filter characteristics be measured, modeled and predicted

- d) The response of the filter/sensor combination be evaluated and compared to the sensor response above.
 - e) Repeatability and uniformity of filter characteristics.
- 5) Determine if a filter can be successfully removed from a silicon sensing device to allow recovery from improper deposition.
 - 6) Determine the effects of wafer dicing, mounting etc. and other techniques required to fabricate a focal plane assembly.

Most of these goals were met and results are described in detail in the following sections.

2.0 FILTER TECHNOLOGY AND CCD OPERATION

2.1 FILTER FABRICATION

Filter deposition is being done by Optoline Corporation of Wilmington, Massachusetts. Optoline specializes in doing multi-discipline precision geometry multiple filter coatings in such areas as precision reticle fabrication, high efficiency mirrors, stripe filters for TV cameras and infrared resolution target reticles for Sidewinder missiles.

The filters are composed of alternate layers of two dielectrics, Zinc Sulfide and thorium fluoride, having respectively a high and low index of refraction, with an intermediate silver spacer layer. The filter designs used for most of the data shown in this report are given in Table 2.1-1.

In the deposition process actual thicknesses are not measured, but rather the optical transmission through a glass witness plate which is in the deposition chamber is monitored at a particular wavelength. The silver layer thickness is determined by looking for a particular valley in the transmission curve. The deposition itself is done in an evacuated chamber by means of thermally filament heating of the source material.

The filter material exhibits very strong adhesion to the substrate silox material. Etch solutions have not been established for defining the material; therefore, photo definition is accomplished using a lift-off process. The basic concepts of lift-off photodefinition are shown in Figure 2.1-2. A resist

TABLE 2.1-1 FILTER DESIGN DATA

BAND 2 = 5600A, Air/Vacuum

MATERIAL	THICKNESS (A)
ZnS	549 = $\lambda/4$
ThF ₄	831 = $\lambda/4$
ZnS	549 = $\lambda/4$
ThF ₄	1662 = $\lambda/2$
Ag	--
ThF ₄	1662 = $\lambda/2$
ZnS	549 = $\lambda/4$
ThF ₄	831 = $\lambda/4$
ZnS	549 = $\lambda/4$
ThF ₄	831 = $\lambda/4$
ZnS	549 = $\lambda/4$

Substrate

Test Wavelength 505 nm

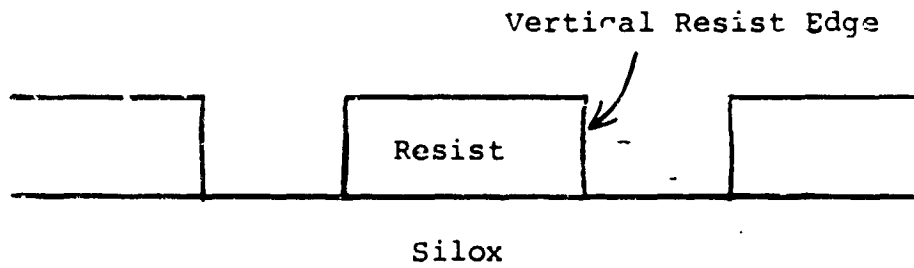
Band 3 = 6600A, Air/Vacuum

MATERIAL	THICKNESS
ZnS	549 = $\lambda/4$
ThF ₄	831 = $\lambda/4$
ZnS	549 = $\lambda/4$
ThF ₄	1662 = $\lambda/2$
Ag	--
ThF ₄	1662 = $\lambda/2$
Ag	--
ThF ₄	1662 = $\lambda/2$
ZnS	549 = $\lambda/4$
ThF ₄	831 = $\lambda/4$
ZnS	549 = $\lambda/4$

Substrate

Test wavelength 630 nm

Define Photoresist Pattern:



Deposit Filter Layers:



"Liftoff" Resist:



Figure 2.1 - 2 Liftoff Process Sequence

pattern is defined, leaving holes in the resist where the filter material is to remain. The resist edge is of sufficient height and steepness that the filter material will be discontinuous crossing the step. A subsequent immersion in a photoresist solvent dissolves away the remaining resist, lifting off the unwanted filter material with it.

The resolution of this process is essentially as fine as one can define the photoresist pattern. In this program we have defined 20x50 um elements in a dual filter deposition process as shown in Figure 2.1-3. SEM analysis as shown in Figure 2.1-4 shows excellent edge acuity and step coverage for the liftoff defined filter edges. A five micron line is shown, with the filter stripe passing over steps approximately 10,000A in height. The bubbles shown in surface texture are due to the underlying silox, not the filter.

ORIGINAL FIGURES
OF POOR QUALITY

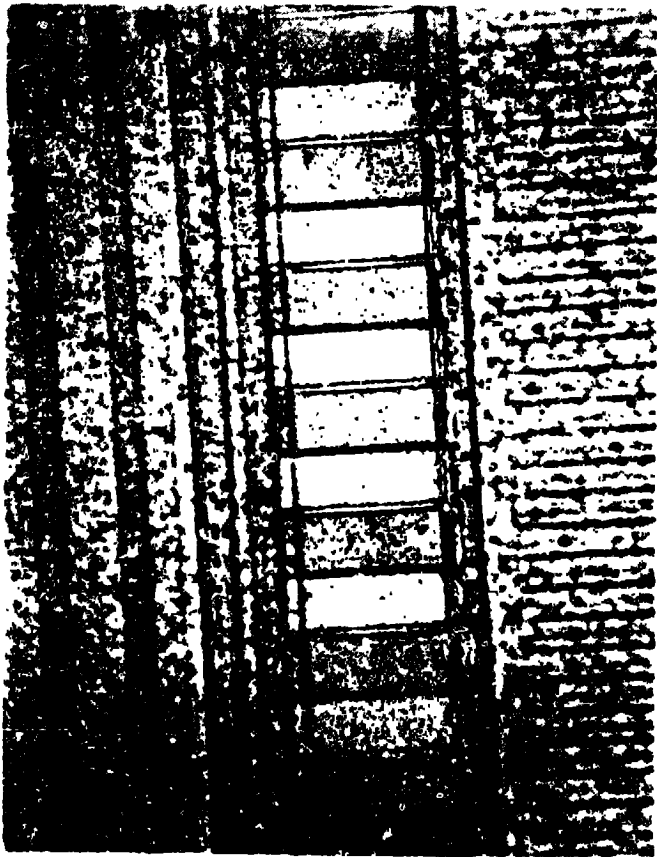
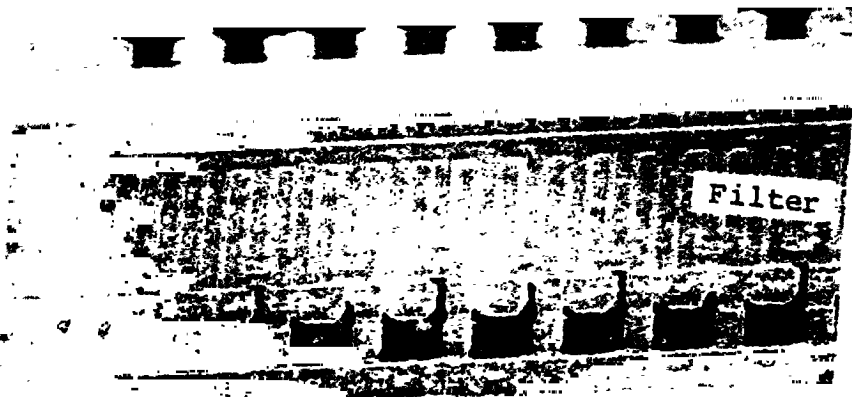


FIGURE 2.1-3 | SECTION OF A 200 ELEMENT LINE ARRAY WITH INTERDIGITATED
20 X 50µm RED AND GREEN FILTERS

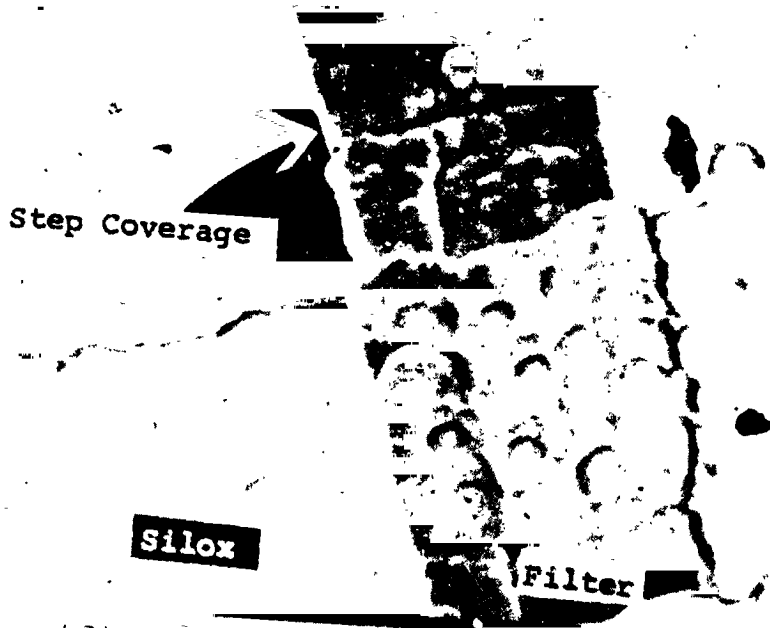
ORIGINAL
OF POOR QUALITY



Silox

10KV X 500

100 010 91681 ATL



Silox

Filter

10KV X 500

100 010 91681 ATL

FIGURE 2.1-4. SURFACE TOPOGRAPHY OF PROCESSED WAFER WITH FILTER

2.2 CCD OPERATION

The device chosen for use in evaluating the filter was a 200-element line array which was part of the mask set identified as 5040.

The line array consists of 200 20umx50um detector elements formed by CCD wells covered by transparent tin oxide. The detector's outputs are transferred in parallel into a four-phase readout register. Dynamic range is limited by a gated blooming control. A metal light shield covers all array area except the imaging area.

A topological schematic illustrating electrode relationship and function is shown in Figure 2.2-1. The timing diagram for the array is shown in Figure 2.2-2. The details of cross section were shown in Section 2.1. As illumination falls on the device the metal aperture allows photons to strike the imaging well only. Electron-hole pairs created within the silicon are separated with the holes being collected under the negatively biased imaging gate (IW). At the end of a frame time the transfer gate (OT) is pulsed negative and the imaging well is pulsed positive transferring charge into the output register gate. The four phases are clocked in sequence to move the charge to the output diode where it is detected and buffered by the output field effect transistor operating as an electrometer. The blooming control line is held at a d.c. value chosen to clip large signals and prevent blooming of signal into the output register. The sink diode is held at a large negative potential to collect charge exceeding the blooming level. In the imaging mode the scupper (SCP), analog input (AI), and input mux (IM)

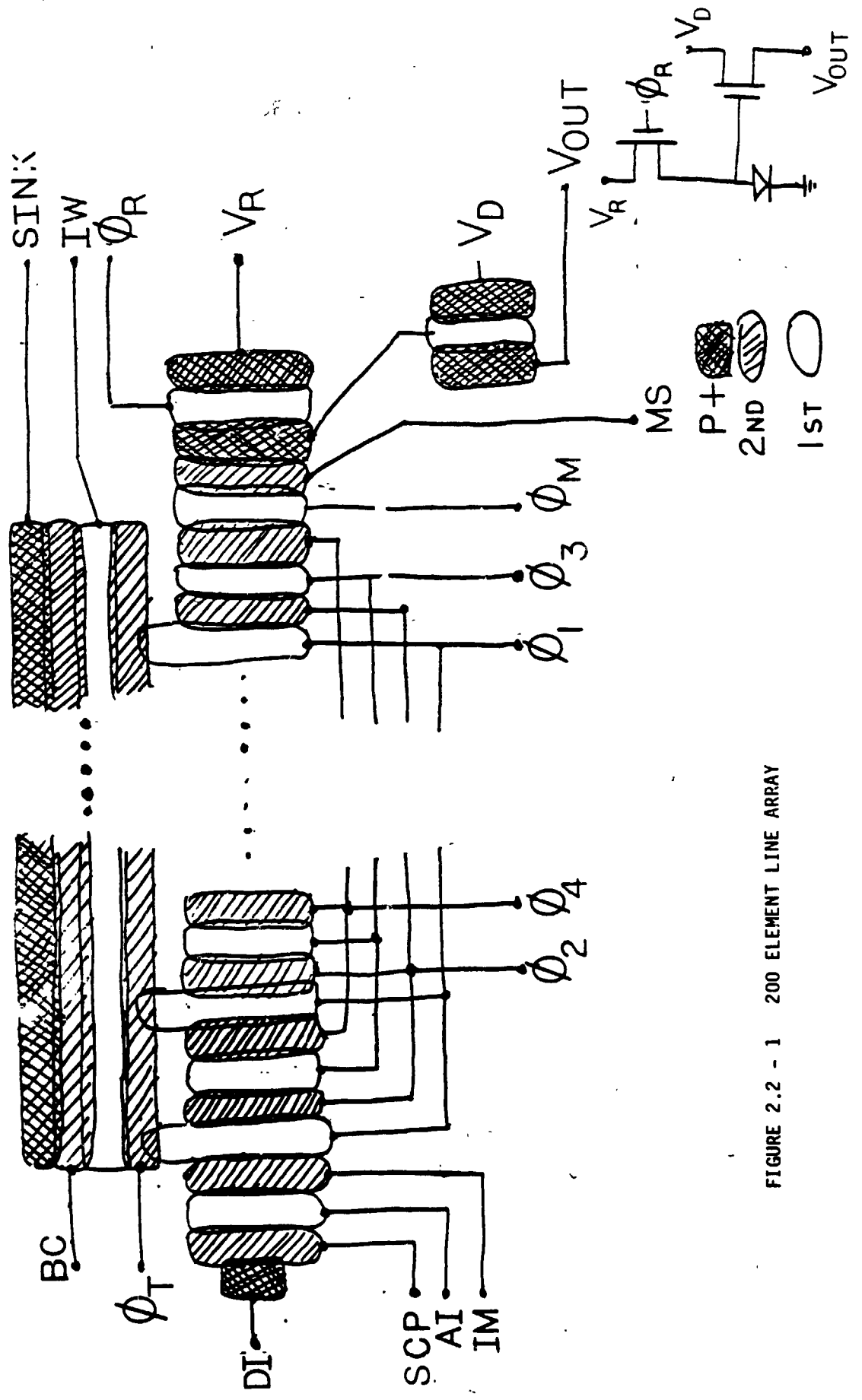


FIGURE 2.2 - 1 200 ELEMENT LINE ARRAY

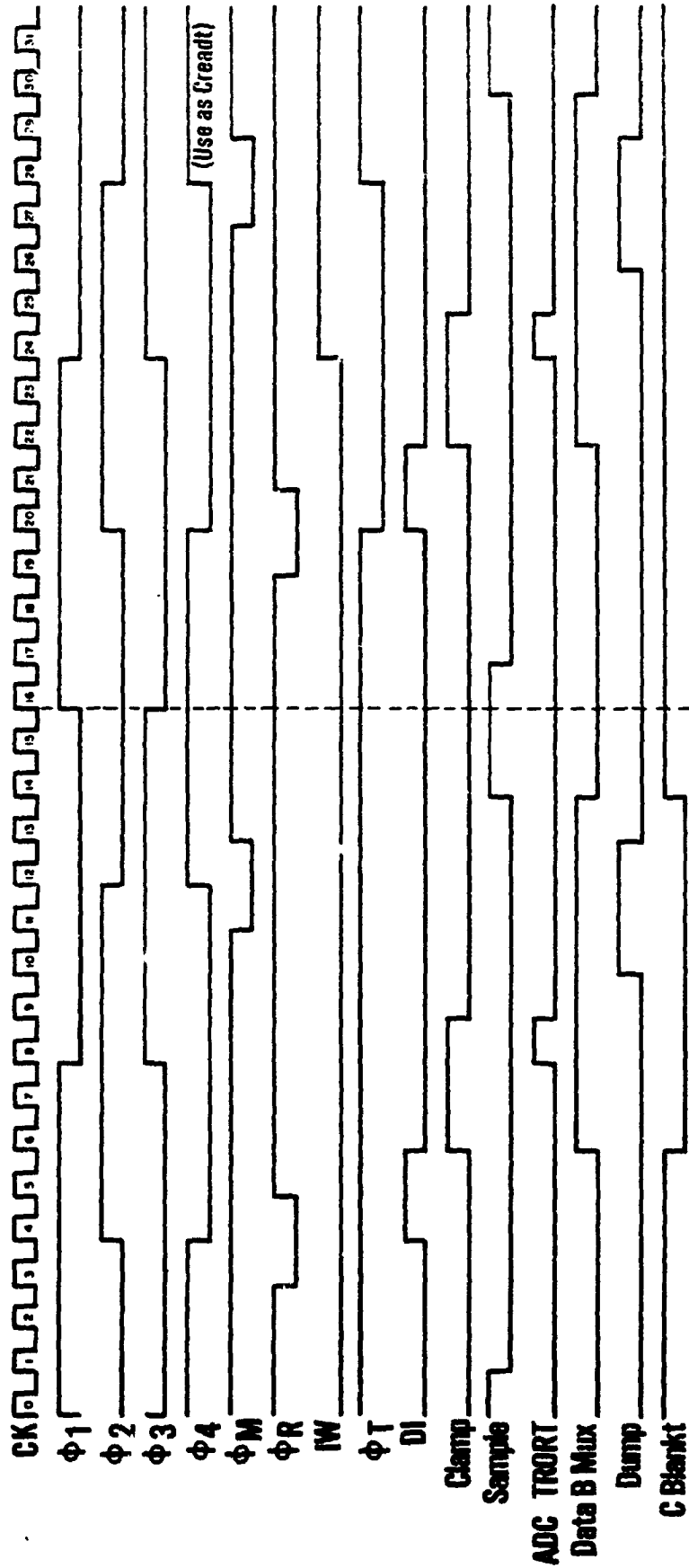


Figure 2.2-2. Test Waveforms

gates are kept blocking such that no charge is injected into the register to interfere with signal.

A top view of the layout showing the imaging well region, channel stops, location of filter stripes and output shift register is shown in Figure 2.2-3. The arrows and dotted path show the direction of charge transfer from the imaging well below the filter into the output shift register. The channel stop diffusion prevents mixing of signals in the imaging well region; the phase voltages on the output register gates prevent mixing there and control charge flow to the output diode. The amount of charge transferred from each pixel is monitored by dumping it into the depletion region of a diode which has been reset to a measured voltage level. The change in voltage across the diode is monitored through a MOS transistor acting as an amplifier. The technique of sampling both the diode reset voltage and signal voltage, known as coherent double sampling, eliminates a lot of noise and uncertainty in the measurement. Computer acquisition and additional signal processing are discussed in Section 4.2.

2.3 FILTER ARRAY MASK DESIGN

To allow easy interpretation of cross talk effects between different filter regions, a mask with a particular bar pattern was designed. The pattern was designed to be used with broad band flat-field illumination and as such contains a number of different sized filtered and non-filtered regions. To eliminate effects of crosstalk due to charge transfer inefficiency, the

ORIGINAL FIGURE
OF POOR QUALITY

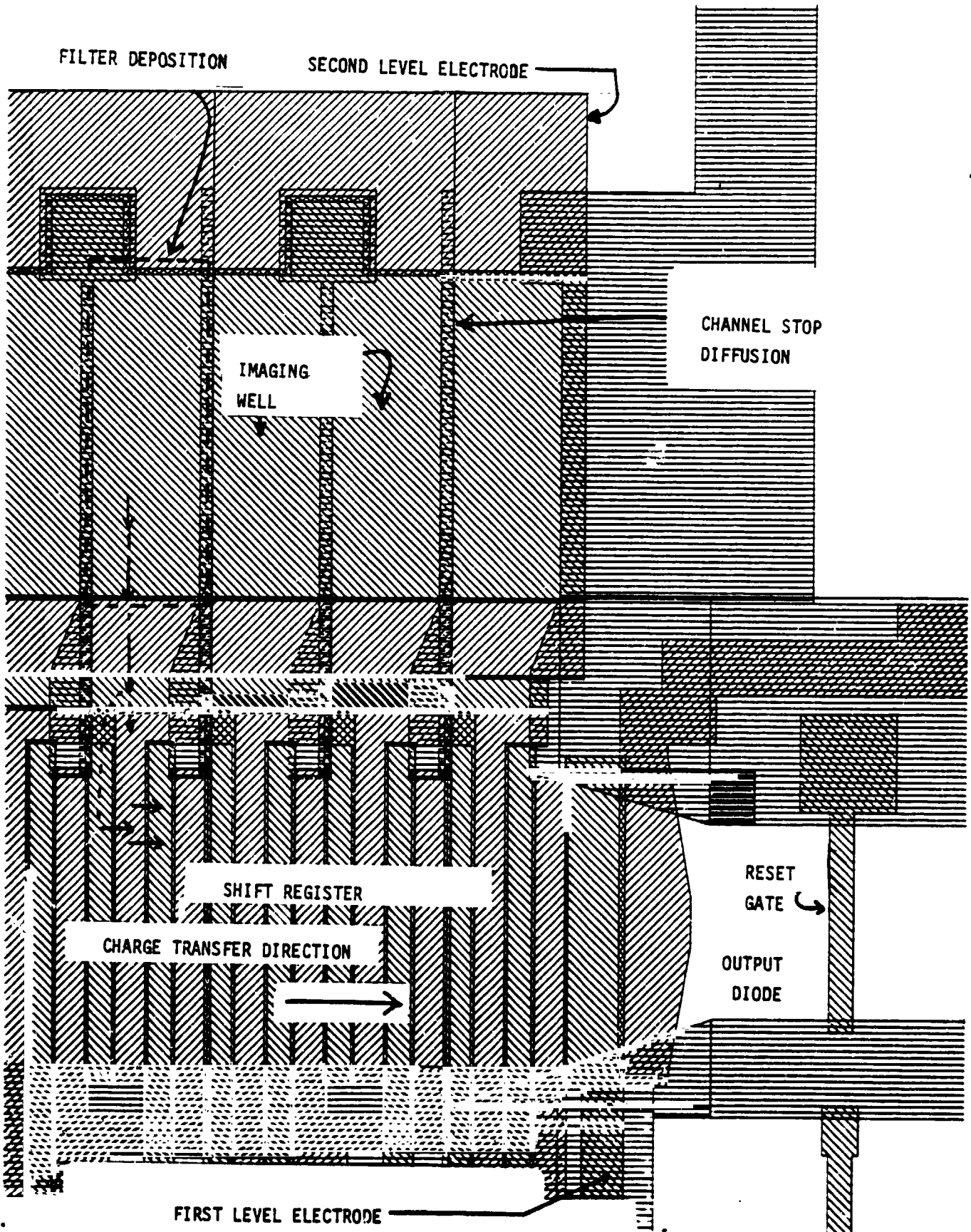


FIGURE 2.2-3 200 ELEMENT LINE ARRAY LAYOUT

array pattern was designed primarily to look for charge spread forward, in the direction of charge transfer, as opposed to bilateral spread. To account for misalignment of the stripe array, filter regions were designed in some cases to overlap into adjacent sensor elements.

Table 2.3-1 lists the type of filter above each cell and the function of that regions. The stripe pattern was formed on all line arrays. Figure 2.3-1 shows the mask design for a completed array, broke into several sections for clarity. To provide an alternate pattern in which effects due to out of band filter transmission were eliminated, a second mask was designed which would mask with aluminum certain regions of this stripe pattern. If this mask were to be used, these cells would be opaque: 11 to 31, 33 to 55, 78 to 96, 98 to 137, 139 to 156, and 180 to 195. After designing this mask, we learned that the filter material was not very tolerant to the chemical etches required to define the aluminum interconnect. This meant that the opaque aluminum regions would have to be formed before filter deposition. As this program was utilizing already fabricated CCD line arrays, it was not considered feasible to incorporate use of this mask design in the program. An alternate and more flexible solution was to use the optical profiler source as described in section 4.2. The aluminum mask design is included here for reference.

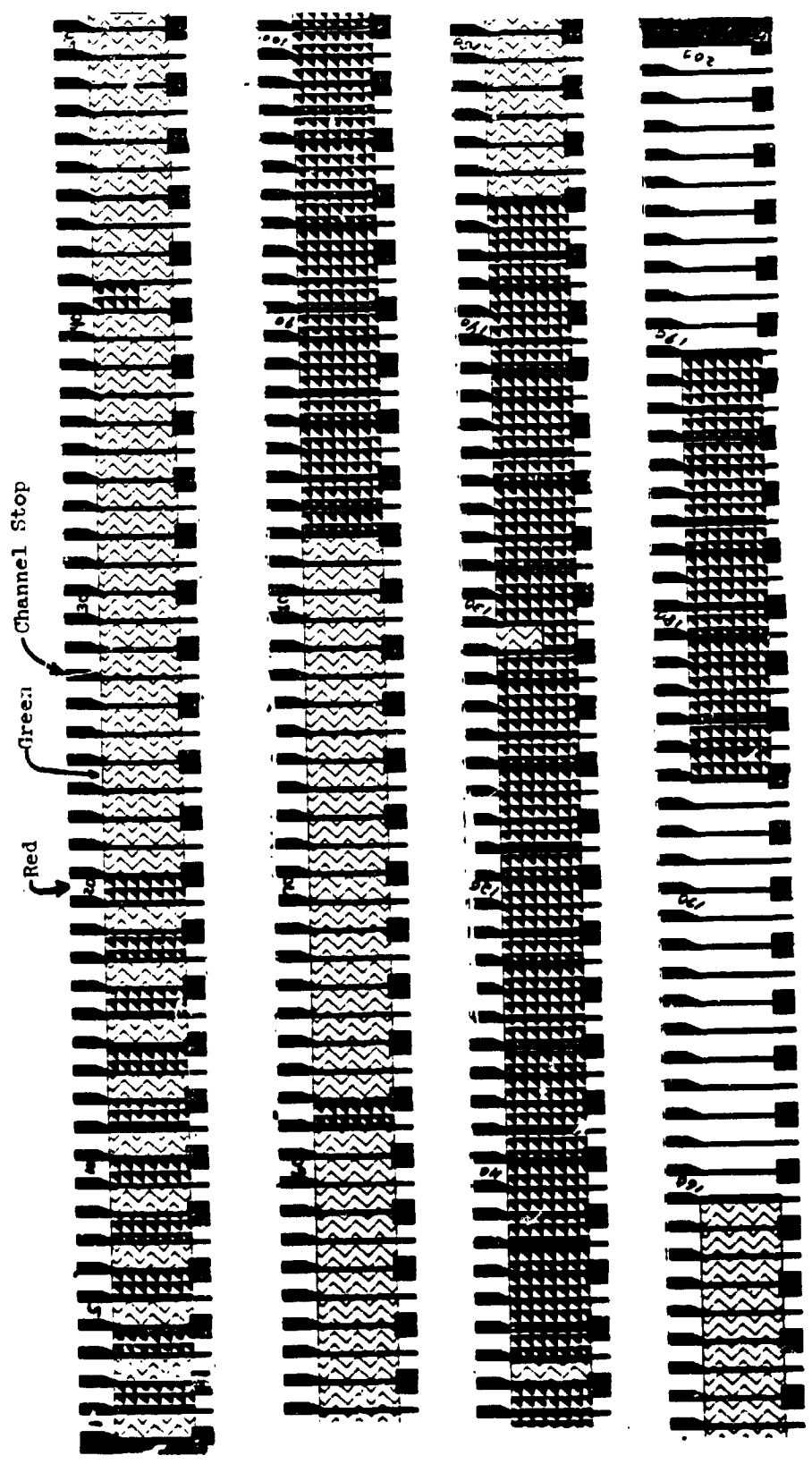
TABLE 2.3-1

<u>*CELL #</u>	<u>COLOR</u>	<u>FUNCTION</u>
1-10	Clear	Clear into Red
11-25	Band 3 Red	Red into Clear
26-40	Clear	Clear into Green
41-55	Band 2 Green	Green into Red
56-71	Band 3 Red	
71	Half-height Band 2	Checks alignment of green filter
72-96	Band 3 Red	
97	Band 2 Green	Single element Green into Red
98-117	Band 3 Red	Red into Green
118-137	Band 2 Green	
138	Band 3 Red	Single element Red into Green
139-158	Band 2 Green	
159	Half-height Band 3	Checks alignment of Red Filter
160-179	Band 2 Green	
180	Band 3 Red	
181	Band 2 Green	
182-200	Alternates Red-Green as above	

*In this table cell #1 is farthest from output end of shift register

Elements are numbered in order
of their electrical output

Figure 2.3 - 1
Filter Mask Design



3.0 MEASURED RESULTS - FILTER CHARACTERISTICS

Essentially two types of measurements were used to characterize the filter layers. Transmission measurements were made by Optoline on glass "witness plates" which were included with each filter deposition. These witness plates had only the filter material present.

When the filter is deposited on completed CCD arrays, some interaction/-attenuation was anticipated because of the underlying gate and insulator levels required to fabricate the array.

To evaluate this interaction, two systems were used to measure spectral reflectance from the filter and array as a unit. These specific systems are described in more detail in the following section. Although initial comparisons between transmission measurements and reflectance measurements looked good, more detailed calibration of the Nanometrics instrument, used at ATL for most of the reflectance measurements, showed a inaccuracy in the wavelength scale. The repeatability of this scale was not affected; therefore, most of the data is valid for uniformity and repeatability measurements but correction is required before comparing results with those from other instruments.

3.1 SPECTRAL REFLECTANCE MEASUREMENT TECHNIQUE

Spectral reflectance measurements on the first group of samples received from Optoline were made at the Westinghouse Research Laboratories in

Pittsburgh using a specially built spectrometry system from another program. This instrument uses a collimated light source. The minimum spot size over which the measurement is made is 100 mils.

The spectral reflectance of these samples and all samples received subsequently were measured at ATL using a Nanometrics Model 010-0180 Film Thickness Meter, operated as a micro spectral reflectometer with an x-y recorder on the output. A block diagram of the measuring system is shown in Figure 3.1-1. The Nanometrics system differs from the Research Laboratories system in two important aspects: (1) it uses a lens-focused converging light beam rather than collimated light, (2) the spot size is approximately 35 microns as opposed to 100 mils minimum. This smaller spot size allowed more detailed measurements of filter uniformity and also allowed measurements on completely processed wafers in the actual imaging well area of the chip where the filters are active. Measurements could also be made using different objective lens powers, permitting some comparison of the effects of the spread in angle of incident light.

The absolute vertical and horizontal scales of the measurements made using the Nanometrics system have not been established. The vertical scale was normalized to the reflectance of an aluminum mirror reference sample. However, since the spectral reflectance of the mirror is not flat and is unknown, efforts were made to find a spectrally flat high reflectance standard. A mirror obtained from NASA suffered from the same problems as the first mirror, in that its reflectance was not spectrally flat and was not

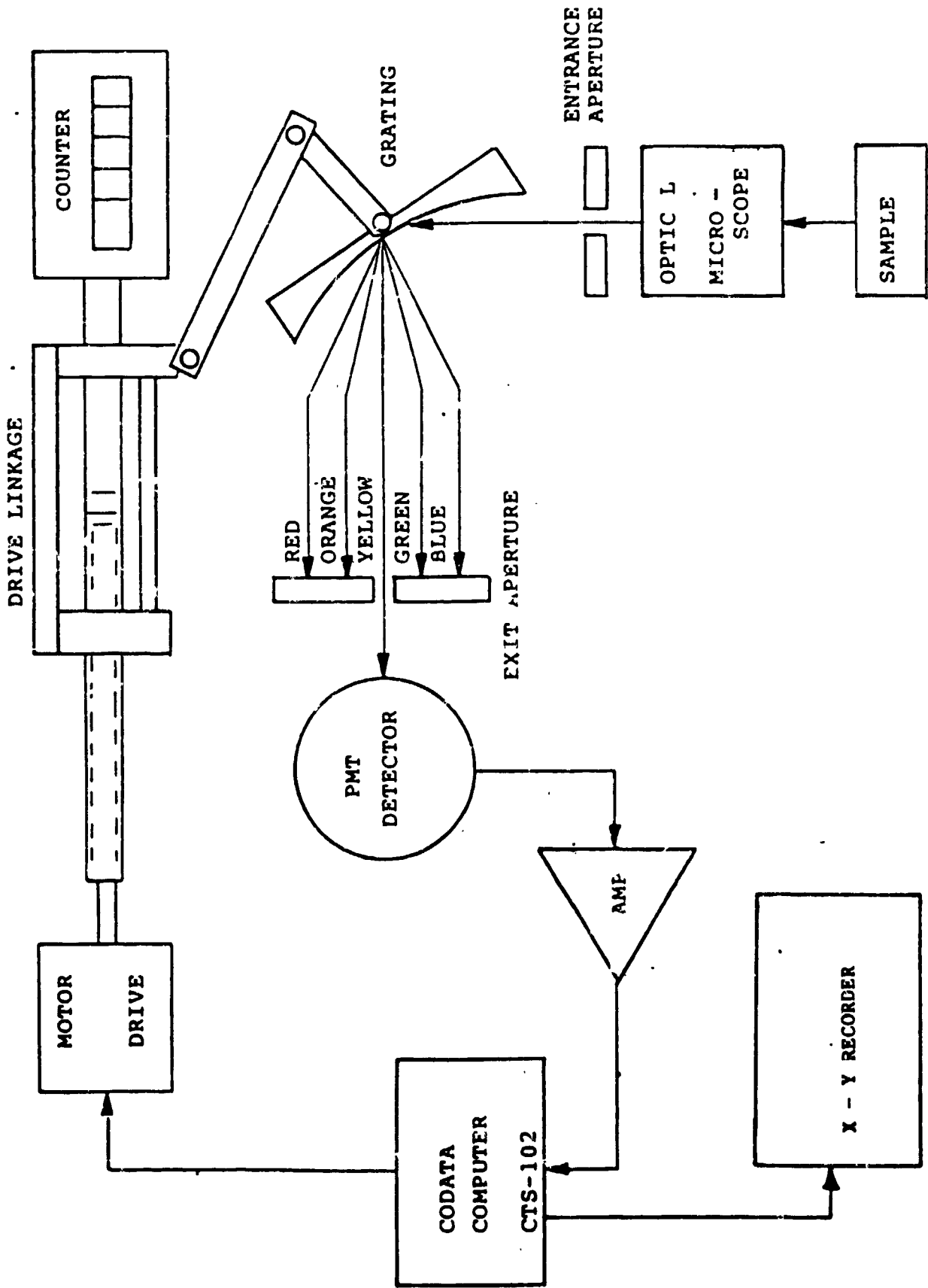


FIGURE 3.1-1 NANOMETRICS MICROSPPECTROPHOTOMETER

known. An attempt was made to use a block of magnesium oxide, which is used as the reference for diffuse reflectance measurements with the Cary 14 Spectrophotometer, as a reference for the Nanometrics instrument. However, since the specular reflectance of magnesium oxide is very low, an amplifier was needed between the output of the micro-spectroreflectometer and the Nanospec computer. Since there was a question of the validity of using a diffuse reflectance standard for a specular reflectance measurement, this approach was not continued.

The horizontal sweep of the x-y recorder was triggered automatically at the start of the Nanometrics sweep. The Nanometrics Instrument measures from 4800A to 8000A in steps of approximately 35.5A. These steps appear as glitches in some of the measured data. Measurements of known narrow-band interference filters, shown in Table 3.1-1, showed that the horizontal scale was non-linearly shifted. The correct wavelength may be calculated from these measurements to be $\lambda = 1.058 \lambda - 467$ Angstroms. This shift in horizontal scale was not detected until nearly the end of the program.

In spite of these slight inaccuracies, measurements were found to be extremely repeatable. As most measurements were significant only on a comparative basis, no attempt was made to correct the data presented in this report except as noted in Section 5 where spectral reflectance is compared to filter transmission.

TABLE 3.1-1 MEASUREMENTS OF KNOWN NARROW-BAND FILTERS
 SHOWING SHIFT IN NANOSPEC HORIZONTAL SCALE

FILTER VALUE (Angstroms)	NANOSPEC SCALE (Angstroms)	SHIFT IN WAVELENGTH (Angstroms)
5461	5600	140
6000	6110	110
6563	6650	90
6943	7000	60

Correction Equation: $\lambda = 1.058 \lambda - 467A$

3.2 FABRICATION EXPERIMENTS

Several sets of wafers were processed during the program. These were identified by wafer number, filter color and the group or batch that they were processed with at Optoline.

Wafer and sample types fell into these categories:

Witness Plates: These are quartz slides with nothing other than filter present, which are included in each run to measure optical transmission

Bulk Wafer Samples: These are silicon wafers with oxide, nitride, silox (etc.) layers which simulate the dielectric structure on completed wafers.

Patterned-non-functional: These are completely processed CCD wafers with no functional chips. A filter array pattern has been defined by liftoff

5048 Diodes: These are large p+/n diodes which were included in one run, with filter material over one-half the diode length. The intent was to give transmission data early in the program by measuring photo induced current while imaging on alternate halves of the diode. Initial measurements were inconclusive and the effort was discontinued as soon as functional wafer samples became available.

Patterned Functional: These are completely processed wafers with functional 200 element CCD line arrays. A filter array pattern has been defined by liftoff. Either one or both filter colors may be present.

TABLE 3.2-1 SUMMARY OF SAMPLES FABRICATED

BATCH SAMPLE TYPE	GREEN FILTER	FILTER TYPE RED FILTER	OTHER	PURPOSE
1. Witness Plate	OK	Broken		Compare spectral transmission to spectral reflectance Measure Reflectance above CCD dielectric structure
First Tin Oxide Bulk Wafer	1234-1	1234-2		
Second Tin Oxide Bulk Wafer	1234-11	1234-17		
2. Witness Plate	OK	OK		Same as above Same as above SEM evaluation Simulated total structure Measure diode leakage
First Tin Oxide Bulk Wafer	1234-7	1234-10		
Patterned non-functional	3712-6	3712-10		
Patterned non-functional	4250-3	4250-6		
5048 diodes	4293-9	4294-4		
3. Witness Plate	OK	OK		First set of functional wafers with both filters.
Patterned functional	4421-8	4421-8		
Patterned functional	4421-9	4421-9		
4. Witness Plate	OK	3 runs done;		To check repeatability of filter deposition when done on successive days without change to deposition system
		Test 2		
		Test 3		
		Device Run		
Patterned functional	4446-10	4446-10		Second set of functional wafers with both filters
Patterned functional	3553-7	3553-7		
Patterned functional	3553-9	3553-9		
Alternate similar CCD chip type with shift registers			3849-10 with no filter	Experiment to isolate transfer efficiency degradation by simulating glw discharge plus thermal cycles
Alternate similar CCD chip type with shift registers			3451-12 with no filter	

TABLE 3.2-1 SUMMARY OF SAMPLES FABRICATED (CONTINUED)

BATCH SAMPLE TYPE	FILTER TYPE		OTHER	PURPOSE
	GREEN FILTER	RED FILTER		
5. Witness Plate	OK			Received filter deposition on surrounding chips - not one measured without glow discharge Patterned with bonding pad mask, filter over entire array, deposited without glow discharge Simulated glow discharge plus thermal cycle without deposition
Alternate similar CCD chip type with chip registers	3875-5			
Patterned functional	4996-15			
Non-patterned functional		4996-15 with no filter		
6. Witness Plate	OK	OK		Transfer efficiency degradation plus single color filter. Experiments - processed with a special version of stripe pattern which leaves open first 10 elements- 4996-1, 4 received both filter depositions on top of one another. Ideal filter deposition above non-ideal substrate: Ideal filter above: psuedo ideal substrate Quartz slide with 550A polysilicon as AR coating Quartz slide without polysilicon
Patterned functional	4996-9			
Patterned functional	4996-13	4996-5		
Patterned functional		4996-6	4996-1	
Patterned functional			4996-4	
Patterned functional			4996-14	
Patterned functional			Ideal Filter	
Patterned functional			#3 Ideal Filter	
Patterned functional			Ideal Filter	
Patterned functional			Ideal Filter	
Bulk Unpatterned				
Witness Plate				
Witness Plate				

A listing of all samples processed during the program is shown in Table 3.2-1.

Optical measurements on these wafers are presented in Section 3.4 and 3.6; electrical measurements are presented in Section 5.0.

3.3 CHIP DIELECTRIC STRUCTURE

The existing CCD process in use at Westinghouse uses a four phase two-level transparent tin oxide gate structure and two levels of aluminum. The first aluminum level serves to interconnect gates and diffusions and the second level serves as a light shield. There are several layers of oxide, nitride and silox used as insulators between various interconnect levels. These are shown in cross section in Figure 3.3-1. As the filter material is deposited on top of a completed wafer, the light must pass through all layers to get into the silicon imaging well. In the existing 5040 design the gate which forms the imaging well region is on the first tin oxide level. In other chip designs it could as easily be put on the second tin oxide level. To see if this would be beneficial, the first batch of experiments included samples which measured filter characteristics above both the first and the second tin oxide level. For reasons to be discussed later, this was found to have no benefit and was discontinued after the first experiment set. Figure 3.3-2 shows a SEM photograph of the filter material in cross-section above a bulk test wafer which includes one level of tin oxide and all other levels except the two aluminum interconnect levels.

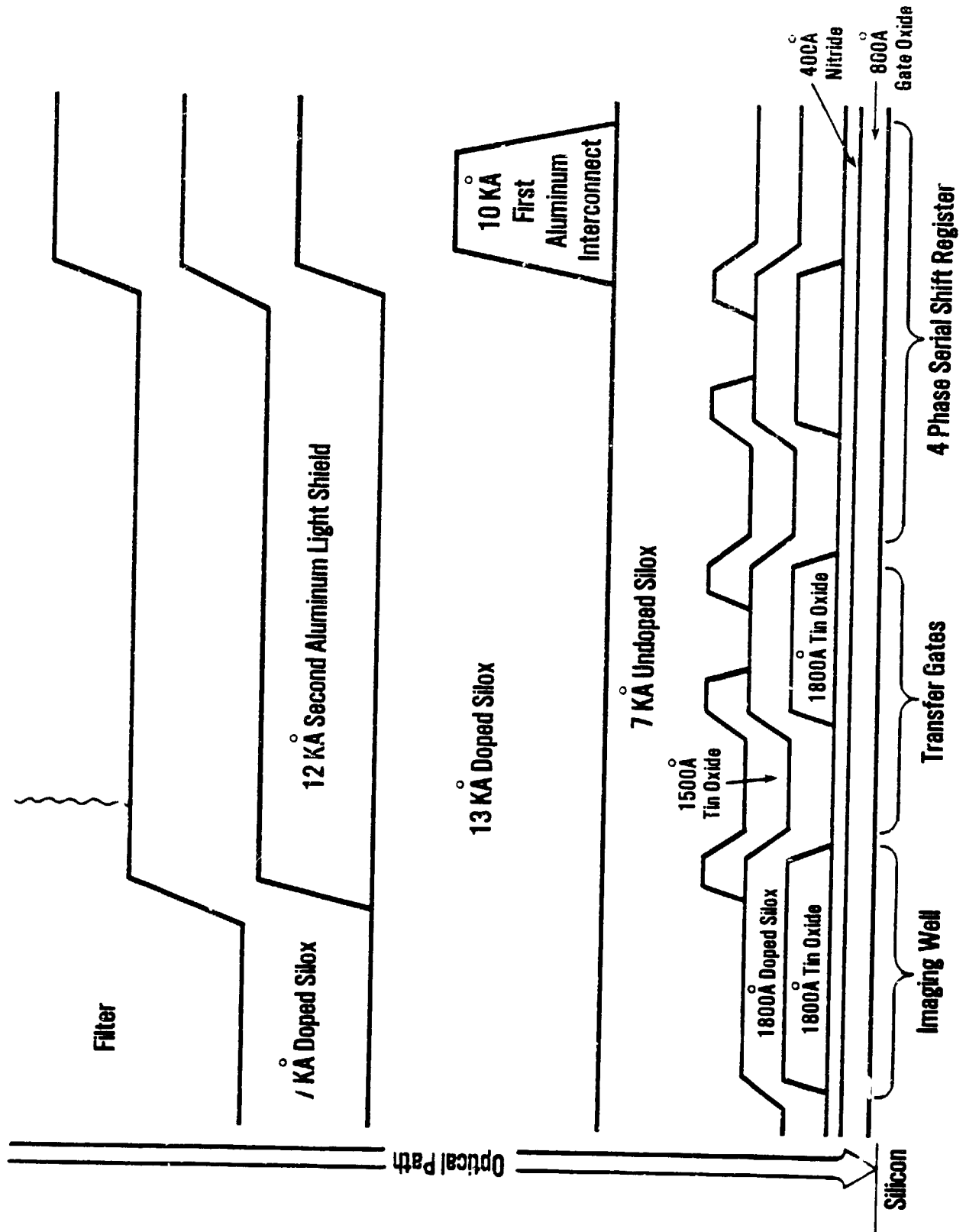
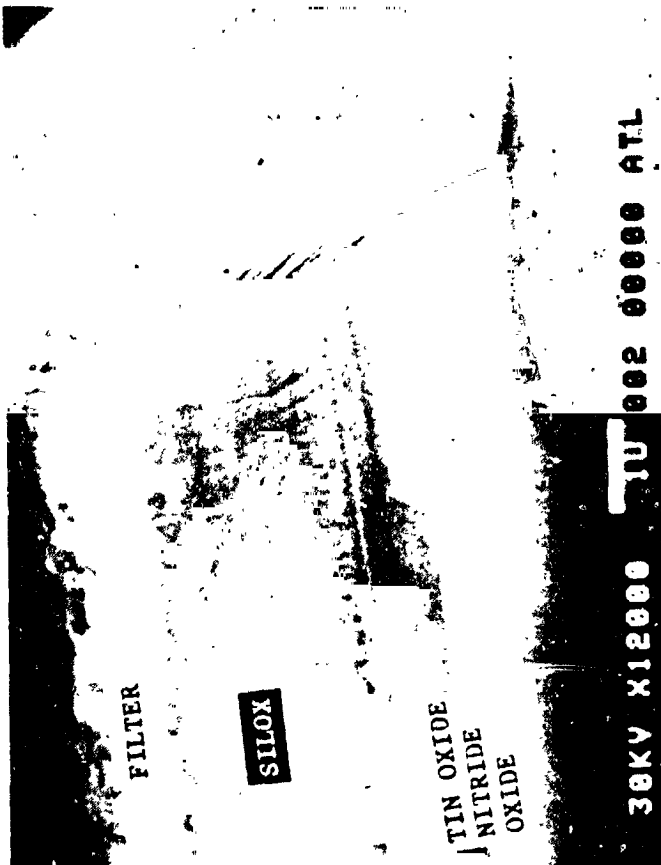
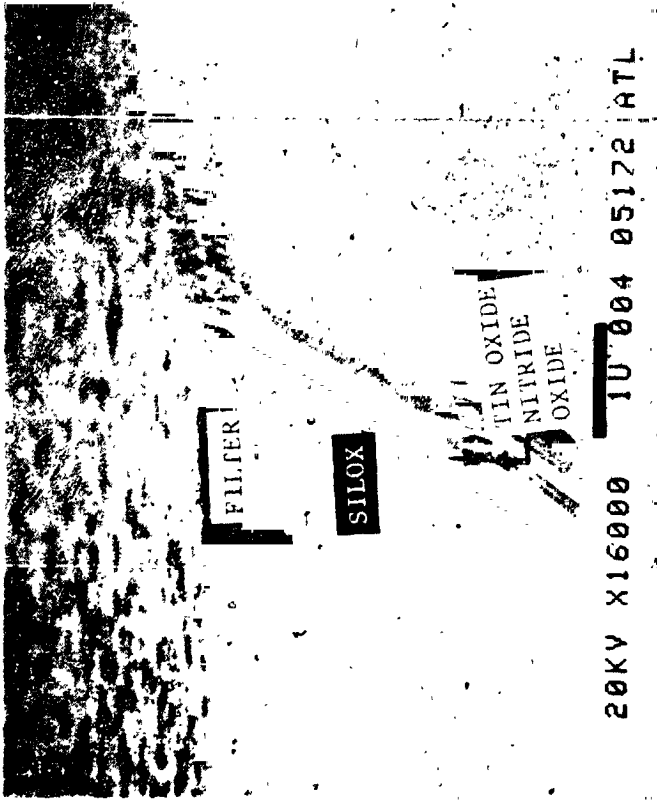


Figure 3.3-1. Chip Cross-Section



ORIGINAL FILE IS
 OF POOR QUALITY

FIGURE 3.3-2 CROSS SECTION OF CHIP DIELECTRIC STRUCTURE

3.4 MEASURED RESULTS

Measurements on the glass witness plate for band 2 for the first filter deposition batch are shown on the following figures. Note that this filter used a standard Optoline recipe intended to approximate the band 2 specification.

Figure 3.4-1 Optical transmission as measured by Optoline

Figure 3.4-2 Spectral reflectance as measured at Westinghouse Research Laboratories

Figure 3.4-3 Spectral reflectance as measured at Westinghouse ATL with the Nanometrics Instrument.

To avoid confusion, charts are labeled with percent transmission at peak and the bandwidth at the 50% point. The point to be noted here is that the curves are smooth and that there is reasonable although not absolute correlation between the different measurement systems.

Figure 3.4-4 shows the transmission measurement for the Band 3 witness plate. Again, this filter used a standard Optoline recipe. This plate was broken at Optoline following deposition so that reflectance measurements could not be made.

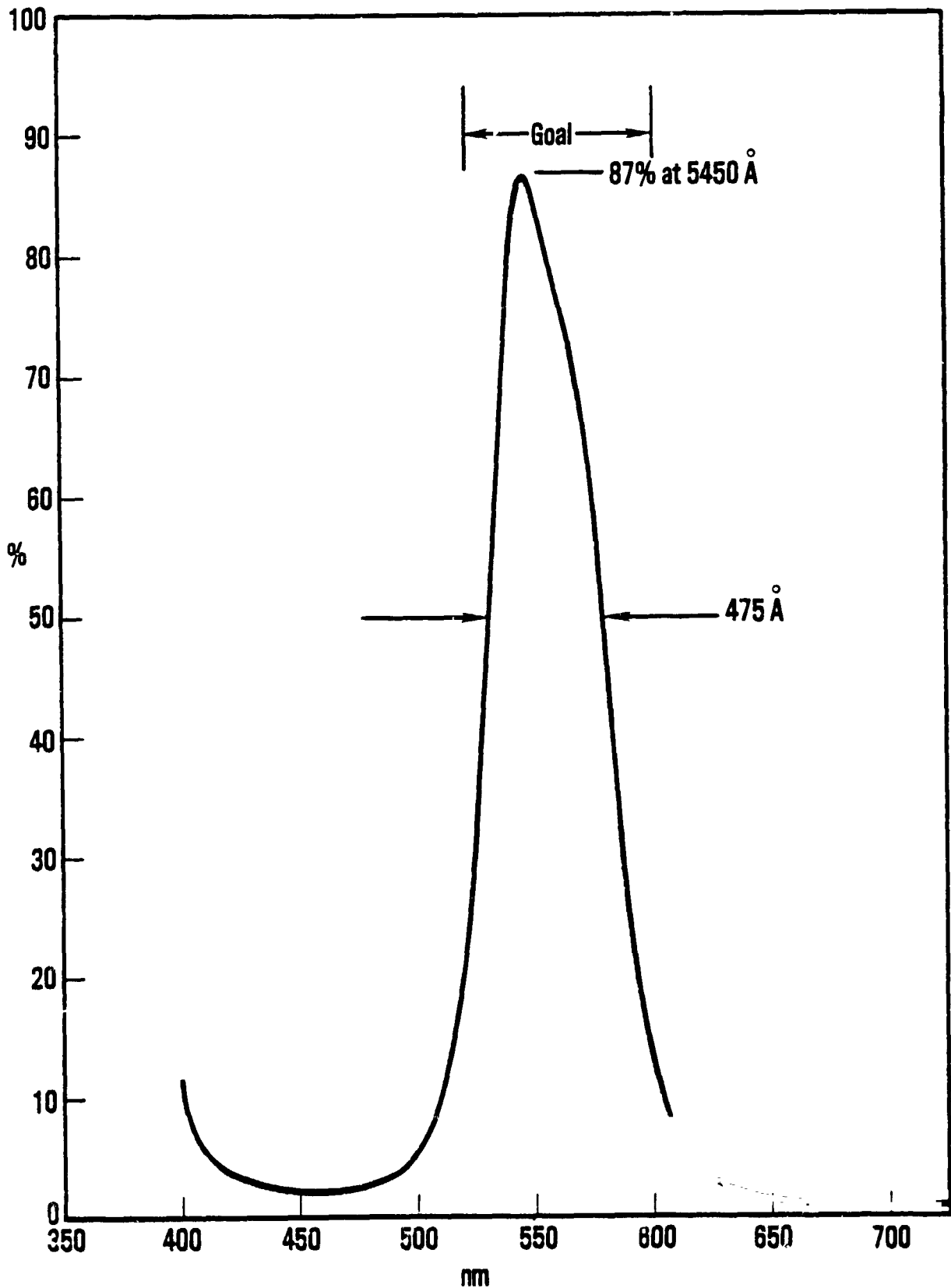


Figure 3.4-1. Glass Witness Plate Transmission

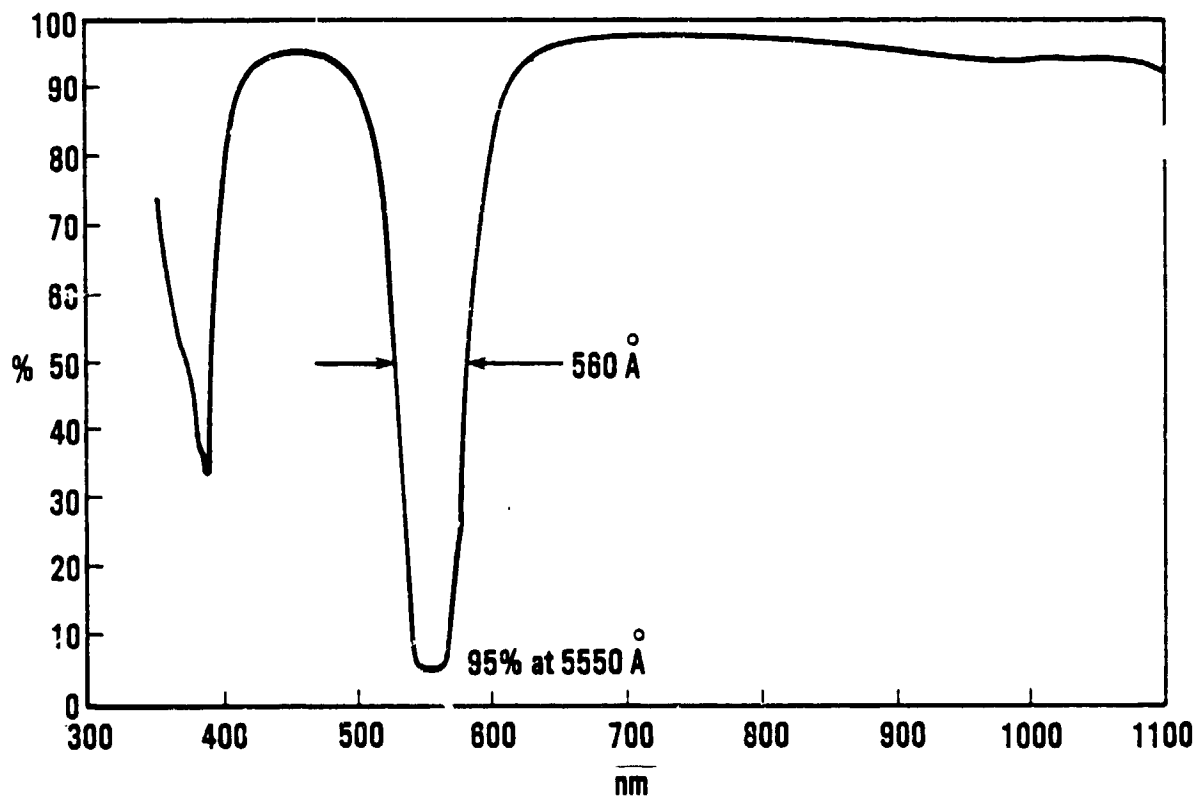


Figure 3.4-2. Spectral Reflectance From Glass Slide Band 2 520-800 nm (Green)

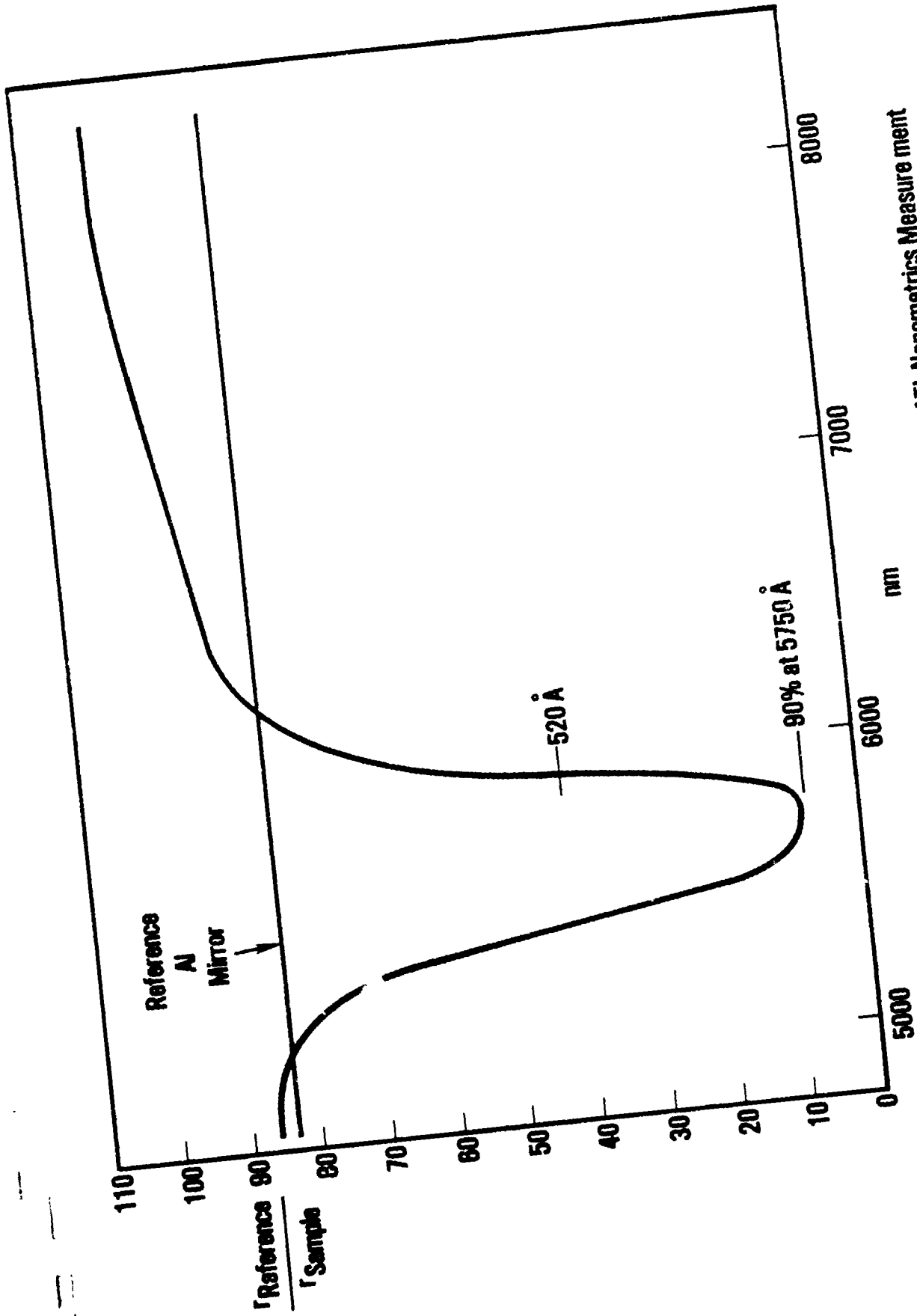


Figure 3.A-3. Spectral Reflectance From Glass Slide Band 2 Westinghouse ATL Nanometrics Measurement

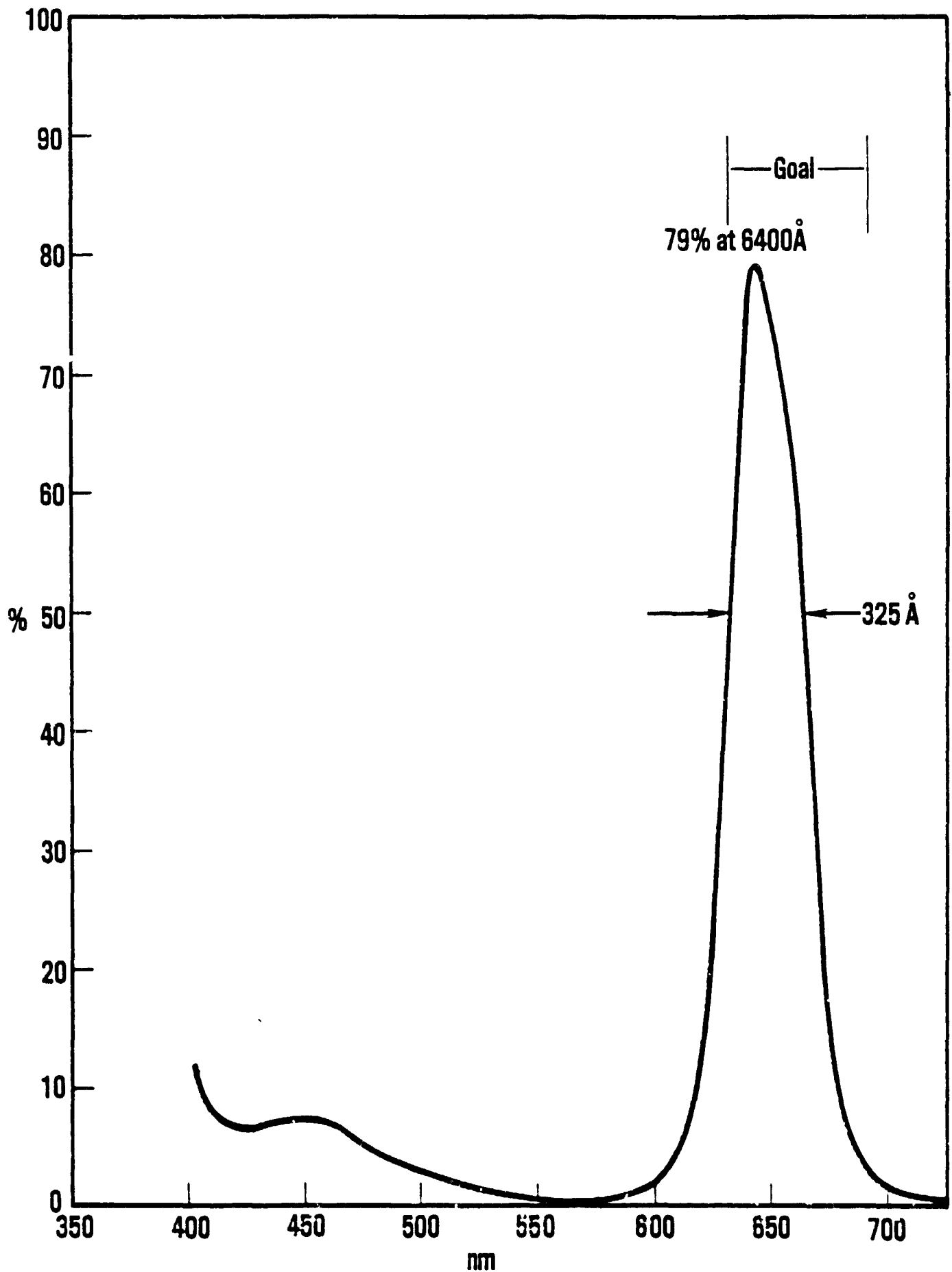


Figure 3.4-4. Glass Witness Plate Transmission - Band 3

Figure 3.4-5 shows the spectral reflectance measurements from these same filter layers when they are placed above bulk silicon wafers with the first tin oxide dielectric substructure required to fabricate CCDs, as illustrated in Figure 3.3-1. There appears now super-imposed on the filter characteristics several sinusoidal components which add fine structure (vs. wavelength) to the overall transmission. Figure 3.4-6 shows spectral reflectance from samples with second tin oxide present.

3.5 FINE STRUCTURE EVALUATION

The fine structure was believed due to reflections occurring at the interfaces between the different dielectric layers in the chip structure and the filters and the silicon surface. Although this type of fine structure had been predicted by computer simulations run previously at Westinghouse for other programs, it had not been measured in the optical response of silicon diode and CCD sensors. It was suggested at one of the review meetings with NASA that this difference between calculated results, which are equivalent to collimated light measurements, and actual system response could be due to the integrated effect of the lens which produces a range of angles of incidence. This concept is supported by the plots shown in Figure 3.5-1 where the same area of a filter sample on a bulk wafer with silox layers is measured using three different microscope objective powers. As the objective power is increased, thereby gathering reflected light from a greater range of angles, more and more of the fine structure disappears.

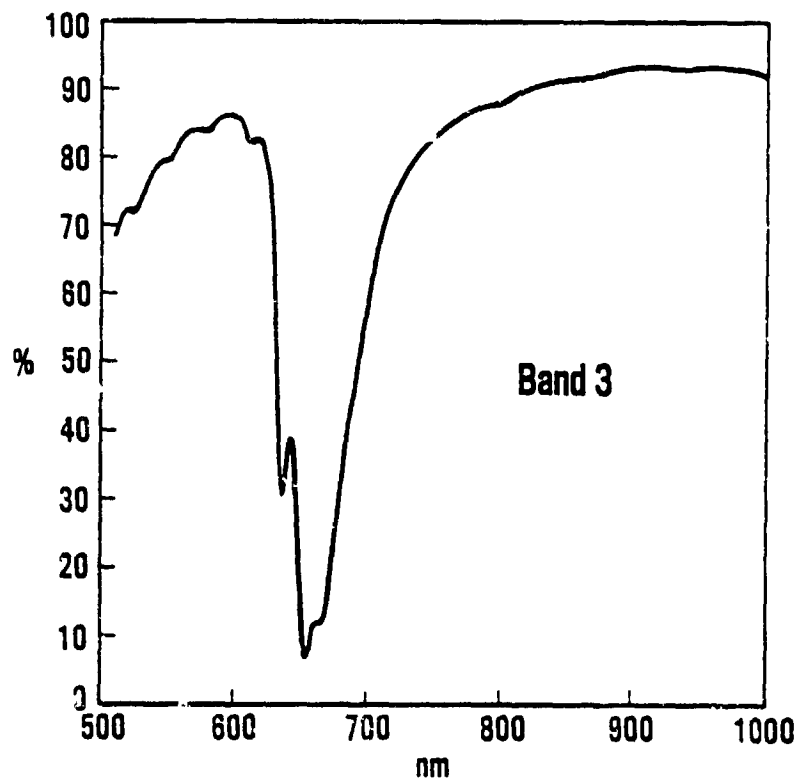
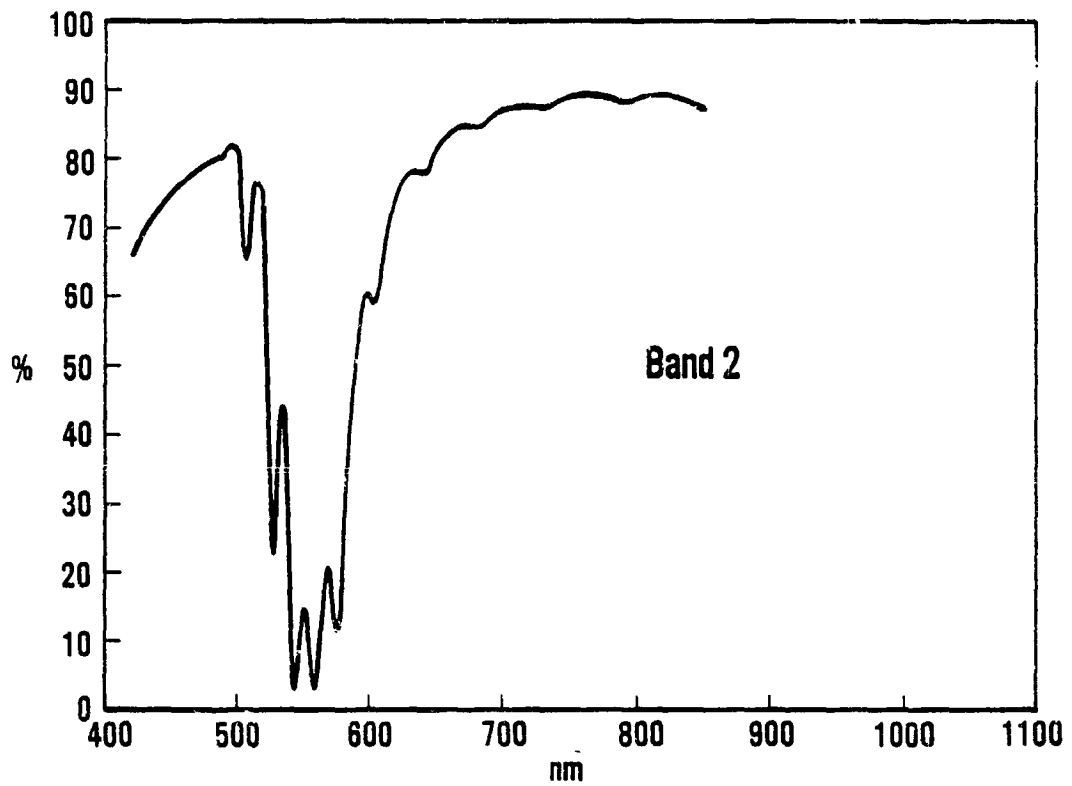


Figure 3.4-5. Spectral Reflectance From Bulk Silicon Wafers With First Tin Oxide Dielectric Structure

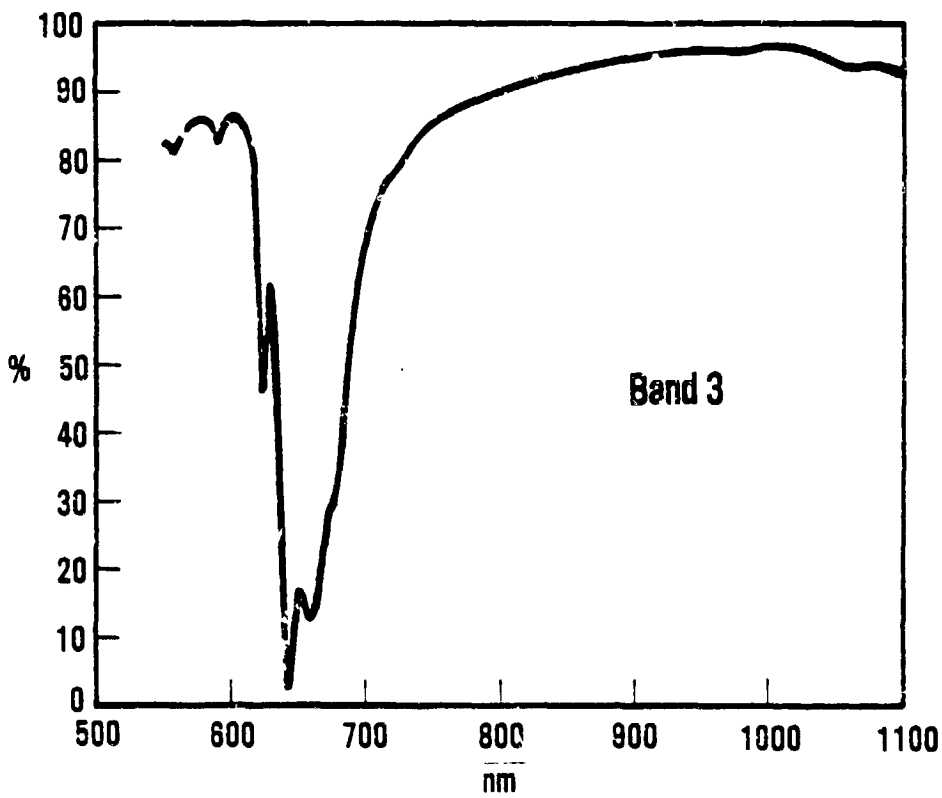
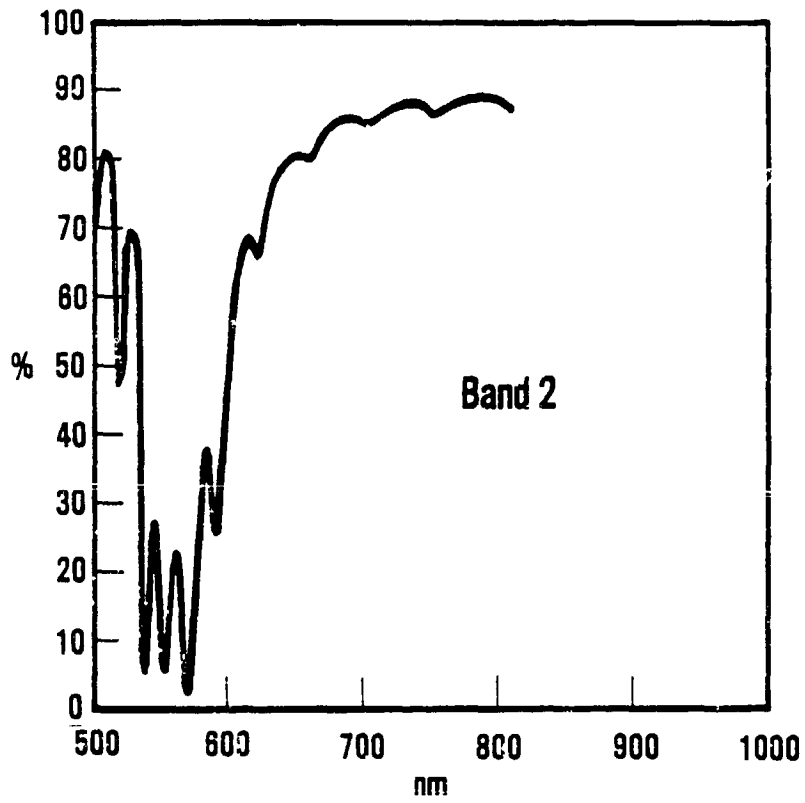


Figure 3.4-6. Spectral Reflectance From Bulk Silicon Wafers With Second Tin Oxide Structure

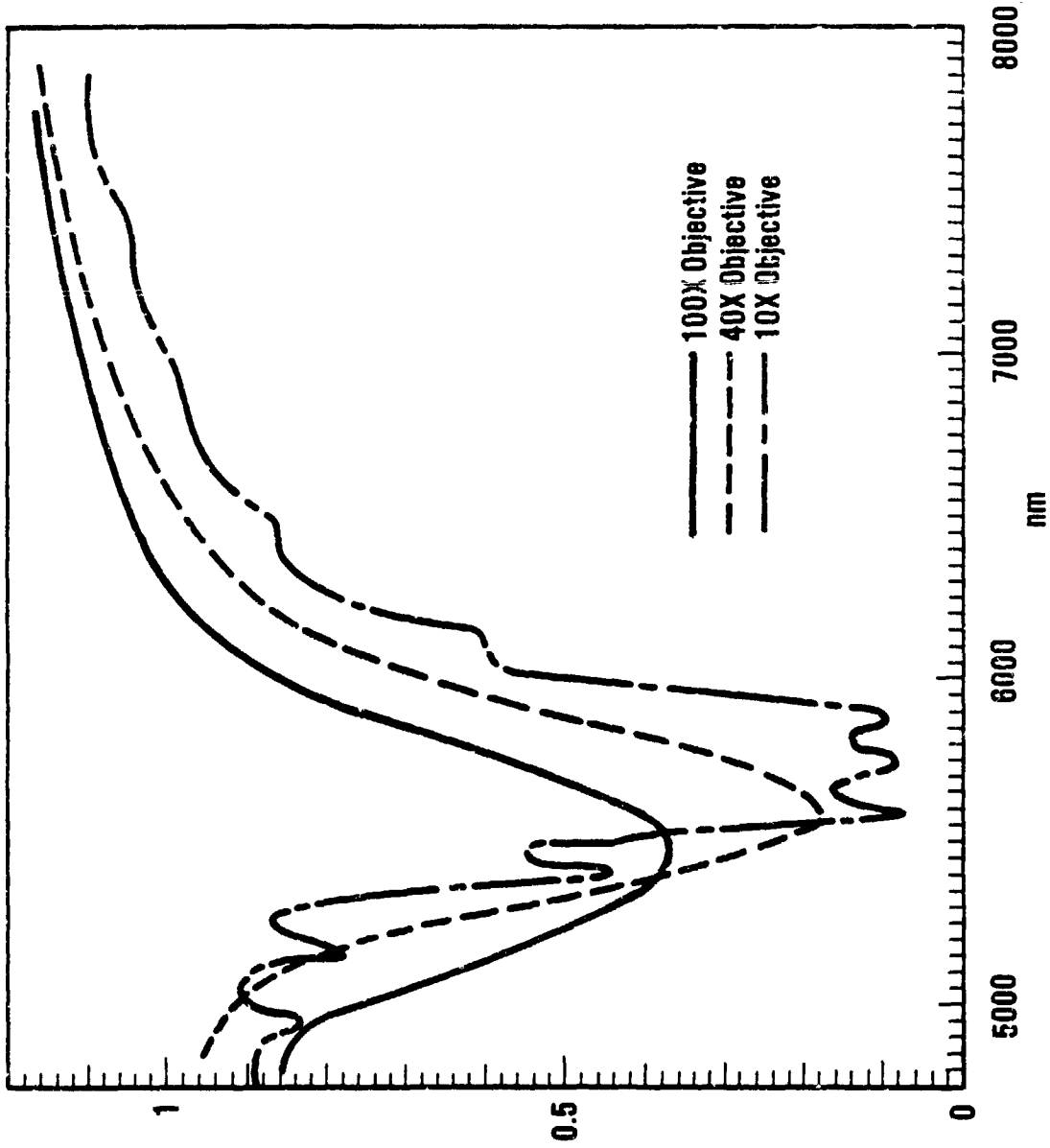


Figure 3.5-1. Filter Response with Different Objective Powers

As supportive evidence, to identify which underlying levels are causing the fine structure, reflectance measurements were made on the completed wafer with its dielectric structure but without the filter material present. This data is shown in Figure 3.5-2 and is qualitatively similar. However, the particular data presented is for another sample and before and after filter deposition overlap comparisons do not show any direct wavelength correlation in the positions of the peaks and valleys of the fine structure, indicating that normal thickness variations in this coating are sufficient to shift the fine structure significantly.

Elimination or reduction of the fine structure seemed necessary both to keep in-band transmission within 10% of peak as requested in the Thematic Mapper specification, and to avoid the probability that small variations in SiO_2 thickness from chip-to-chip could shift the phase of the fine structure and in effect shift the passband.

As modeling performance was one of the goals included in the Statement of Work, it was decided to use computer analysis to verify the measured results as well as to predict a solution. A sophisticated optical design program was in use by Dr. T. W. O'Keefe of the Westinghouse R&D Center. O'Keefe's program can not only compute the spectral transmission from air into silicon through a specified set of filter layers deposited over the gate and insulator structure, but can perturb all or some of the layer thicknesses within limits set by the experimenter to produce an optimum design. Initially these limits,

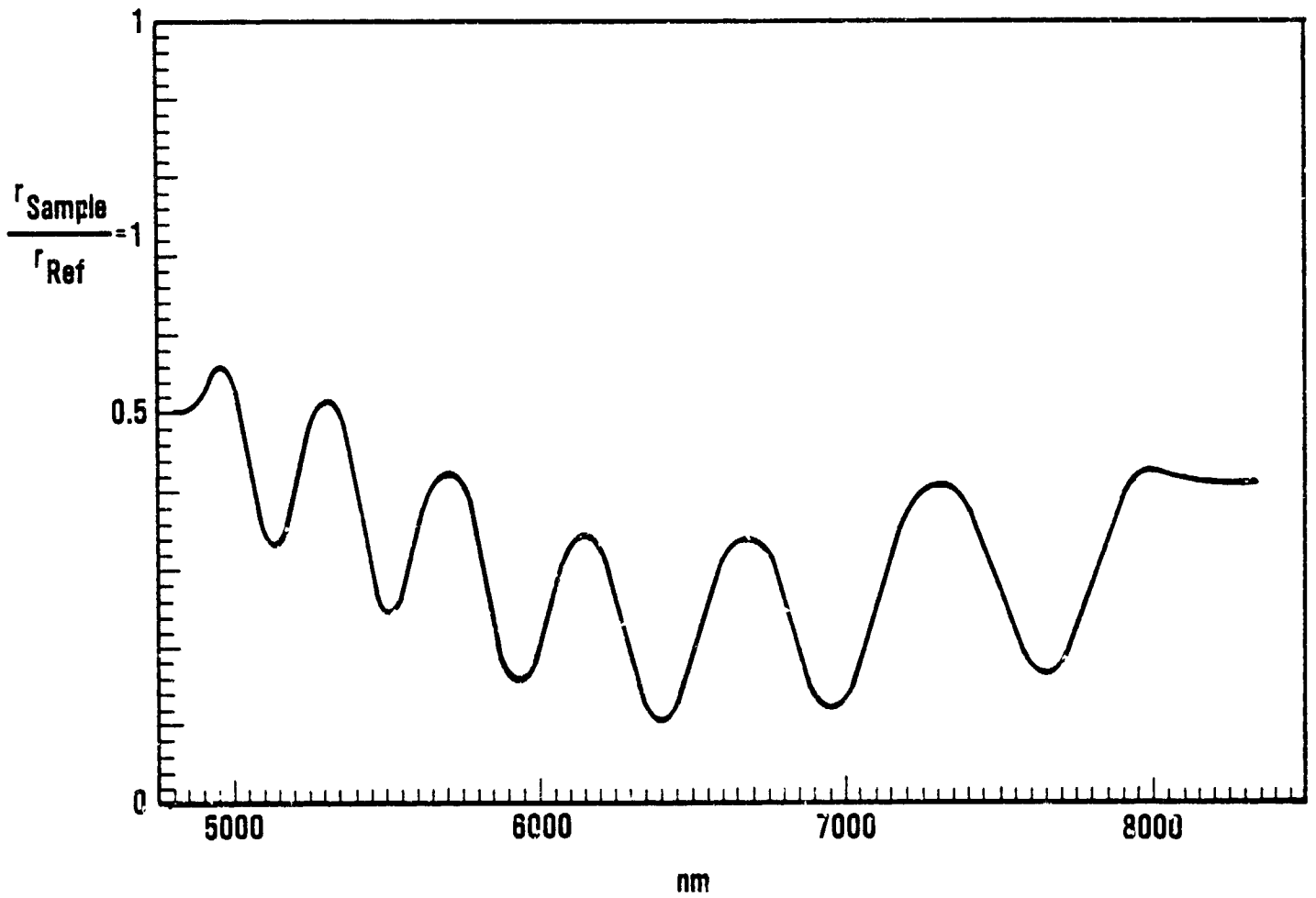


Figure 3.5-2. Spectral Reflectance of Imaging Region Without Filter

following Optoline practice, were only that all the ThF_4 layers had the same thickness, and that all ZnS layers had the same thickness.

The optimization criteria, also chosen by the experimenter, can include, for example, minimizing the transmission variations within the passband, maximizing overall transmission within the passband, achieving the desired passband width and center wavelength, maximizing the slopes at the edges of the passband, or minimizing out-of-band transmission within the range of silicon device response. Combinations of those criteria can be made into a self optimizing tool, limited only by the ingenuity of the experimenter in devising an equation which properly weights the several features as components of a single number to be minimized by the program. For example, the figure of merit used in late August was:

$$\begin{aligned} F &= 100 + T_{\text{average}} (4000 \text{ to } 5100 + 6100 \text{ to } 9000) \\ &\quad - T_{\text{average}} (5200 \text{ to } 6000) \\ &\quad + 2T_{\text{st.dev.}} (4000 \text{ to } 5100 + 6100 \text{ to } 9000) \\ &\quad + T_{\text{st.dev.}} (5200 \text{ to } 6000) \\ &\quad + 10 (T-5\%) \text{ if } T_{\text{average}} \text{ 5\% outside the transmission band.} \end{aligned}$$

This equation heavily weights undesirably high out-of-band transmission. A later variation narrowed the passbands slightly to concentrate on the center 75% wavelength interval, following the Thematic Mapper specification.

In fabricating filters, Optoline does not measure layer thicknesses directly. Rather, they measure the change in optical transmission of the

partial filter structure on a glass substrate as they form each dielectric layer, generally adding material until the transmission at a chosen optical wavelength reaches a maximum or a minimum. The thickness of the silver layer is also determined by a change in transmission, but by an empirical recipe not obviously specifying thickness. As shown by the Optoline recipes for filter fabrication that were given in Section 2.1, the band 3 filter is a symmetrical "double cavity" filter, while the band 2 filter has a "single cavity" with an extra "high-low" film pair on the substrate side. The real part of the index for silver is much less than unity, about 0.05, hence the descriptive title.

The first step in analysis was to determine whether a structure with the dielectric layer thicknesses Optoline believes they have deposited would give the measured transmission on a glass slide. The silver layer thickness is of concern since it determines the width and shape of the passband. Since Optoline had no direct silver thickness data, we simply tried several silver thicknesses with the Optoline dielectric layer thicknesses, and tried to match the computed passband with the measured values. Figures 3.4-1 and 3.4-4 show measured transmission for Optoline filters on glass for bands 2 and 3. Figure 3.5-3 shows the simulated band 2 transmission for three silver layer thicknesses. The 450A curve is close to the measured data.

The next step was to evaluate the filter performance on bare silicon, to determine how much effect a change in substrate index would have. Comparing the computer 400A Ag film filter data on silicon, Figure 3.5-4 with the same filter on glass, Figure 3.5-3, we find the peak shifted 100A from 5400 to

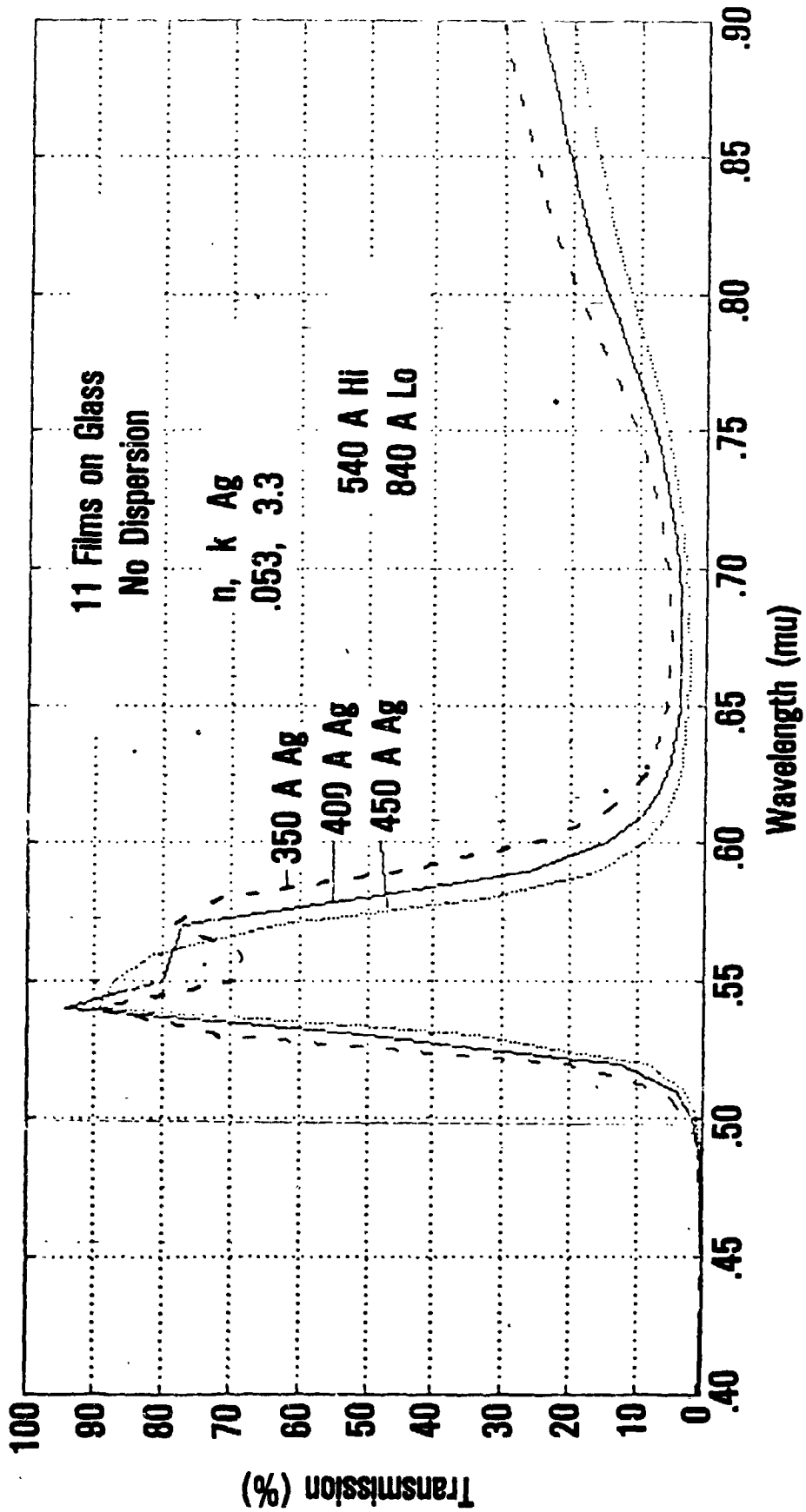


Figure 3.5-3. Computed Band 2 Transmission for Optolines Filter With Several Silver Layer Thicknesses

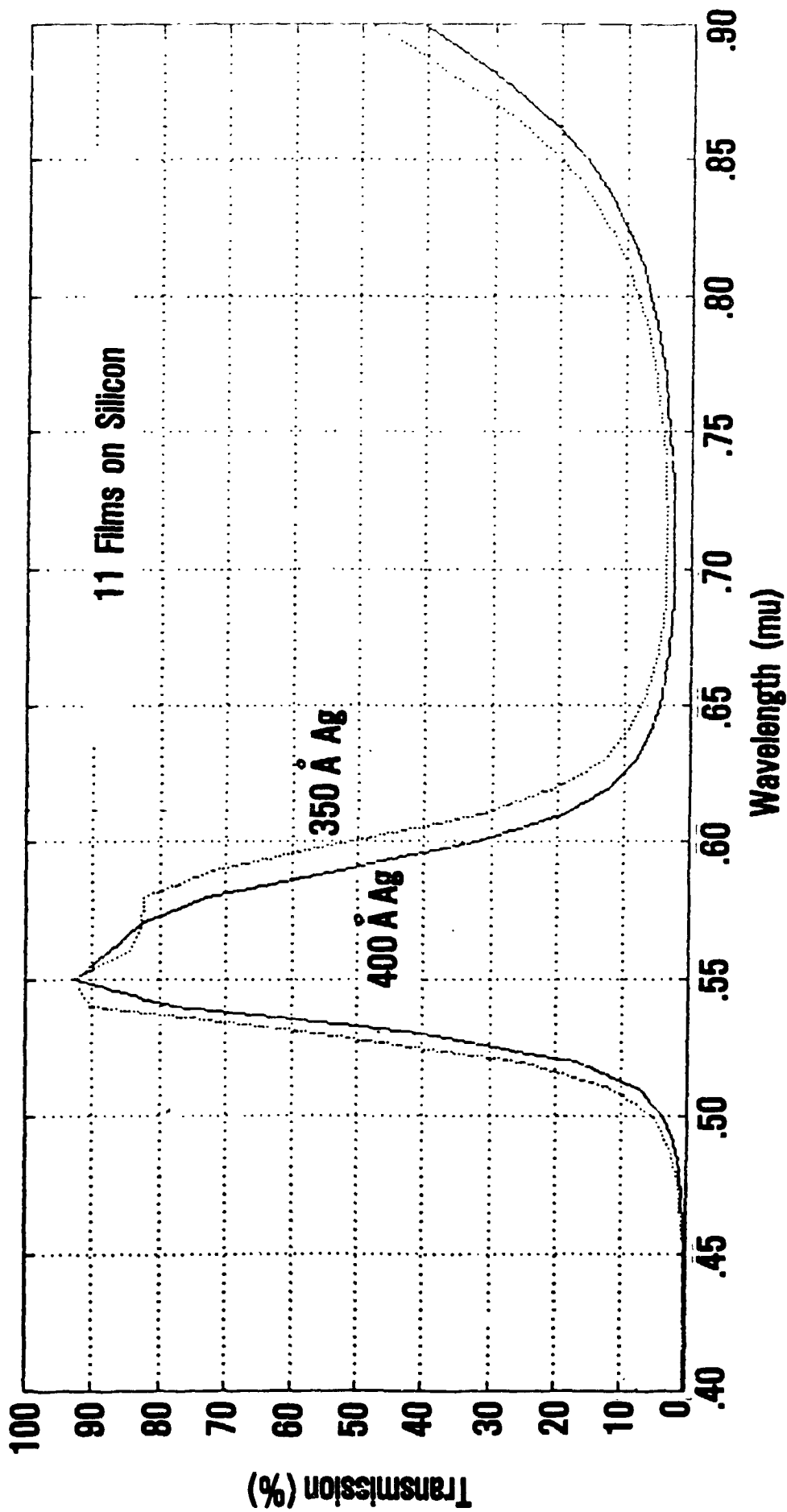


Figure 3.5-4 Computed Transmission of Optoline Filter on Bare Silicon

5500, a change in shape near the peak, and a change in the out-of-band transmission curve near 9000A; but in general only a small change from the computed transmission curve for a glass substrate. No experimental data was available for comparison.

When the same filter was interfaced with a chip with a simplified gate structure, i.e., a 28,800A silox layer over the silicon, the computed transmission curve changed greatly, see Figure 3.5-5, similar to the corresponding measured reflectance data for a band 2 filter on an actual CCD gate/insulator structure, Figure 3.4-5, 3.4-6. Except for the obvious inversion to convert reflection to transmission, there is similarity, with four or five peaks across the intended passband and smaller peaks outside the band. Thus the fine structure appears primarily related to the thick silox layer, which is common to both the experimental chip and to the simulation. The silox layer is both an intermetal insulator and overall protection against scratches.

Later in the program, mid-August, the simulation was changed to include dispersion relations for all indices of refraction, using data given in Figures 3.5-6 through 3.5-11. This change improved agreement with experiment significantly.

The next goal was to design a filter/CCD structure which would eliminate this fine structure in the spectral response. The approach taken was first to make the gate and insulator structure as thin as possible, so that reflection

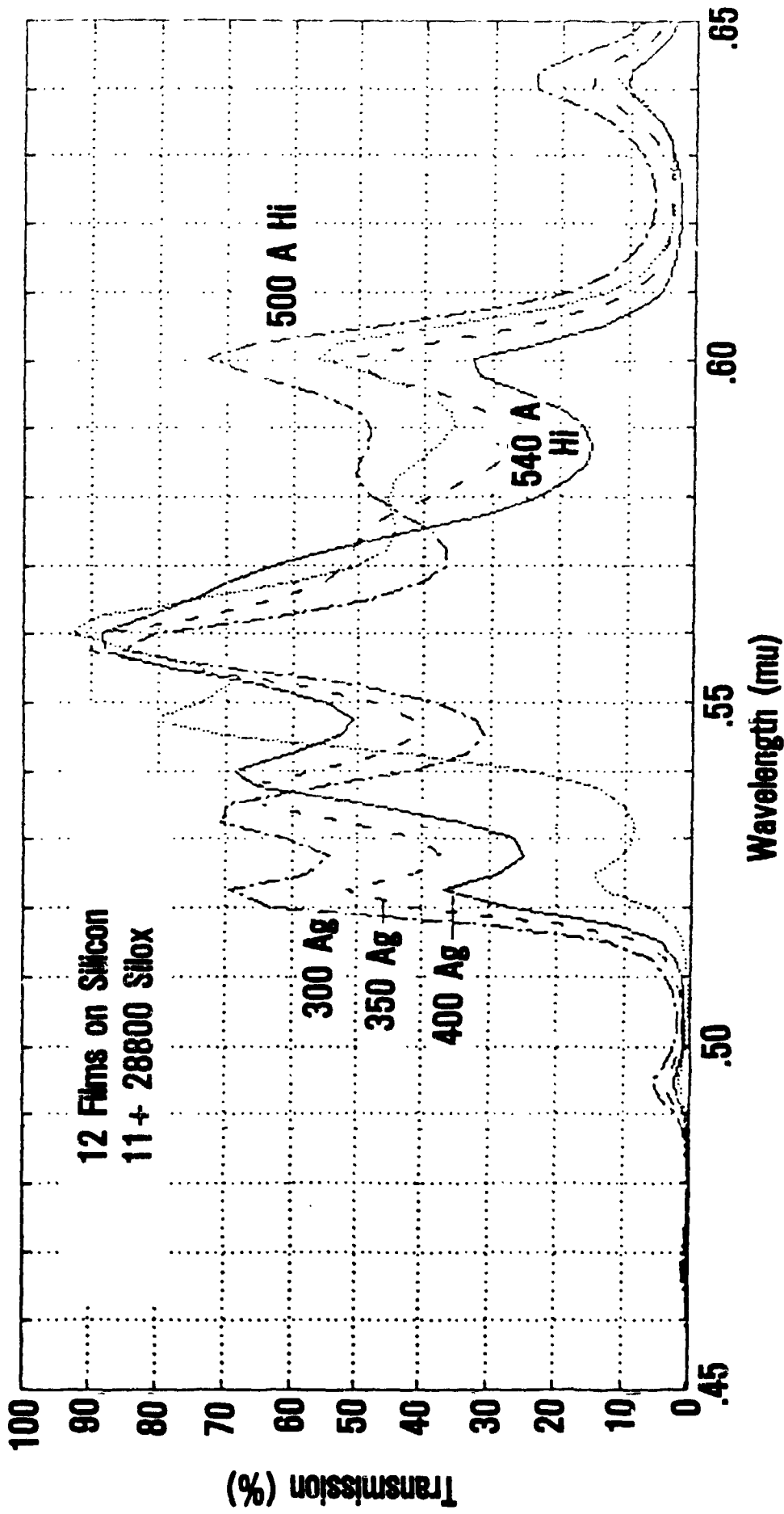


Figure 3.5-5. Computed Transmission Through Optoline Filter and Simplified Gate Structure

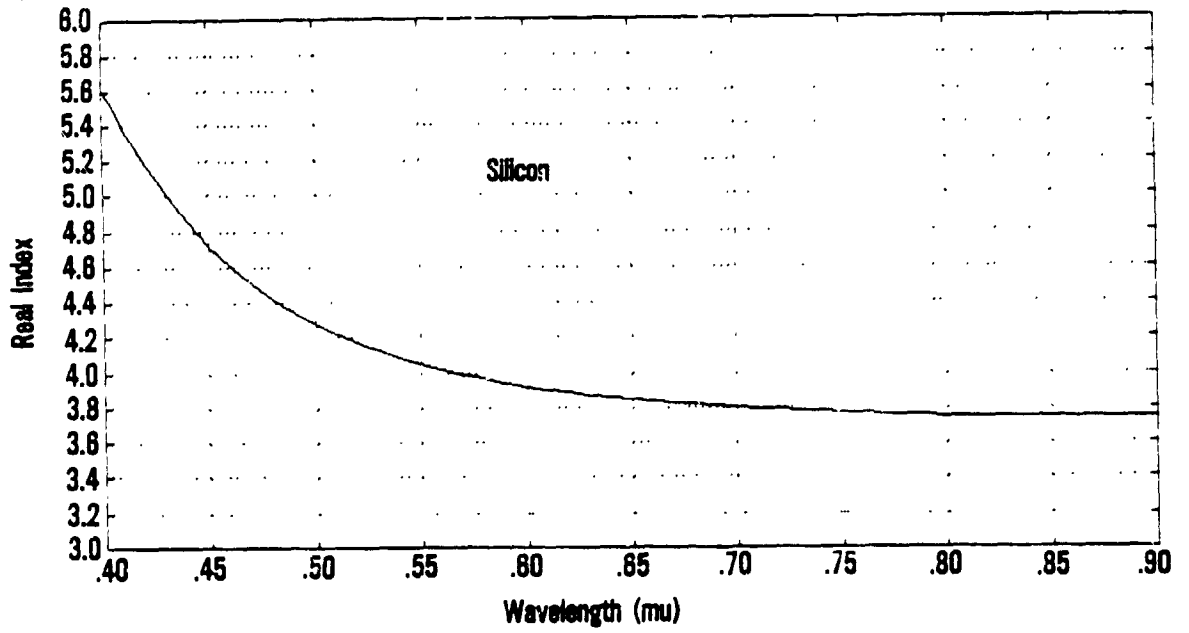


Figure 3.5-8. Index of Refraction for Silicon-Bands 1 Through 4

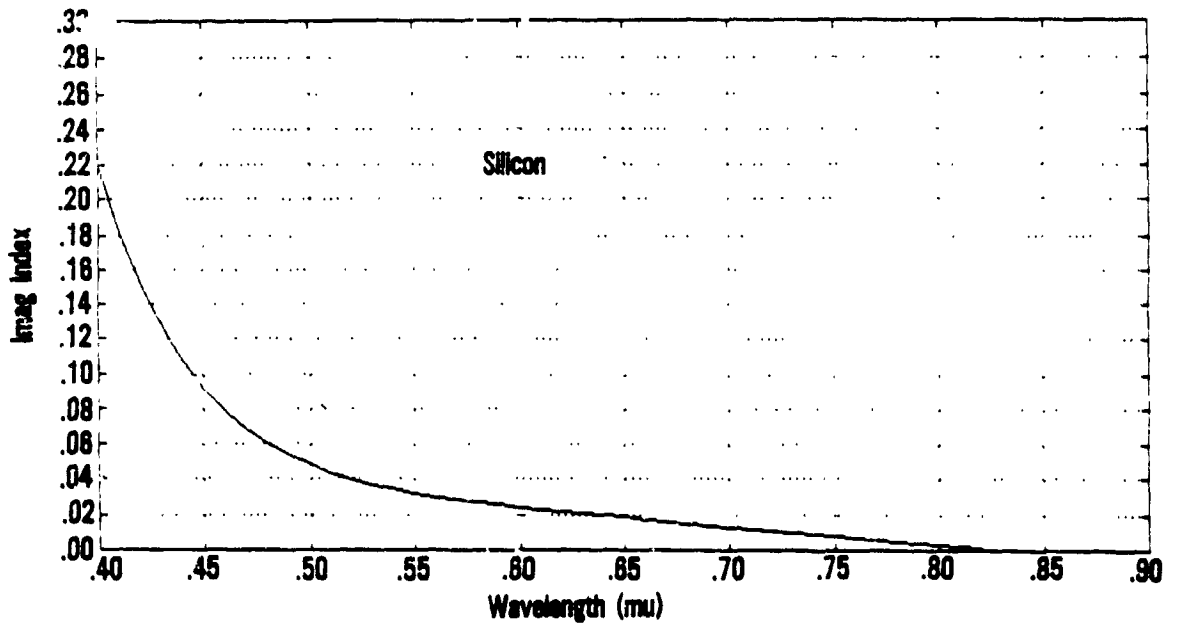


Figure 3.5-7. K for Silicon, Bands 1 Through 4

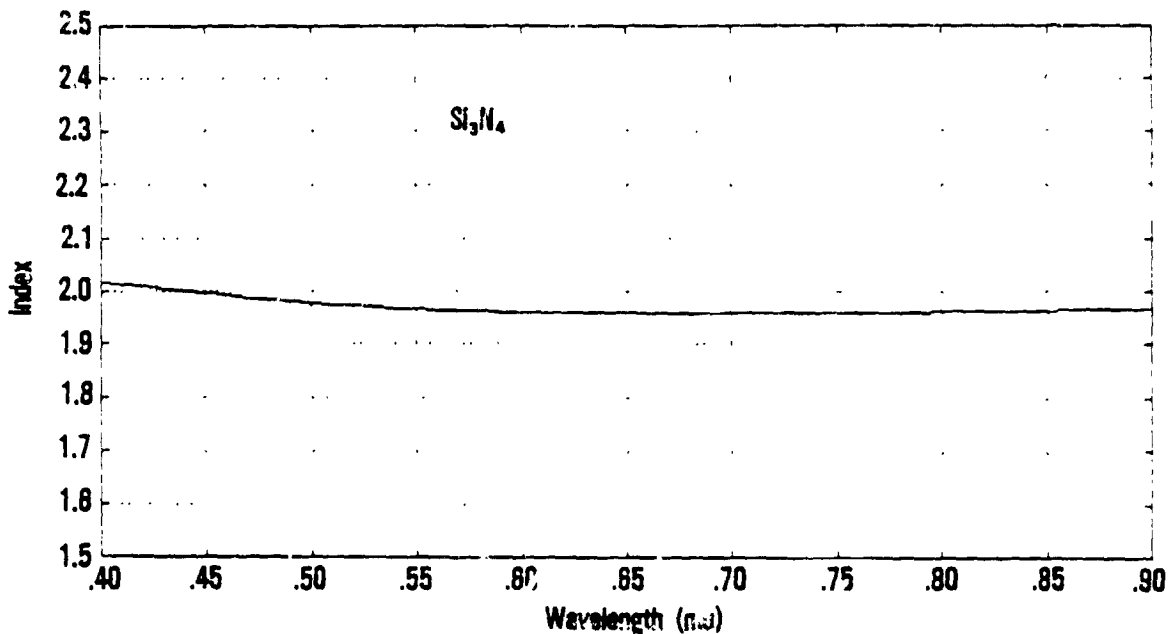


Figure 3.5-8. Index of Refraction for Si_3N_4

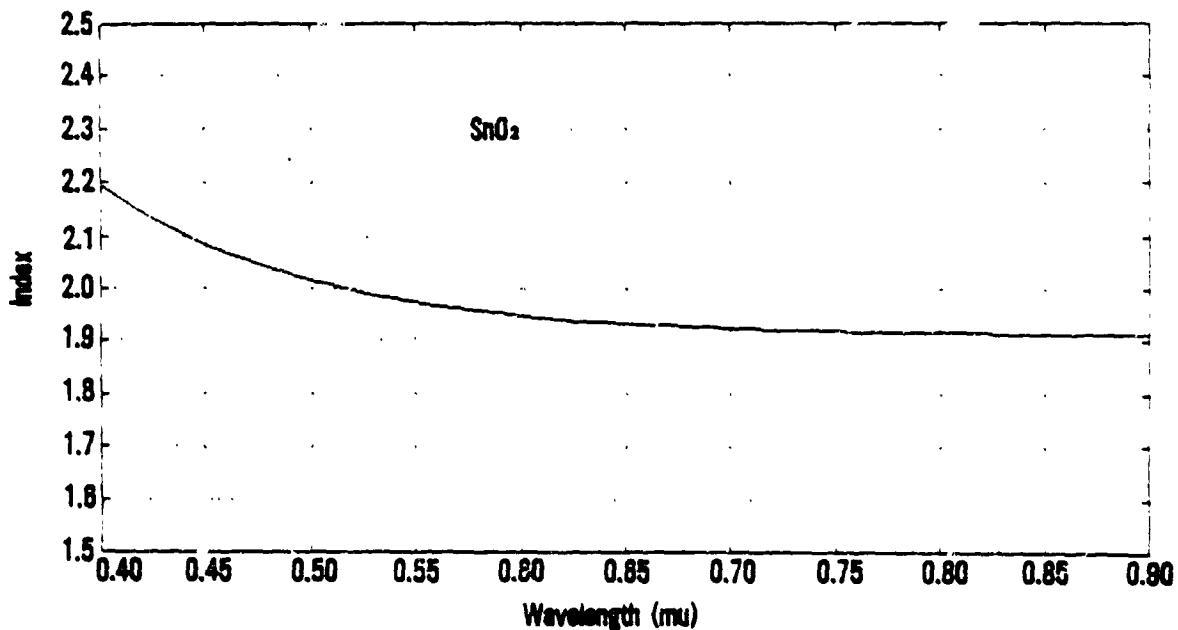


Figure 3.5-8. Index of Refraction For SnO_2

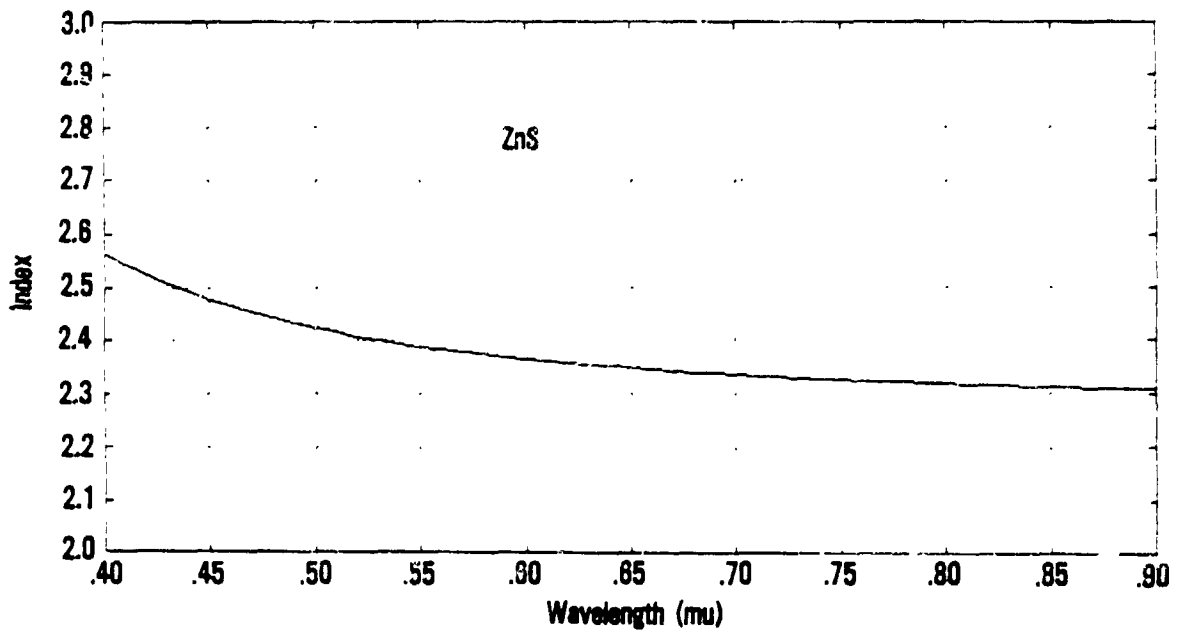


Figure 3.5-10. Index of Refraction for ZnS, Bands 1 Through 4

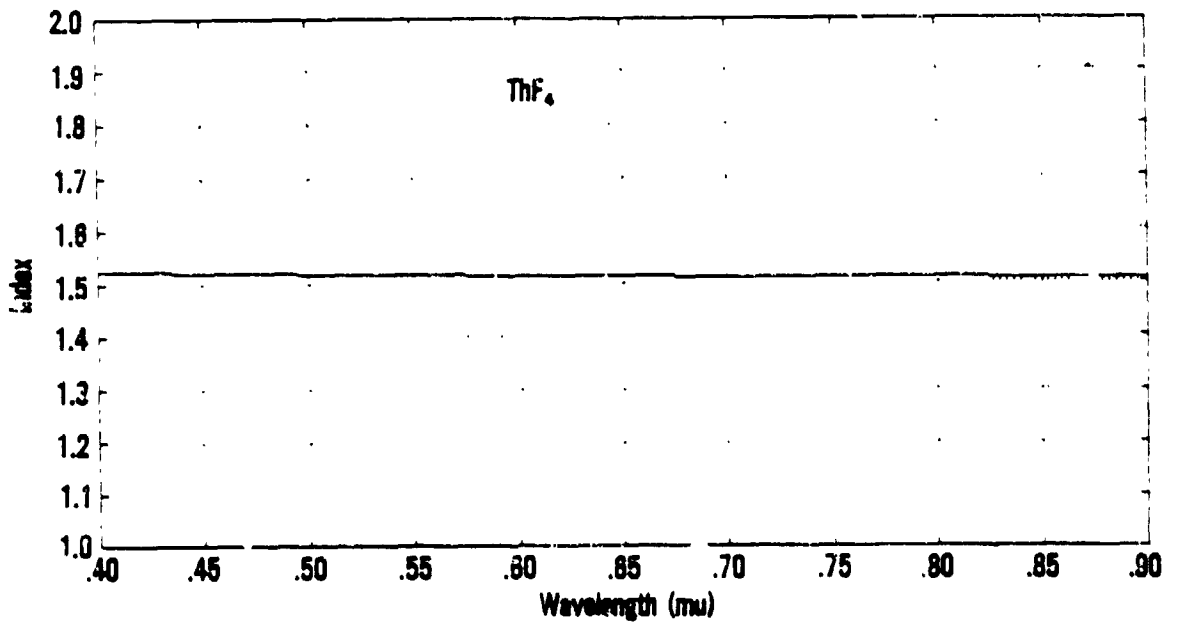


Figure 3.5-11. Index of Refraction for ThF₄

phase relationships would change only slowly with wavelength, then to try to design the structure to form an anti-reflecting coating when placed in contact with the overlying filters. For this conceptual design, we estimated a minimum thickness gate/insulator structure which would still be manufacturable as: Silicon substrate, 150 to 200A SiO_2 , 300A Si_3N_4 , and 500A SnO_2 , plus any coatings needed to form the optical interface with the filter. To protect these coatings against the HF etches used to remove silicon dioxide from the sensitive areas, the design may include a nitride layer over the tin oxide gate. To make the gate structure anti-reflecting when in contact with ThF_4 a layer of polycrystal-line silicon is deposited over the nitride, in place of the first high index (ZnS) layer of a symmetric filter. When this structure was optimized using a formula like that given above, we obtained a band 2 filter and gate combination with the computed transmission curve found in Figure 3.5-12. This is very nearly the goal characteristic for that band. As the filter deposition technique does not monitor actual thickness but rather transmission through a witness plate, it was necessary to generate a recipe for filter deposition which identified when to terminate deposition on each layer. Such a recipe is shown in Figure 3.5-13, where the transmission through each successive layer is indicated by its respective curve and the point to stop deposition is shown by the vertical hash marks.

Two types of bulk wafer samples were fabricated with the oxide, nitride, tin oxide thicknesses calculated in the simulation. As the target thicknesses were not obtained exactly, a second simulation was made with the actual thicknesses and is shown in Figure 3.5-14. The samples were processed at

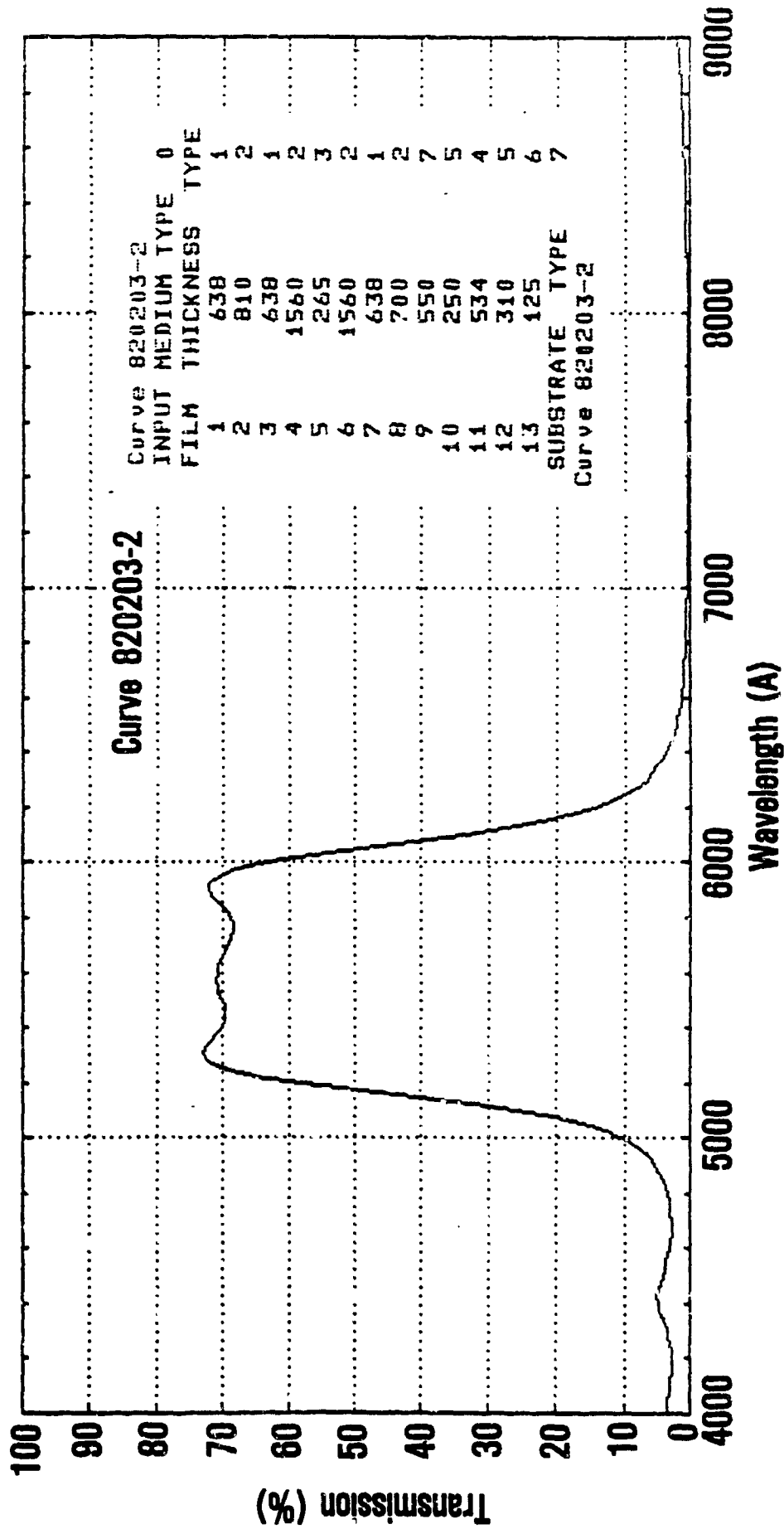


Figure 3.5-12 Ideal Filter Simulation Optimum Calculated Thicknesses

For Curve 820203-2
 NO. OF FILMS = 9 WAVELENGTH = 5600 ANGLE = 0
 INC MED N=1.0000, K=0.0000
 FILM 1 N=2.3480, K=0.0000, D= 638
 FILM 2 N=1.5150, K=0.0000, D= 786
 FILM 3 N=2.3480, K=0.0000, D= 638
 FILM 4 N=1.5150, K=0.0000, D= 1560
 FILM 5 N= .0490, K=3.3330, D= 265
 FILM 6 N=1.5150, K=0.0000, D= 1560
 FILM 7 N=2.3480, K=0.0000, D= 638
 FILM 8 N=1.5150, K=0.0000, D= 700
 FILM 9 N=4.0170, K= .0300, D= 550
 SUB MED N=1.5150, K=0.0000

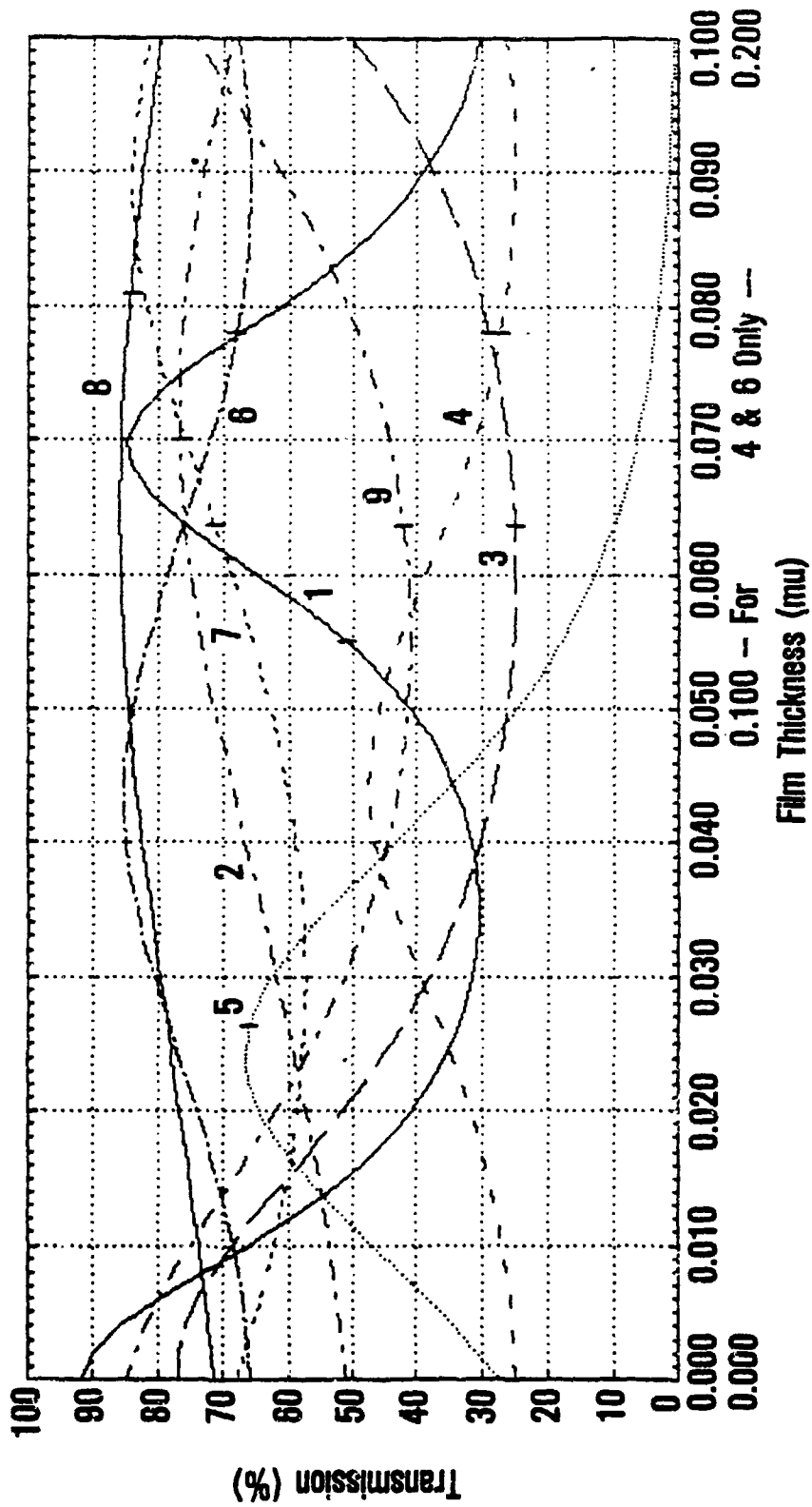


Figure 3.5-13 Deposition Recipe "Ideal" Filter Experiment

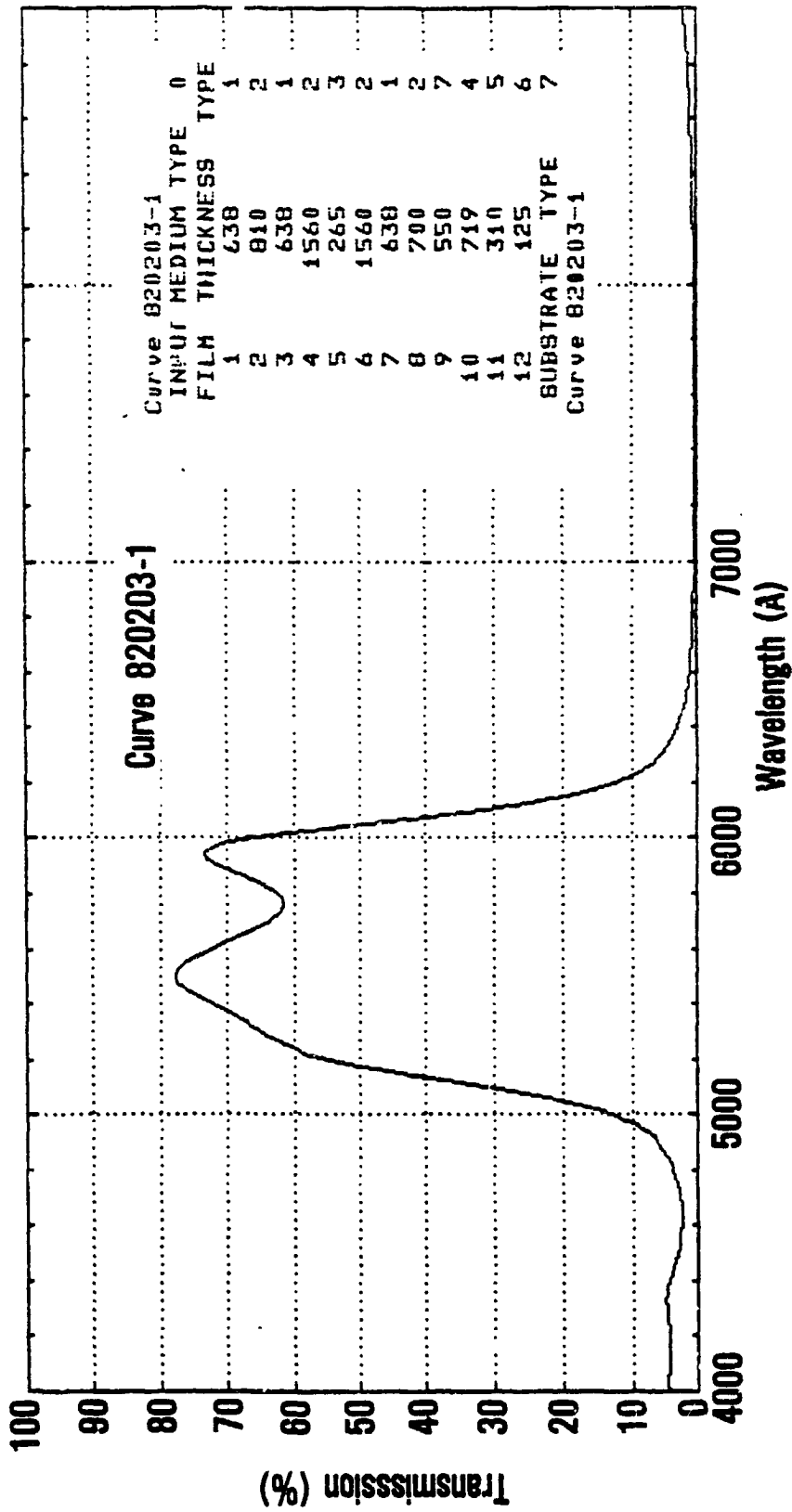


Figure 3.5-14. Ideal Filter Simulation Optimum Calculated Thicknesses

Optoline using the recipe of Figure 3.5-13. A plot of the measured filter transmission on a witness plate is shown in Figure 3.5-15, and measured spectral reflectance above the bulk wafer with the designed substructure is shown in Figure 3.5-16.

Although that more fine tuning of the fabrication process is required, to equalize the transmission peaks, the lack of fine structure and the generally correct center wavelength and bandpass in Figure 3.5-15 shows that the phase shift and bandwidth control problems caused by interaction with underlying layers can be eliminated by proper filter design and process fabrication control.

As these results were obtained near the end of the program, it was not possible to incorporate these computed filter designs operating CCD sensor chips with thin gate and insulator structures. Several chips were evaluated, however, with the standard Optoline filters.

3.6 FILTER UNIFORMITY AND REPEATABILITY

One of the concerns about the integral filter technique is the uniformity and repeatability of filter characteristics. Uniformity was measured across a chip and at various chip sites on the same wafer. When discussing filter uniformity, it must be remembered that there are two components to the uniformity; the filter itself and the underlying wafer substructure. Figure 3.6-1 shows the spectral reflectance uniformity of the filter alone as

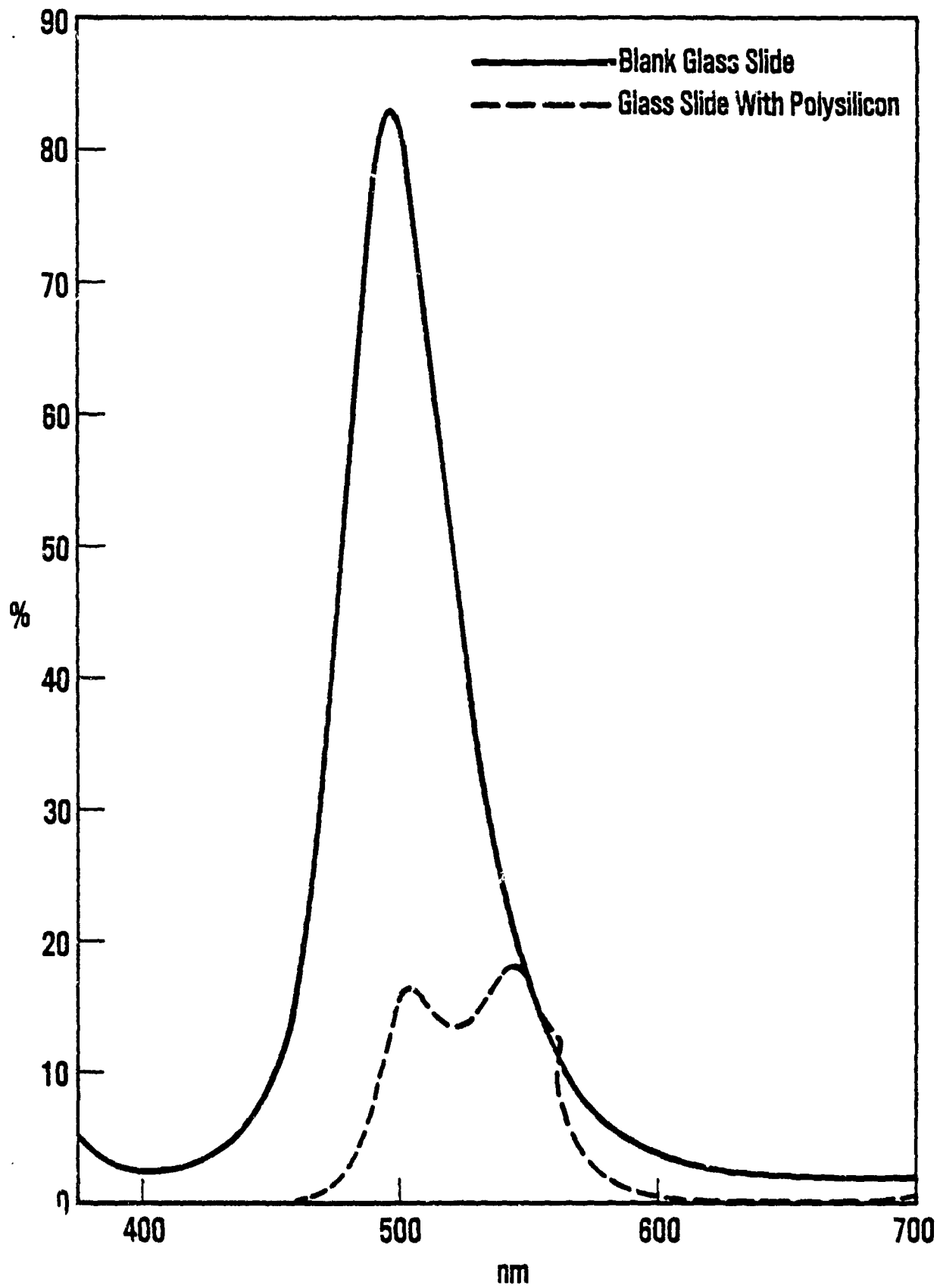


Figure 3.5-15. Optoline Transmission Measurement – Ideal Filter

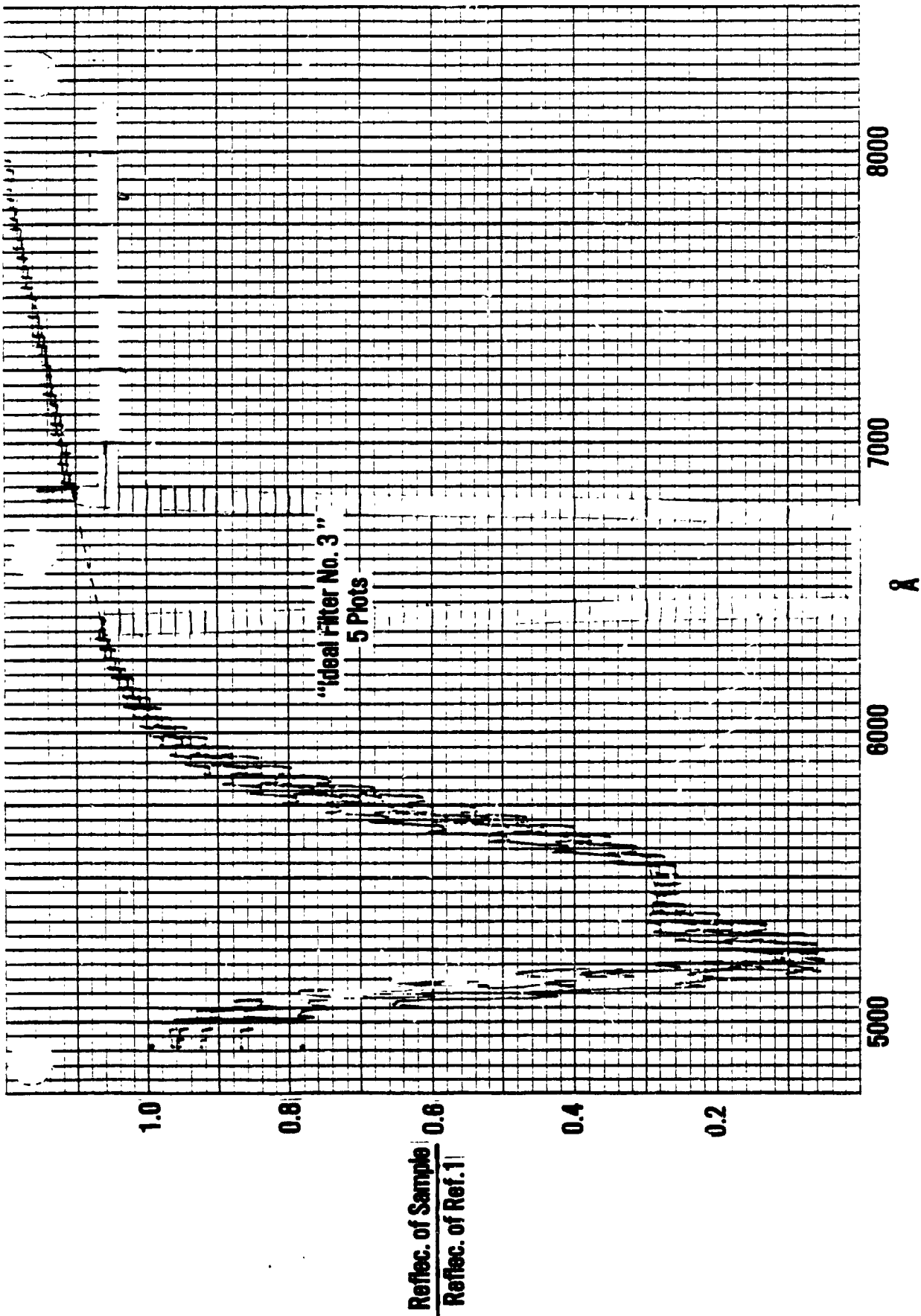


Figure 3.5-16 Ideal Filter on Test Wafer 5 Measurements Superimposed

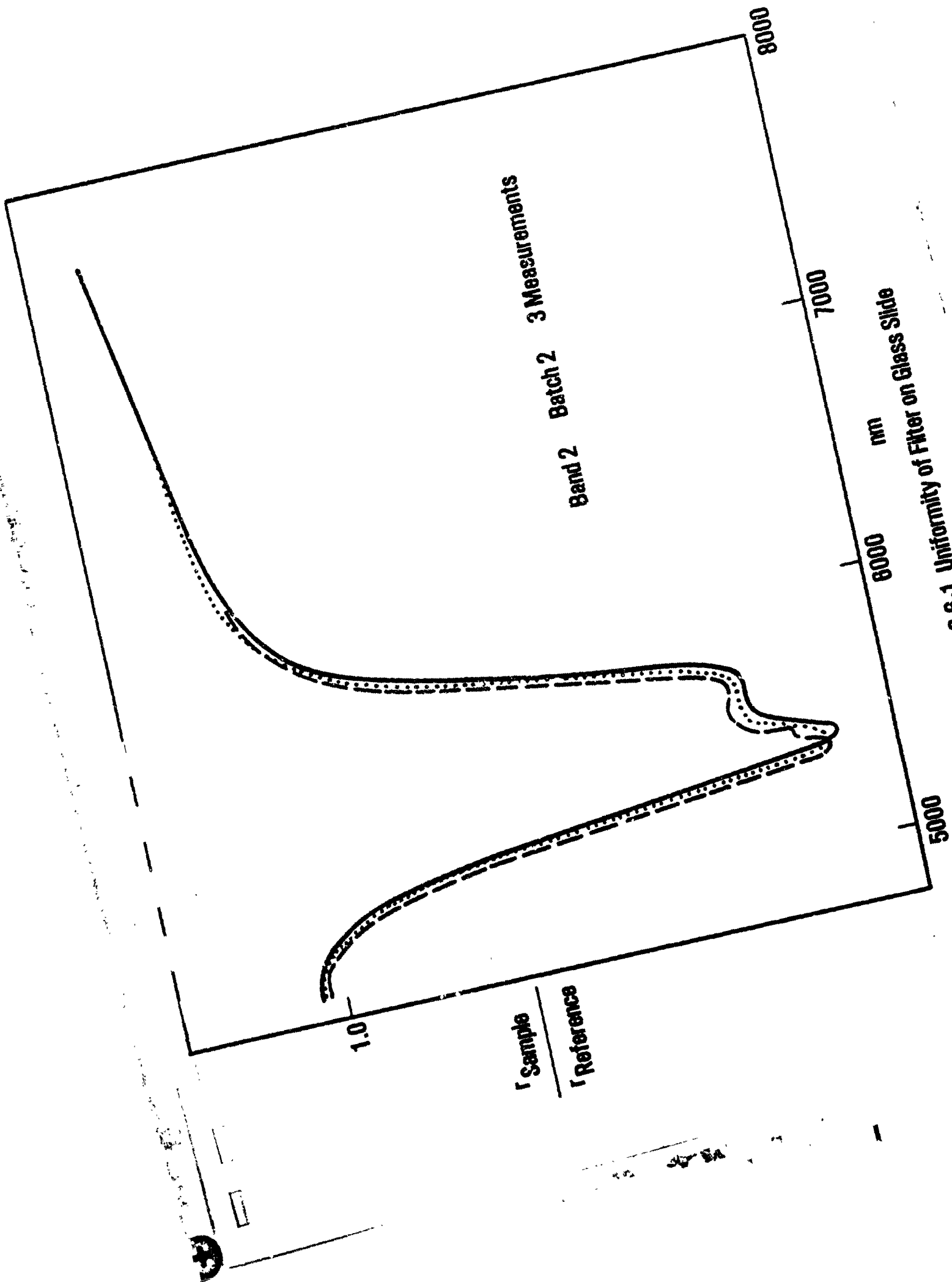


Figure 3.6-1. Uniformity of Filter on Glass Slide

measured across a 2-inch glass witness plate. Figure 3.6-2 shows the spectral reflectance uniformity of a band 2 filter when measured across a 200-element line array. This represents a distance of 4000 microns or about 0.15 inches. Of the five regions measured, only one showed any shift, and that shift occurred in the fine structure rather than the bandwidth edges.

Figure 3.6-3 shows spectral reflectance measurements made in three different imaging well regions scattered across a 2-inch completely processed wafer. There appears here much more shift in the fine structure than on a single array, as would be expected considering the typical 10% uniformity of silox thicknesses across a wafer. In the recommended ideal filter structure described in Section 3.5, the fine structure disappears and a sampling of 5 regions on the wafer shows all edges within a 100A width, attesting to the uniformity of the filter itself.

Another area of concern is the filter repeatability from one deposition run to the next. Figure 3.6-4 shows drawn on one plot the variability of band 2 and 3 filters from the first three deposition runs. Some of this variation is because the deposition recipe was changed by Optoline after the first run, but most of it is believed due to the fact that the thermal evaporation units used to deposit the filter could not be dedicated to a single fabrication operation. Removing the source material and frequently reconfiguring the vacuum chamber equipment over a several month period does not lend itself to repeatable results.

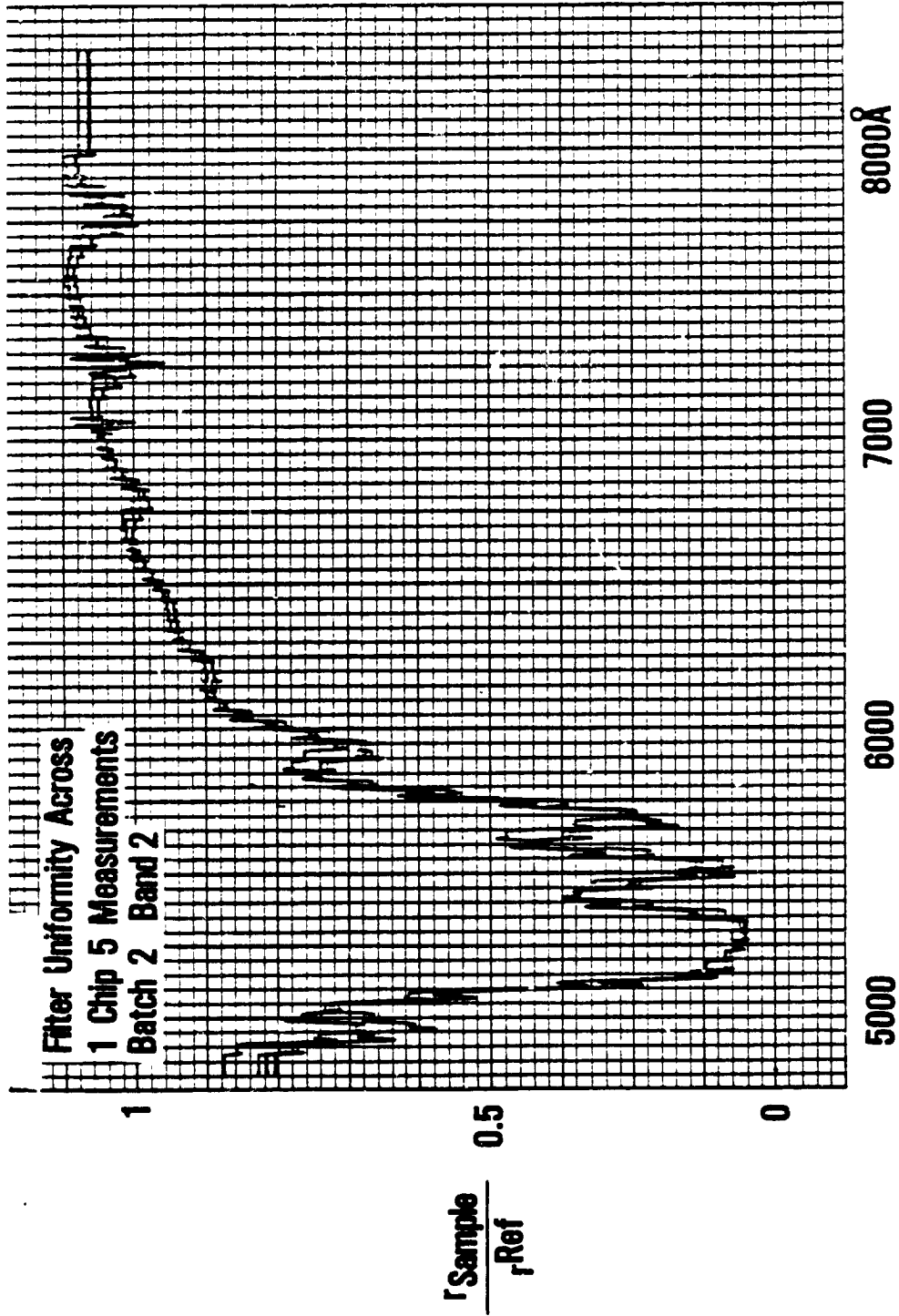


Figure 3.6-2 Uniformity of Filter Plus SiOx Spectral Reflectance
Across a Single 200 Element Array

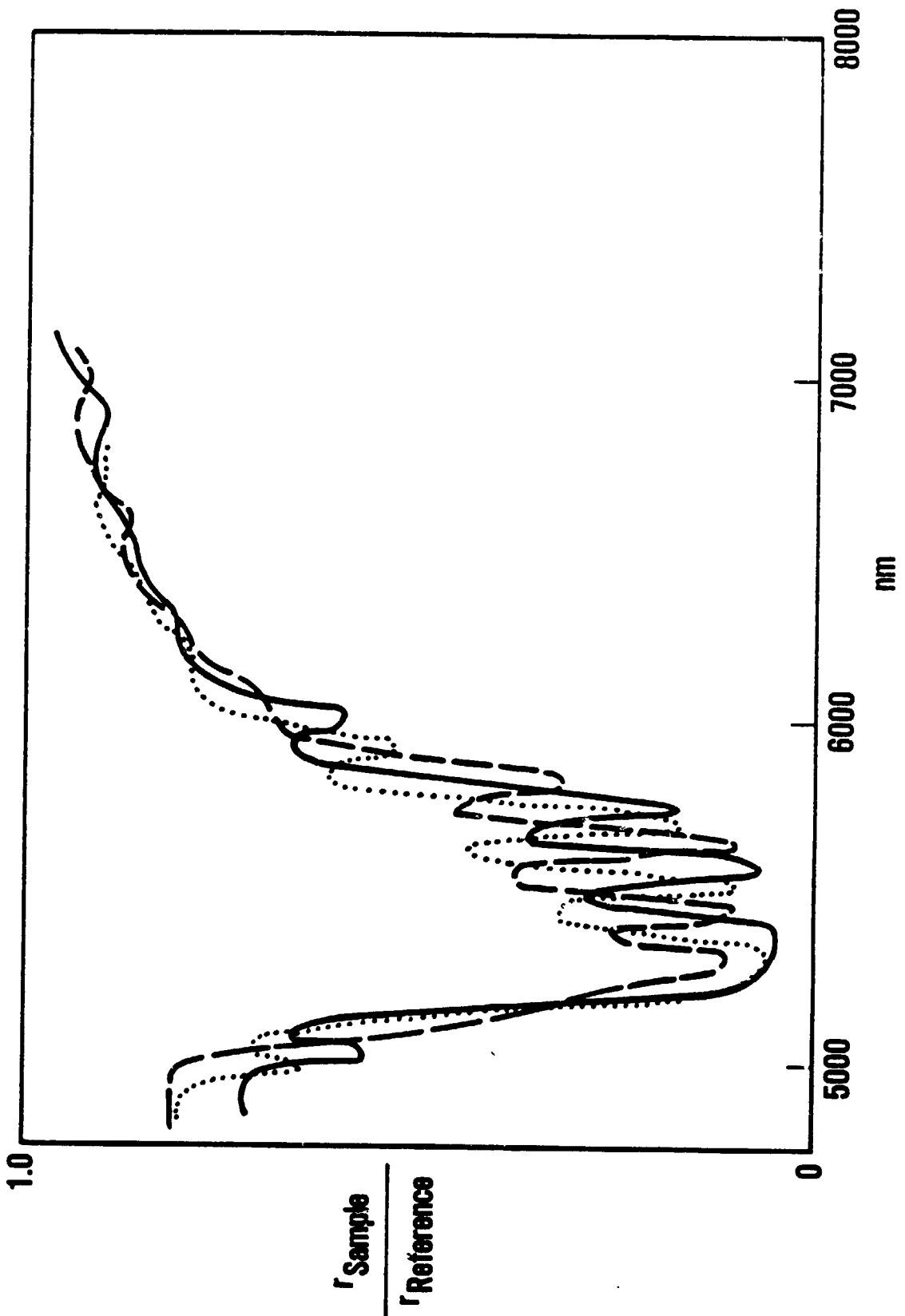


Figure 3.6-3. Band 2 Uniformity of Filter Across 2 Inch Wafer

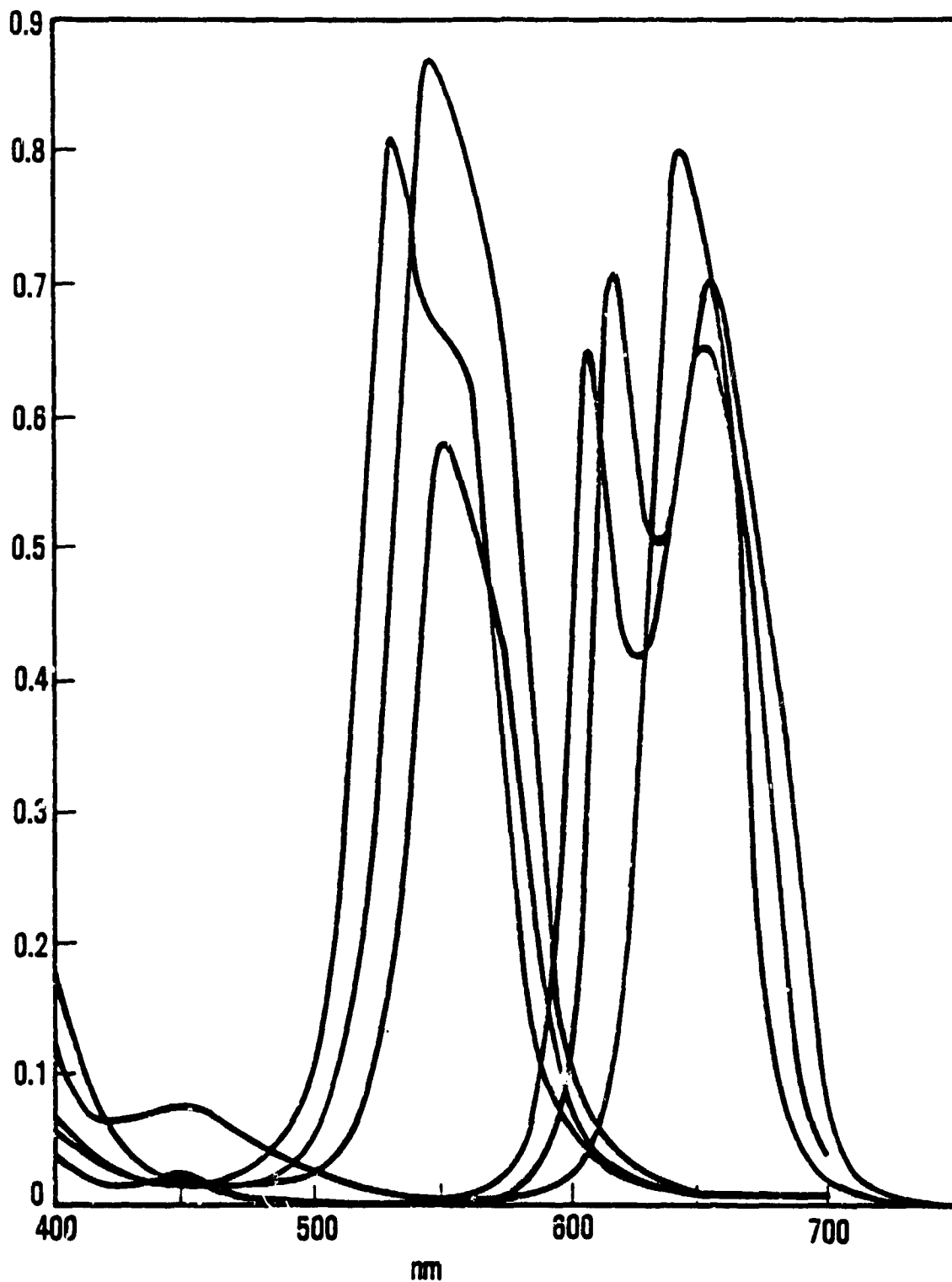


Figure 3.6-4. Repeatability – Run to Run on Glass Witness Plates
Optocline Transmission Measurement

Optoline felt that with a dedicated system and more frequent use, the deposition characteristics could be made significantly more uniform. To verify this, we requested a special test run where a band 3 filter would be deposited on sequential days without a change to recipe or fixturing. The results of this test are plotted in Figure 3.6-5. Although the two curves are much closer together, there is still a need for improvement. More sensitive monitoring techniques and perhaps more modern equipment would help, but that was out of the scope of this program.

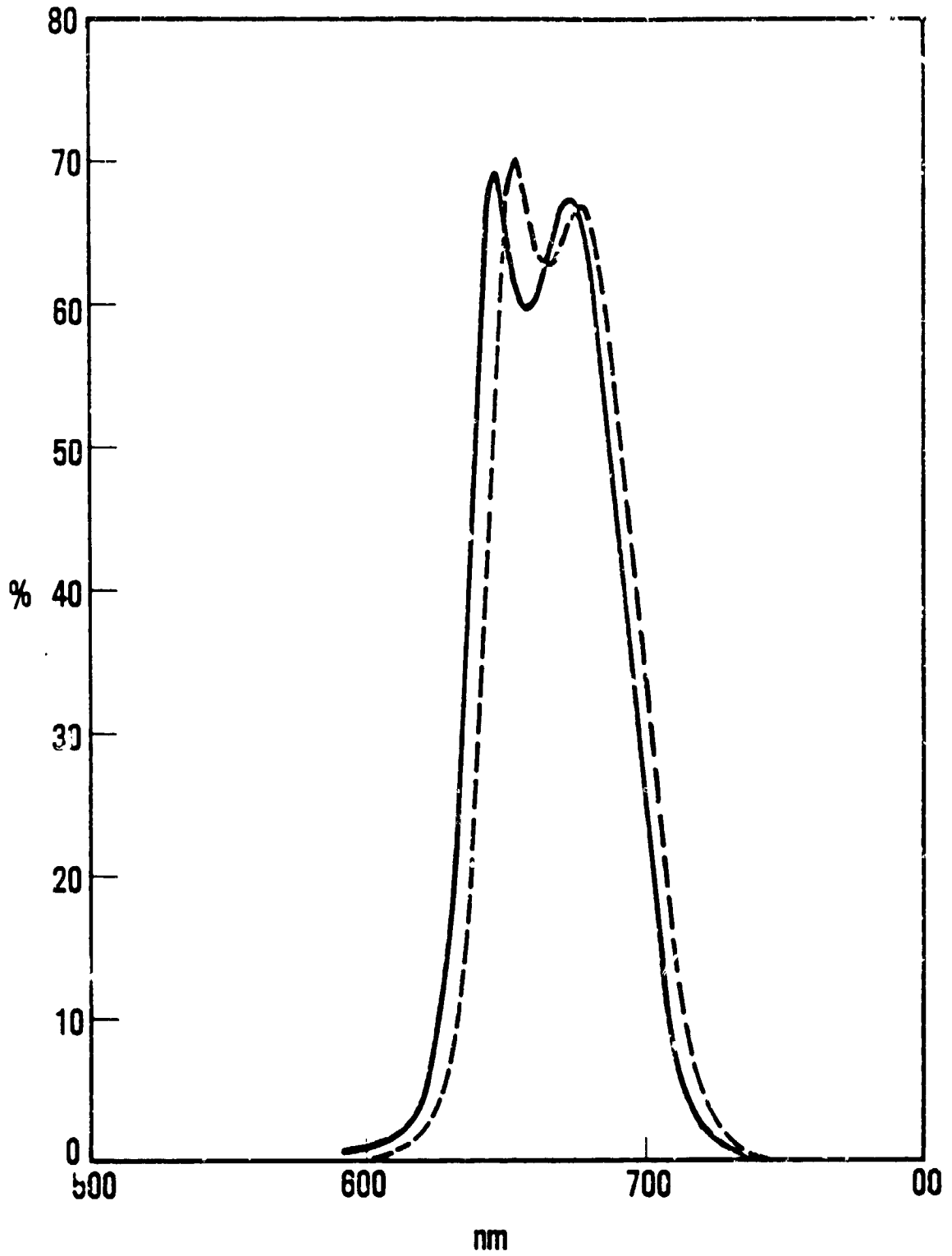


Figure 3.6-5. Filter Uniformity With Two Successive Depositions.

4.0 ELECTRICAL AND OPTICAL CHARACTERIZATION

4.1 INITIAL WAFER CHARACTERIZATION

Before shipment of wafers to Optoline for filter deposition, a four part electrical characterization test was performed. These tests consisted of a Keithley short test, imaging test, transfer efficiency test and leakage test. An explanation of these tests follows.

The Keithley short test was performed on all available 5040 line arrays. The test determines whether the conductive electrodes comprising the gates of the CCD are electrically isolated from each other and from the substrate. It also checks basic transistor action in the output circuitry. Only those line arrays which passed the Keithley testing were given additional electrical screening.

Imaging ability was determined by illuminating the array through a narrow slit which was free to move across the entire array. If all 200 pixels were sensitive to the illumination and responded uniformly, the array was graded good. All preliminary testing was done at a phase clock frequency of approximately 340KHz. Voltage levels were optimized to provide the most

efficient charge transfer, and the input circuit was biased to prevent inadvertent charge injection. The optimum voltage levels were recorded, in order that set-up time for packaged chip testing could be minimized.

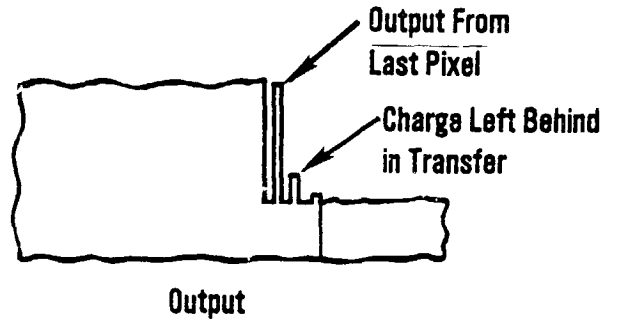
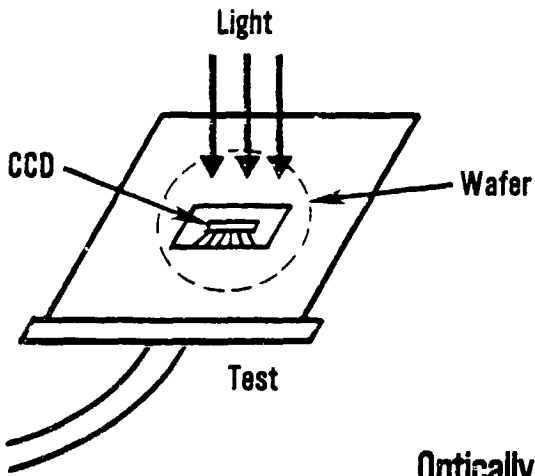
Leakage current was determined by measuring the difference in output voltage between a reference voltage (resulting from charge leaking into the output register only) and imaging well voltage (resulting from charge leaking into the output register + charge leaking into the imaging well). The current represents the amount of charge leaking into one pixel during an integration time of .76 msec and was calculated using the following equation:

$$I_{\text{leakage}} (C_{\text{output}}) = (\text{GAIN}) (\Delta V / \Delta t).$$

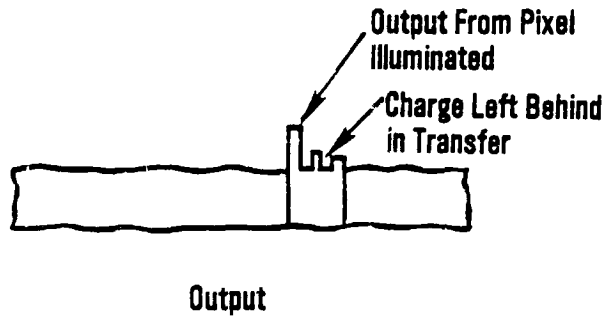
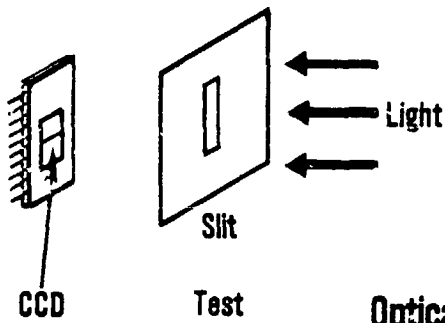
Transfer efficiency was measured by illuminating the array at a level well below saturation and comparing the output voltage of the last pixel read out (V_{last}) and the voltage level of the next transfer (charge left behind, V_{trans}). Transfer efficiency was then calculated using:

$$\eta = (1 - V_{\text{trans}}/V_{\text{last}})^{1/800}$$

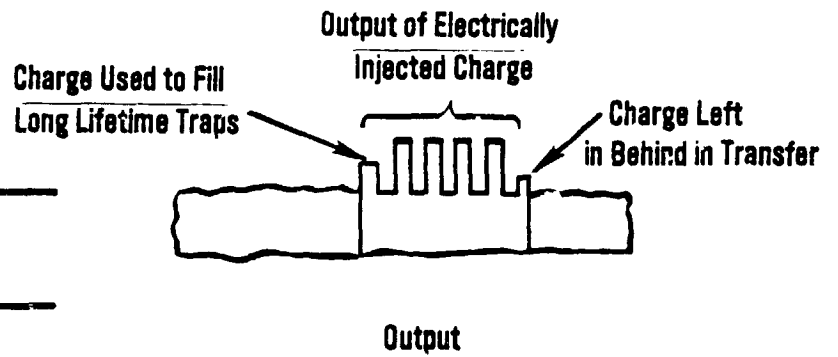
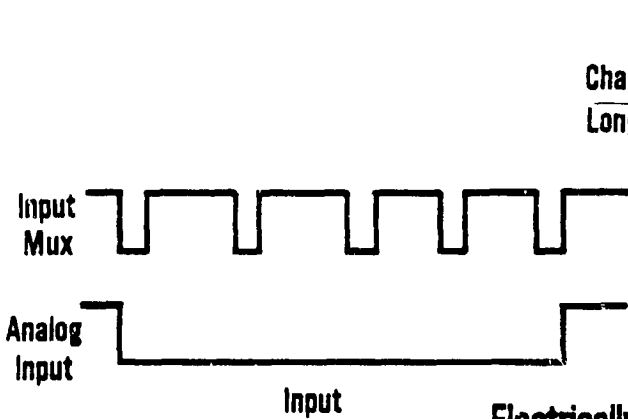
Figure 4.1-1 illustrates how a signal was optically injected into all the pixels. Table 4.1-1 gives the results of this preliminary testing. Table 4.1-2 is a list of chips with deposited filter which were packaged and are available for test.



Optically Injected Signal Into All Pixels



Optically Injected Signal Into Signal Pixel



Electrically Injected Signal

Figure 4.1-1. Three Methods of Measuring Transfer Efficiency

TABLE 4.1-1 RESULTS OF INITIAL CHARACTERIZATION

WAFER NUMBER	GOOD ARRAYS (FROM INITIAL CHARACTERIZATION)
4421-8	11
4421-9	2
4446-10	15
3553-7	3
3553-9	4
4139-13	2
4139-14	1
4996-1	2 Chips Passed Short Test
4996-2	2 Chips Passed Short Test
4996-3	2 Chips Passed Short Test
4996-4	3 Chips Passed Short Test
4996-5	7 Chips Passed Short Test
4996-6	7 Chips Passed Short Test
4996-7	26 Chips Passed Short Test
4996-8	1 Chip Passed Short Test
4996-9	3
4996-10	4 (5 More Chips Passed Short Test)
4996-11	1 Chip Passed Short Test
4996-12	3 (4 More Chips Passed Short Test)
4996-13	4 (2 More Chips Passed Short Test)
4996-14	1 (2 More Chips Passed Short Test)
4996-15	2 (3 More Chips Passed Short Test)

TABLE 4.1.2 INVENTORY OF PACKAGED ARRAYS

LOT/WAFER/CHIP	FILTER	COMMENTS
4421-8-11	BAND 2, BAND 3	Poor TX. Eff.
4421-8-22	BAND 2, BAND 3	Poor TX Eff.
4421-8-25	BAND 2, BAND 3	Poor TX. Eff.
4421-8-26	BAND 2, BAND 3	Poor TX. Eff.
4421-8-27	BAND 2, BAND 3	Poor TX. Eff.
4421-8-28	BAND 2, BAND 3	Poor TX. Eff.
4421-8-33	BAND 2, BAND 3	Poor TX. Eff.
4421-8-37	BAND 2, BAND 3	Poor TX. Eff.
4221-9-27	BAND 2, BAND 3	BROKEN
4221-9-41	BAND 2, BAND 3	Poor TX. Eff.
4446-10-23	BAND 2, BAND 3	Poor TX. Eff.
4446-10-27	BAND 2, BAND 3	Poor TX. Eff.
4446-10-29	BAND 2, BAND 3	Poor TX. Eff.
4446-10-30	BAND 2, BAND 3	Poor TX. Eff.
4446-10-40	BAND 2, BAND 3	Poor TX. Eff.
4996-15-7	BAND 2	NOT TESTED
4996-15-8	BAND 2	NOT TESTED
4996-15-9	BAND 2	GOOD
4996-15-10	BAND 2	NOT TESTED
4996-15-13	BAND 2	GOOD
4996-9-7	BAND 2	GOOD
4996-9-16	BAND 2	NOT TESTED
4996-9-17	BAND 2	NOT TESTED
4996-9-44	BAND 2	NOT TESTED
4996-5-32	BAND 3	Leaky Junctions
4996-5-37	BAND 3	Floating Reset Gate
4996-5-40	BAND 3	Floating Reset Gate
4996-5-41	BAND 3	Transfer Gate Breakdown
4996-5-46	BAND 3	Floating Scupper Gate
4996-5-47	BAND 3	Floating Scupper Gate
4996-4-9	BAND 3 Over BAND 2	GOOD
4996-4-10	BAND 3 Over BAND 2	NOT TESTED

BAND 2 FILTER

WAFER/CHIP	INITIAL TRANSFER EFFICIENCY	PACKAGED TRANSFER EFFICIENCY
9-7	.993	.9998

BAND 3 FILTER

WAFER/CHIP	INITIAL TRANSFER EFFICIENCY	PACKAGED TRANSFER EFFICIENCY
5-32	-	Leaky Junctions
5-37	-	Floating Reset Gate
5-40	-	Floating Reset Gate
5-41	-	Transfer Gate Breakdown
5-46	-	Floating Scupper Gate
5-47	-	Floating Scupper Gate
*6-38	-	.9998
*6-40	-	.9995
*6-46	-	.9998

BAND 2 and BAND 3 FILTER

4-8	-	.9996
4-9	-	.9997

*WAFER LEVEL TEST

Two techniques were used to determine the transfer efficiency of packaged arrays with deposited filters. Both methods are illustrated in Figure 4.1-1. A description of each of these techniques follows.

The first method generates charge by optically illuminating a single pixel with a $\approx 10\mu\text{m}$ wide slit of light. The output voltage (above dark level) of the illuminated pixel and all subsequent voltage readouts which are a result of transfer inefficiency are recorded. These voltages are summed and the ratio of the voltage output of the illuminated pixel to the sum of the output voltage is taken. Since $V_{\text{out}}(e1xx) \propto Q(e1xx)$ and $\sum V_{\text{out}} \propto Q_{\text{total}}$ we can determine transfer efficiency by:

$$\eta = \frac{(Q(e1xx)/Q_{\text{total}})^{1/\text{total transfers}}}{1} = \frac{(V_{\text{out}}(e1xx)/\sum V_{\text{out}})^{1/\text{total transfers}}}{1}$$

This technique can be used to determine transfer efficiency of devices too poor to be analyzed by other techniques.

In the second method, charge is electrically injected into the serial output register by biasing the analog input gate to accept charge for the desired period. This period is shown in Figure 4.1-1. After 200 phase clock cycles the electrically injected charge is read out. The transfer efficiency is then calculated using the same method used in wafer level testing by comparing the voltage level of the last charge packet injected to the voltage level of the trailing charge packet resulting from transfer inefficiency.

4.2 OPTICAL/ELECTRICAL CHARACTERIZATION OF CHIPS

4.2.1 Description of Optical Test Station

The optical test system defined for studying the characteristic of Band 2 and Band 3 filters is presented here. Figure 4.2-1 illustrates the optics required to image a slit of monochromatic light on the device and filter being characterized. The slit image focused on the surface of the device is approximately 8 micrometers wide by 200 micrometers long.

Monochromator: A Bausch & Lomb Diffraction Grating Monochromator was used for the study. The diffraction grating used had a range of 350 nanometers to 800 nanometers. A second grating with a range of 700nm to 1600nm was used for near infrared measurements. The spectral purity of the output was determined by the relative widths of the entrance and exit slits. All measurements in this report were taken with the control slits adjusted for a minimum bandpass. The tungsten light source for the monochromator was powered by a regulated constant current DC supply. This keeps the lamp operating at nearly constant temperature and power which assures constant spectral output over time.

Profiler: The output of the monochromator was then focused onto the desired portion of the device being characterized by use of an optical profiler. The profiler contains an image slit which can be projected to the device being tested. The focused image on the device is one-tenth that of the image slit (see Figure 4.2-1). To aid in alignment, a

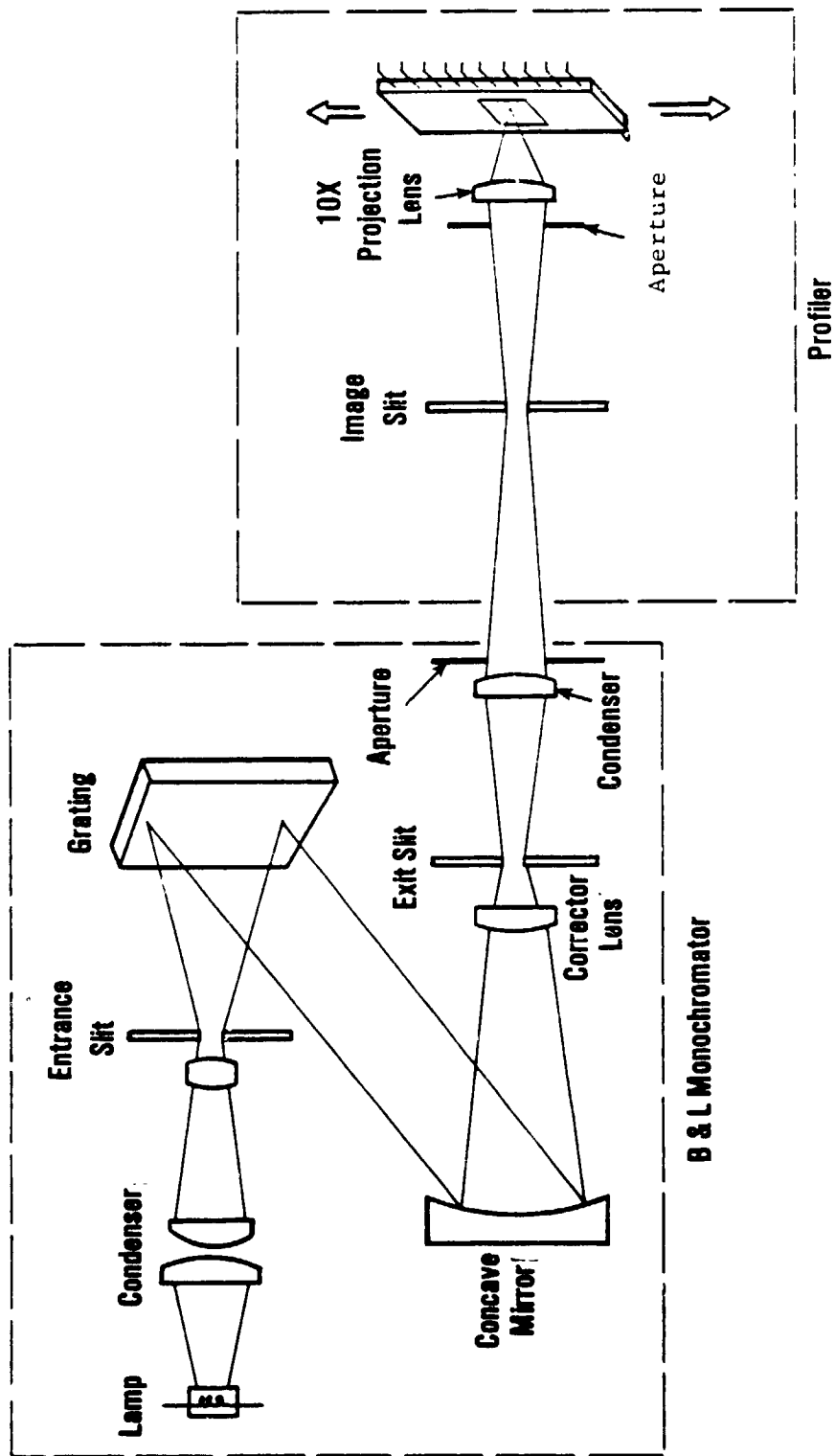


Figure 4.2.-1. Optical Test System

pellicle beam splitter can be moved into the optical path for viewing of the slit image on the device.

The optical profiler is also capable of translating the device relative to the optical path in 2-micrometer steps over the entire range of interest.

4.2.2 Description of Electrical Test System

A block diagram of the electrical test system and its interface to the optical test system is shown in Figure 4.2-2. A brief description of each block follows.

Signal Generation Board: This unit generates all of the TTL signals necessary to drive the device being tested, the analog processor and the trigger timing for the Analog to Digital conversion (see Figure 2.1-2).

Head: The head contains the clock drivers used to translate the clocks from TTL to that necessary for CCD operation. All D.C. voltages are generated in the head. The analog processor is also contained here. This consists of a gain stage and correlated double sampling used for reset noise subtraction.

A/D Converter: A 12-bit A/D converter then digitizes the analog output of the AP. The A/D has a dynamic range of 2.0 volts. Its resolution is 0.49 mv/bit.

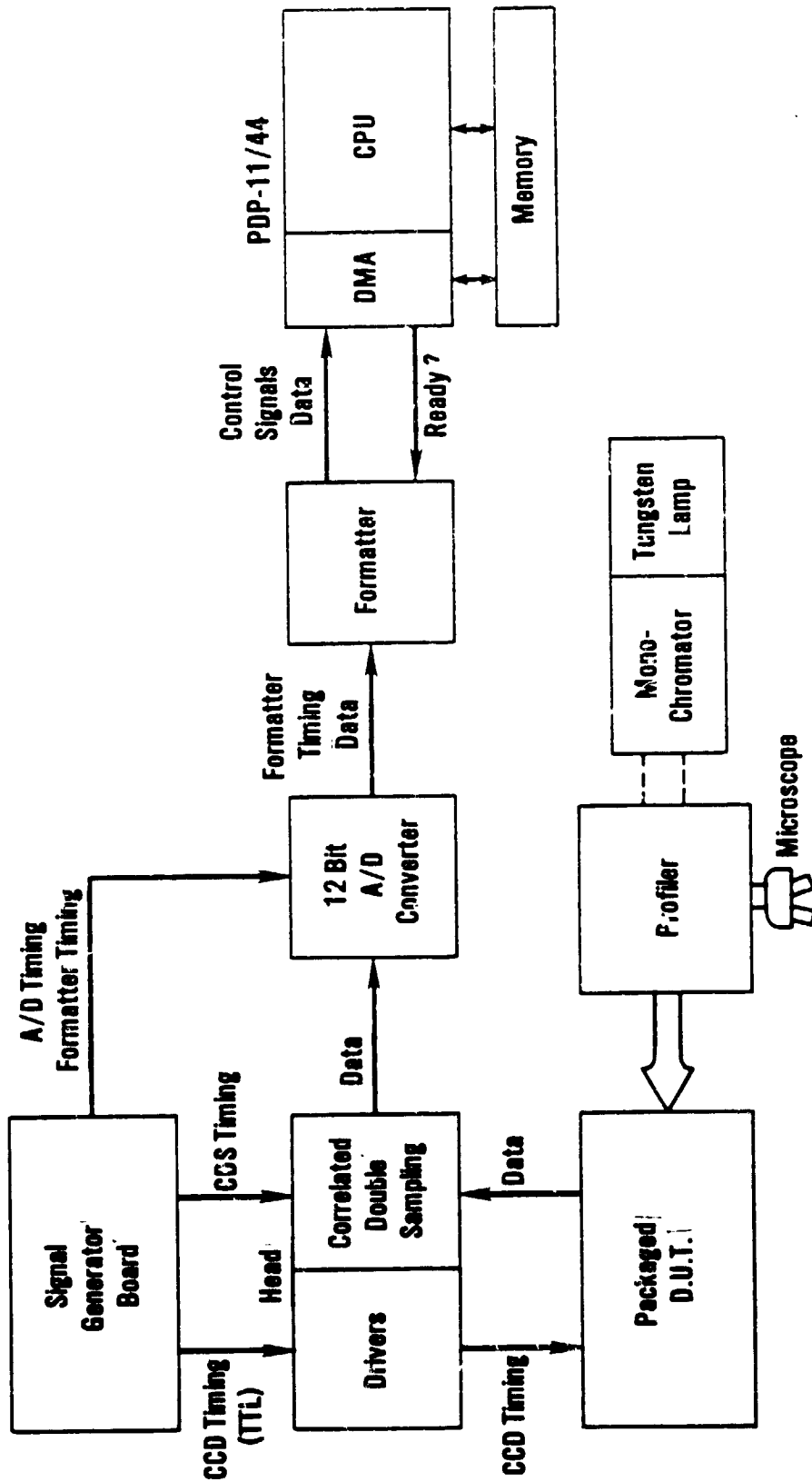


Figure 4.2-2. Test Equipment Layout for Data Acquisition

Formatter: The digital output of the A/D is then sent to the formatter whose purpose is to hold the data in storage for high speed data acquisition. The formatter also generates the necessary timing and synchronization signals for the direct memory access (DMA) input channel of the computer.

PDP 11/44 Computer: A PDP 11/44 Computer is used to acquire the digitized output signal of the device under test. Sums and Sum of Squares of each element are stored for later processing.

4.2.3 Characterization of Chips

Calibration of Monochromator Dial

The diffraction grating of the monochromator is connected to a dial graduated in 5 nanometer divisions. The calibration of the dial was verified by placing a series of narrow bandpass interference filters into the optical path of the monochromator output. The response of a 5040 device was used to detect the output of the monochromator/filter combination.

With the interference filter in place, the dial of the monochromator was adjusted until the response of the 5040 device was maximized. The results are shown in Table 4.2-1. In the 500 to 700nm region of interest, the largest discrepancy was 3.9nm.

TABLE 4.2-1 BOOTSTRAP CALIBRATION OF MONOCHROMATOR
DIAL BY PLACING INTERFERENCE FILTER IN THE OPTICAL PATH

SERIES INTERFERENCE FILTER BANDPASS	MONOCHROMATOR DIAL READING	DIFFERENCE
404.7nm	405nm	+ 0.3nm
500.0nm	500nm	0.0nm
546.1nm	550nm	+ 3.9nm
600.0nm	602nm	+ 2.0nm
656.3nm	658nm	+ 1.7nm
767.0nm	768nm	+ 1.0nm
794.7nm	800nm	+ 5.3nm

Calibration of Monochromator Light Source

In order to calculate the Relative Spectral Response (RSR) of the CCD detectors, it first becomes necessary to determine the Relative Spectral Output (RSO) of the monochromatic light incident on the CCD.

This is accomplished by replacing the CCD with a calibrated silicon diode. The NBS calibrated diode has a surface area of 1cm^2 and is temperature controlled to $19^{\circ}\text{C} \pm 0.1^{\circ}\text{C}$. The reverse biased current of the diode is measured using an EG&G Picoammeter (see Figure 4.2-3). The spectral output of the monochromator was measured in 20 nm steps from 360 nm to 500 nm and from 720 nm to 800 nm. The output was measured in 10 nm steps from 500 nm to 720 nm.

This measured current (I_M) when divided by the calibrated response of the diode (R_{SD}) to a uniform intensity light source of the same wavelength will give the Relative Spectral Output (RSO_{λ}) of the monochromator.

$$RSO_{\lambda} = I_M_{\lambda} / R_{SD_{\lambda}} \text{ (normalized)}$$

Data Acquisition: The data acquisition program is user prompted for the number of detectors to be acquired and the number of samples of each detector to be acquired. The sum of the responses and the sum of the squares of the responses for each detector is calculated and stored.

The Response and Response minus dark for each detector of interest can then be calculated. These terms are defined below:

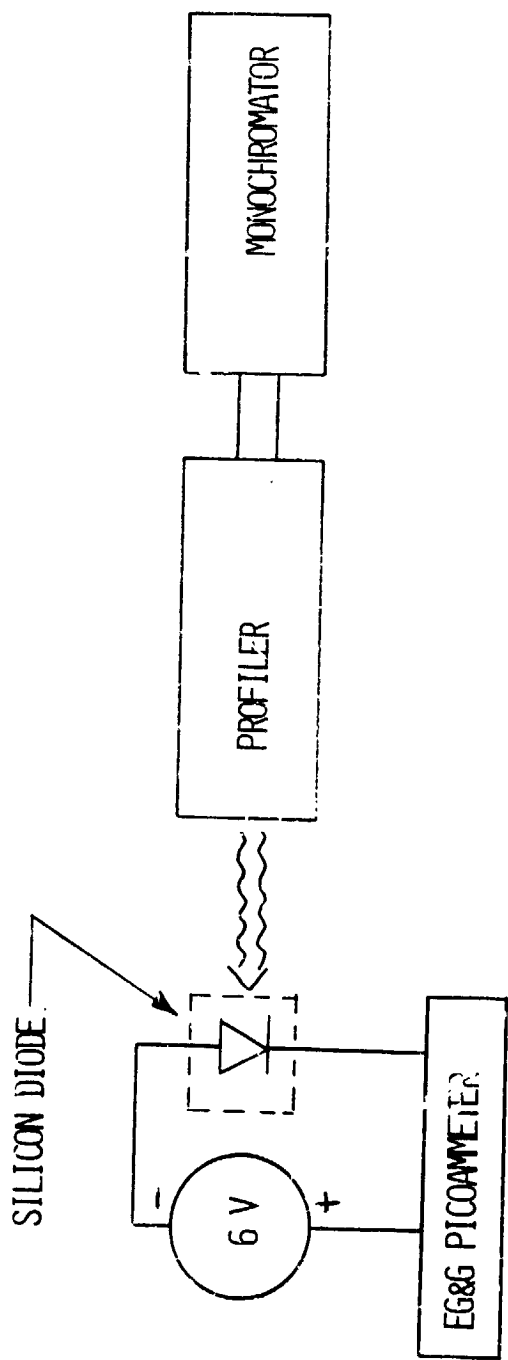


FIGURE 4.2-3 LIGHT SOURCE CALIBRATION

AVERAGE RESPONSE ($R_{i\lambda}$)

$$R_{i\lambda} = S_{i\lambda} / \text{NSAMP}$$

where:

i = i^{th} element

λ = wavelength

NSAMP = number of samples of each element

S = sum of the NSAMP responses

RESPONSE MINUS DARK ($\text{RMD}_{i\lambda}$)

$$\text{RMD}_{i\lambda} = R_{i\lambda} - R_{id}$$

where:

R_{id} = Average response of the i^{th} detector to dark (d)

SUM OF RMDs ($\text{RMDS}_{i\lambda}$)

$$\text{RMDS}_{i\lambda} = \sum_{i=A}^B \text{RMD}_{i\lambda}$$

where:

The RMD of elements A thru B are summed

RMDS is occasionally used when one detector is being illuminated but due to transfer efficiency problems the resultant chip output is smeared over several elements. The sum of the responses of the smeared elements approximates a detectors response with ideal transfer efficiency

Relative Spectral Response:

Relative Spectral Response is the response of a device to a uniform intensity light of wavelength λ .

The device to be tested is placed in the optical path as shown in Figure 4.2-1. The slit is aligned optically to the detector to be characterized. When all inputs to the device have been optimized, the incident light is adjusted via the final aperture in the optical path to utilize the maximum range of the A/D and not saturate the dynamic range of the CCD.

In order to minimize the effects of temperature drift during acquisitions, the dark response of all detectors is taken immediately prior to acquisition of the response to the test wavelength. $RMD_{i\lambda}$ & $RMDS_{i\lambda}$ are then calculated for each wavelength. The number of elements summed is dependent on the CCD transfer efficiency of the sample being tested.

Acquisitions are made at the same wavelengths described in Section 4.2.3 (Calibration of Monochromator Light Source).

The Relative Spectral Response (RSR) can then be calculated with the following equation:

$$RSR_{i\lambda} = RMS_{i\lambda} / RSO_{\lambda} \quad (\text{Normalized})$$

Filter Transmission:

In order to determine the Transmission (T) of a filter deposited on a CCD, two measurements are required:

- 1 - RSR of a nonfiltered CCD Detector (RSR_N)
- 2 - RSR of a filtered CCD detector (RSR_F)

The relative transmission (T) can then be calculated with the following equation:

$$T_{i\lambda} = RSR_{F_{i\lambda}} / RSR_{N_{i\lambda}} \quad (\text{normalized})$$

Spread Function:

The Spread Function or Crosstalk into the CCD array is due primarily to photons which are absorbed deep in the silicon, creating carriers which diffuse randomly until they are collected in a CCD well, or until they recombine in the bulk. Since the minority carrier lifetime is 50usec or more, carriers generated near the rear surface under one CCD well can produce a significant signal in wells several detectors away.

In order to measure the spread function, the focused slit from the profiler was projected onto the center of a detector on a 5040 line array. The response to each detector was acquired at the beginning,

middle, and end of the ideal bandpass for the 4 bands of interest. See Table 4.2-2. The spread function was then determined by measuring the normalized RMD of the neighboring elements readout before the illuminated element. This was done to avoid the confusion with signal associated with transfer in efficiency if elements read out after the illuminated element were used.

One additional error source in this type of measurement is the spread function (stray light) of the optics used to define the slit. The following method was used to minimize its contribution. One of the 5040 wafers sent to Optoline received a Band 2 and a Band 3 filter deposition, but received only one masking. This resulted in a device covered by both filters except in certain detector sites where there was no filter (see Figure 4.2-4).

The Band 2 and Band 3 filters with different bandpasses would collectively block approximately 99% of the stray light from being collected by neighboring detectors.

TABLE 4.2-2 TEST WAVELENGTHS FOR SPREAD FUNCTION ACQUISITIONS

BAND	BEGINNING	MIDDLE	END
1	450nm	485nm	520nm
2	520nm	560nm	600nm
3	630nm	660nm	690nm
4	760nm	830nm	900nm

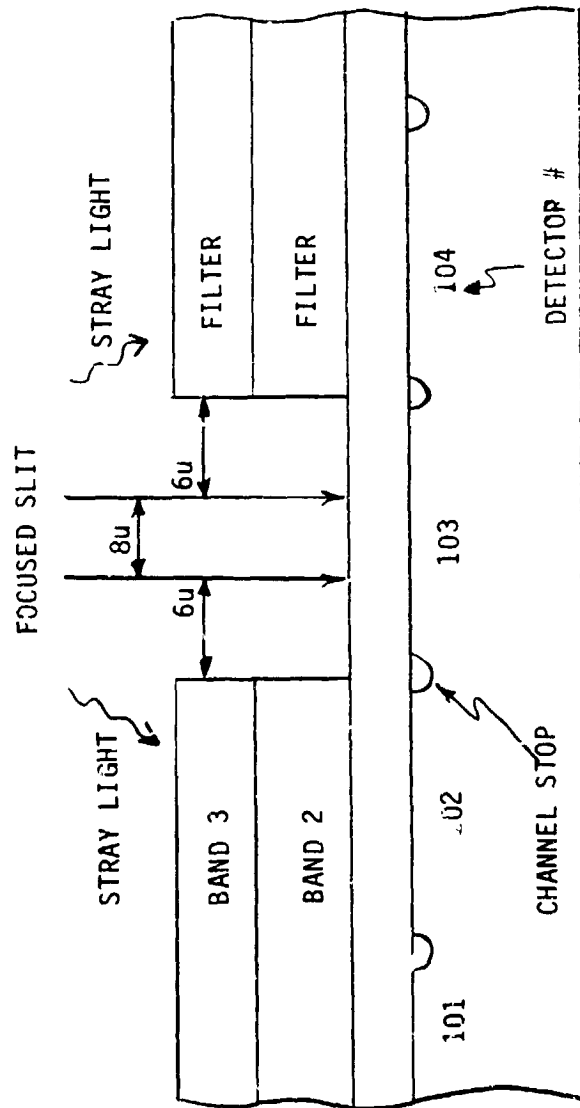


FIGURE 4.2-4

CROSS SECTION ILLUSTRATING SPREAD FUNCTION ILLUMINATION

5.0 MEASURED RESULTS ON CHIPS

Several 5040 line arrays were characterized after stripe filter depositions. Relative spectral response, filter transmission and spread function results will be reported here. Also to be discussed are comparisons of transmission and reflectance data as well as the repeatability of RSR from one filter deposition to the next.

5.1 RELATIVE SPECTRAL RESPONSE

Chip 4446-10-29 which received a patterned, Band 2 and Band 3 filter definition was characterized for RSR. Since transfer efficiency for this sample was less than .999, the resultant output was spread over several elements and the RMDS technique was used. One hundred and twenty-eight samples of each element were acquired.

The lamp calibration, Nonfiltered RSR and RSR of Band 2 and Band 3 are shown in Figures 5.1-1, 5.1-2, 5.1-3 and 5.1-4 respectively.

The following Table summarizes the results compared with the ideal filter.

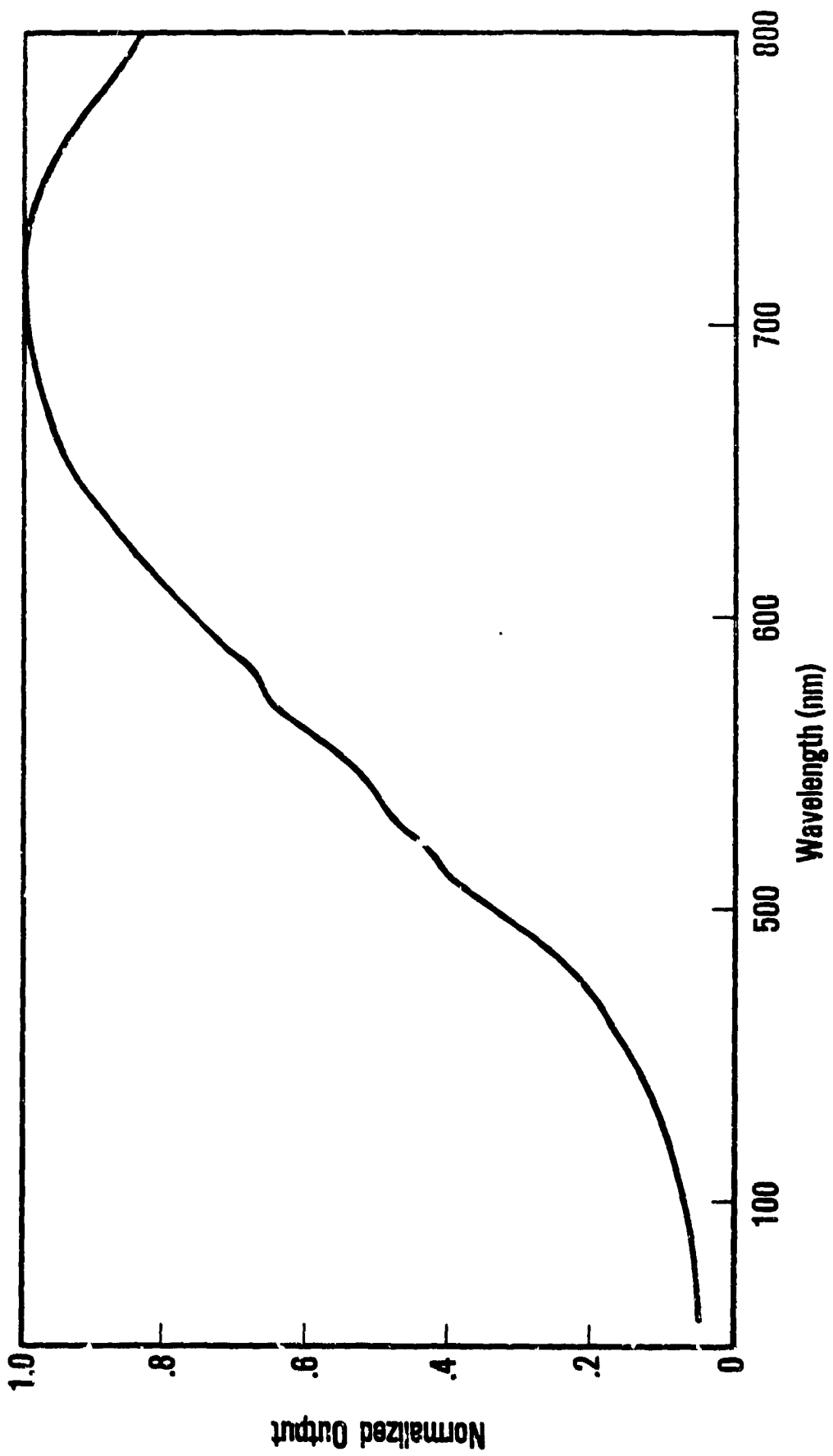


Figure 5.1-1 Relative Spectral Output of B & L Monochromator

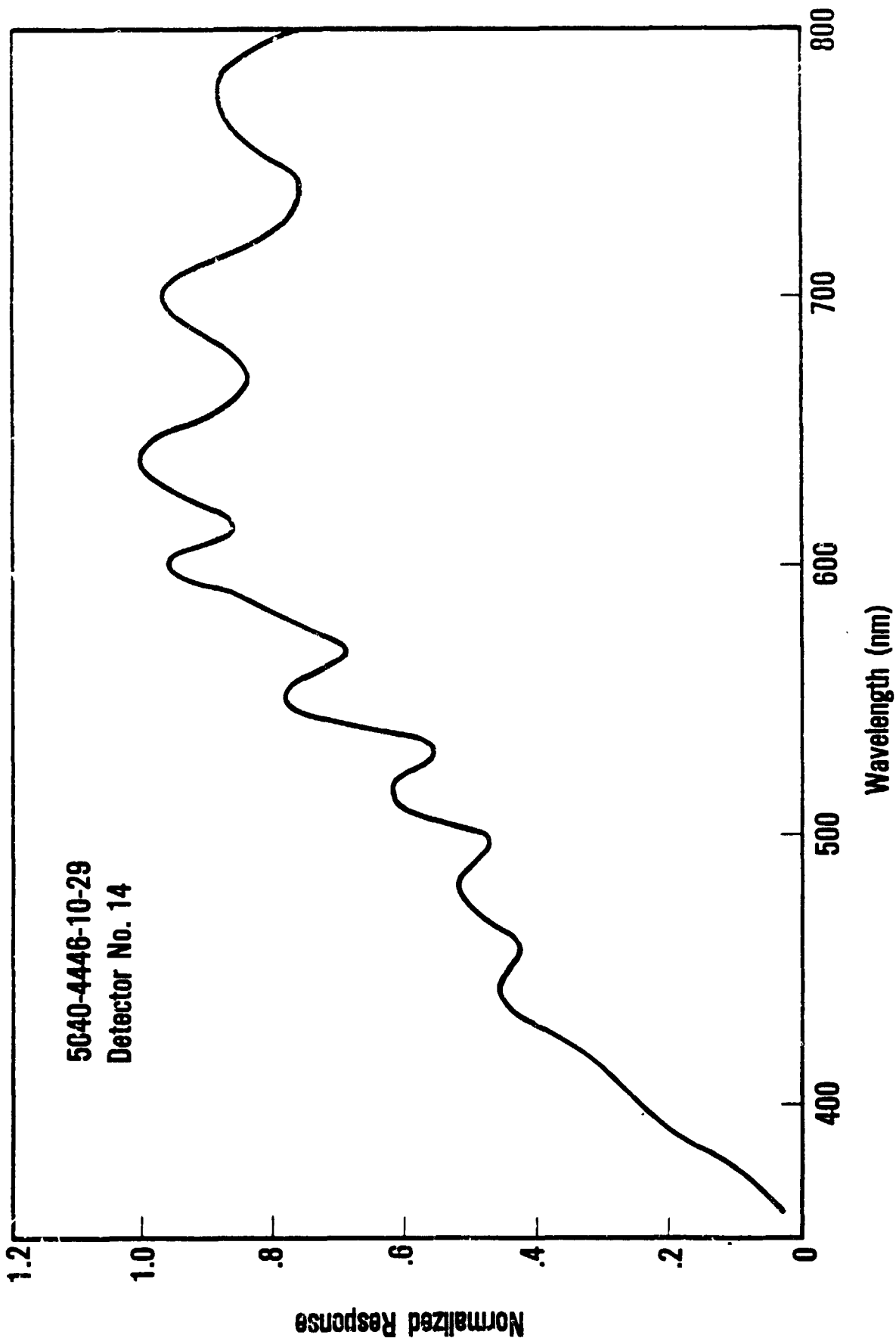


Figure 5.1-2. Relative Spectral Response of Unfiltered Silicon

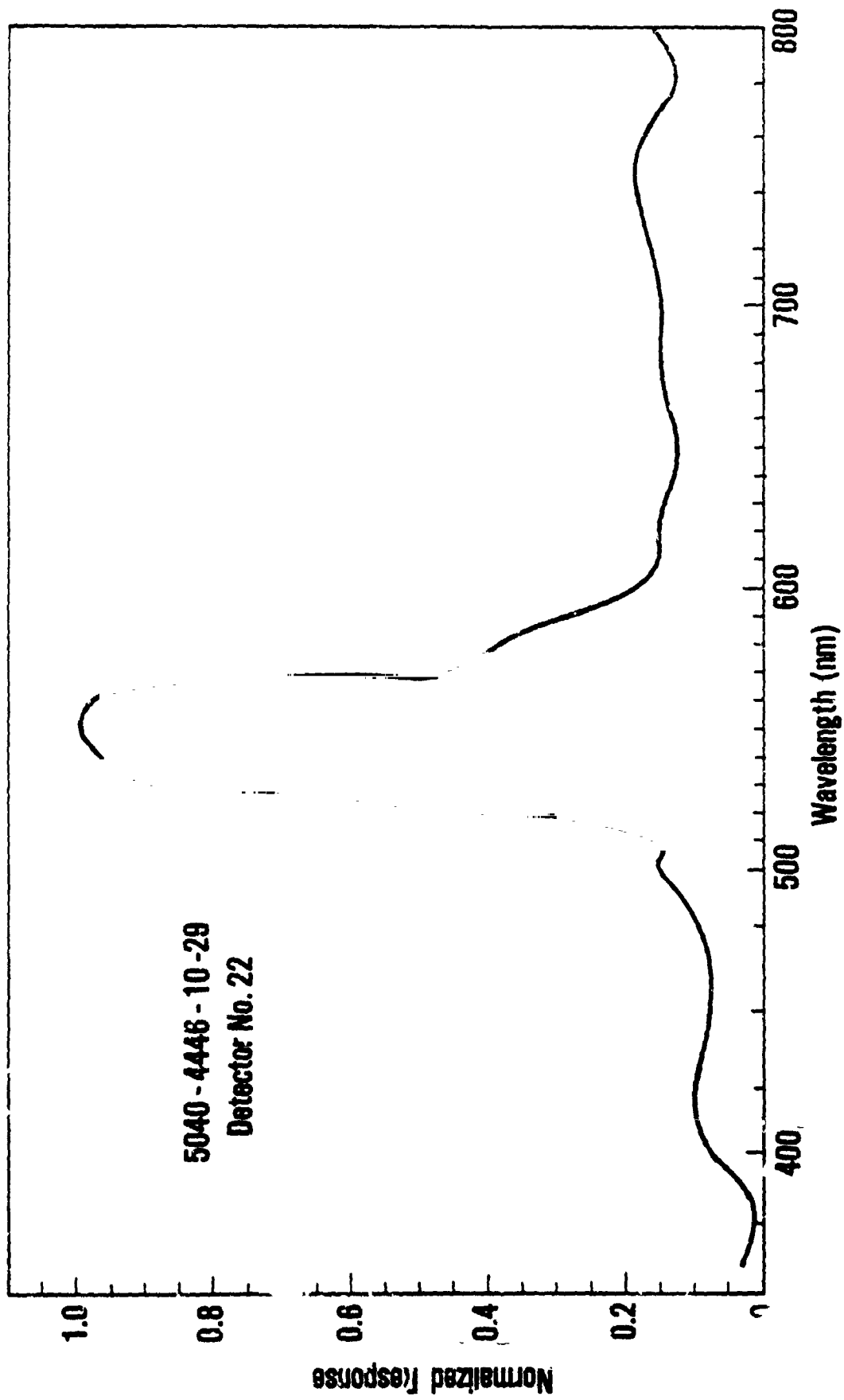


Figure 5.1-3. Relative Spectral Response of Band 2 Filter on Silicon

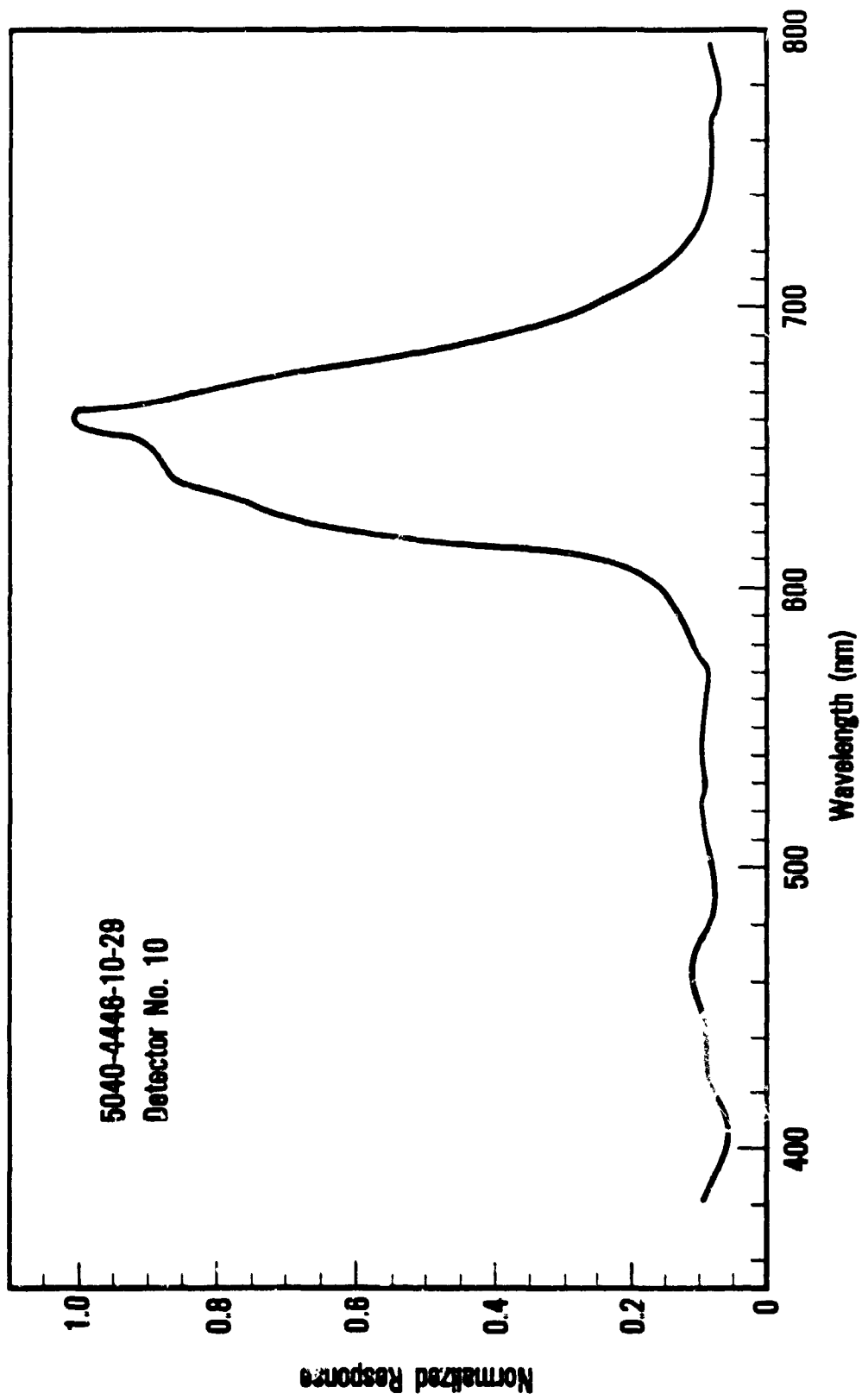


Figure 5.1-4. Relative Spectral Response Band No. 3 Filter

TABLE 5.1-1 COMPARISON OF DEPOSITED FILTER BAND EDGE
TO DESIRED BAND EDGE

	Band 2		Band 3	
	50% Point		50% Point	
	Lower Edge	Upper Edge	Lower Edge	Upper Edge
Desired	520 nm	600 nm	630 nm	690 nm
Measured	522 nm	568 nm	618 nm	686 nm

Figure 5.1-5 shows the variation in Relative Spectral Response between two separate filter runs made weeks apart. The differences in their bandpass regions is approximately 10nm.

5.2 FILTER TRANSMISSION

The relative spectral transmission of the Band 2 and Band 3 filters was calculated using the formulas described in Section 4.2-3. The resultant transmission plots for Band 2 and Band 3 are shown in Figures 5.2-1 and 5.2-2 respectively.

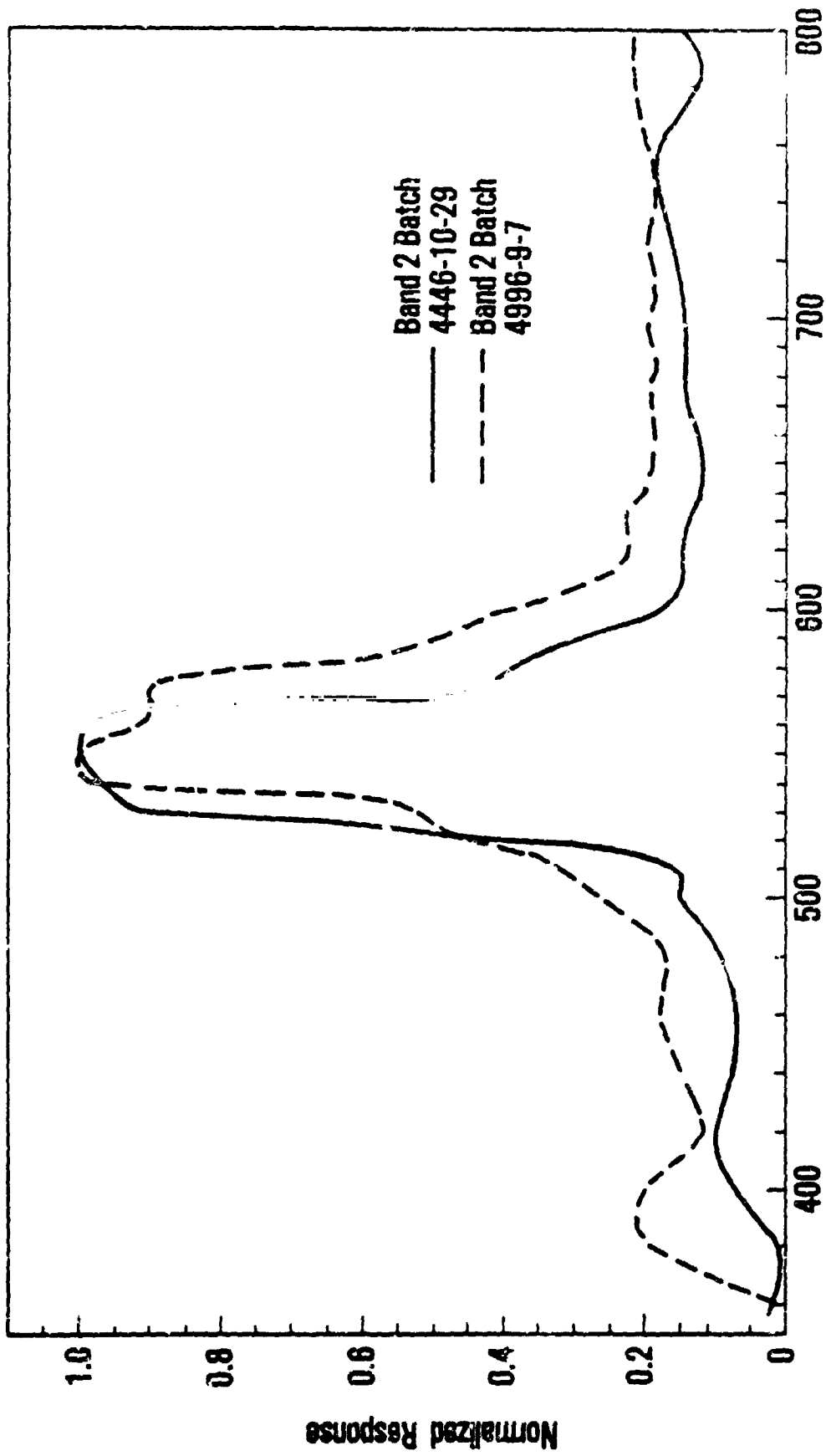


Figure 5.1-5. Comparison of RSR Between Two Separate Filter Runs - Band 2

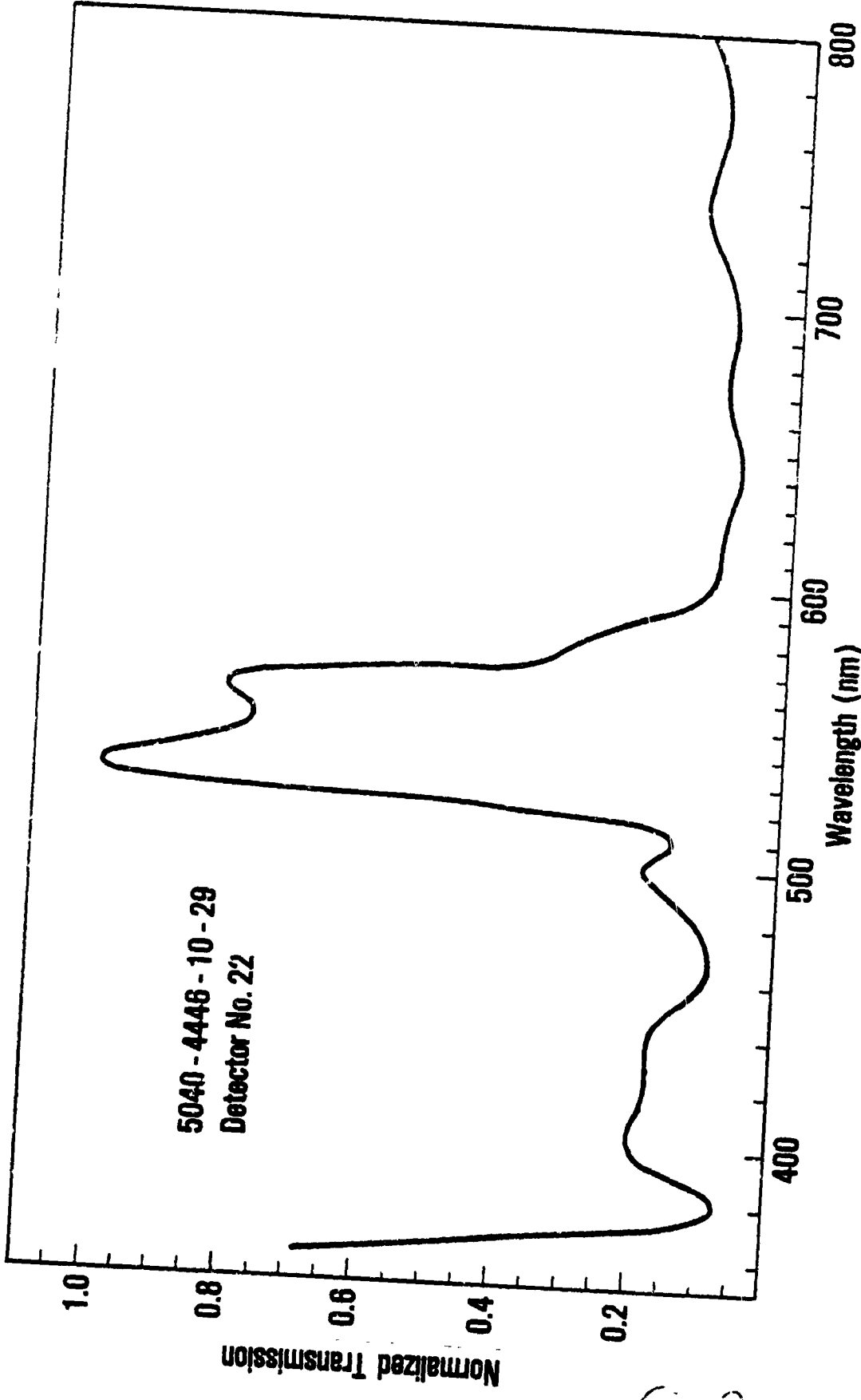


Figure 5.2-1. Transmission of Band 2

C-2



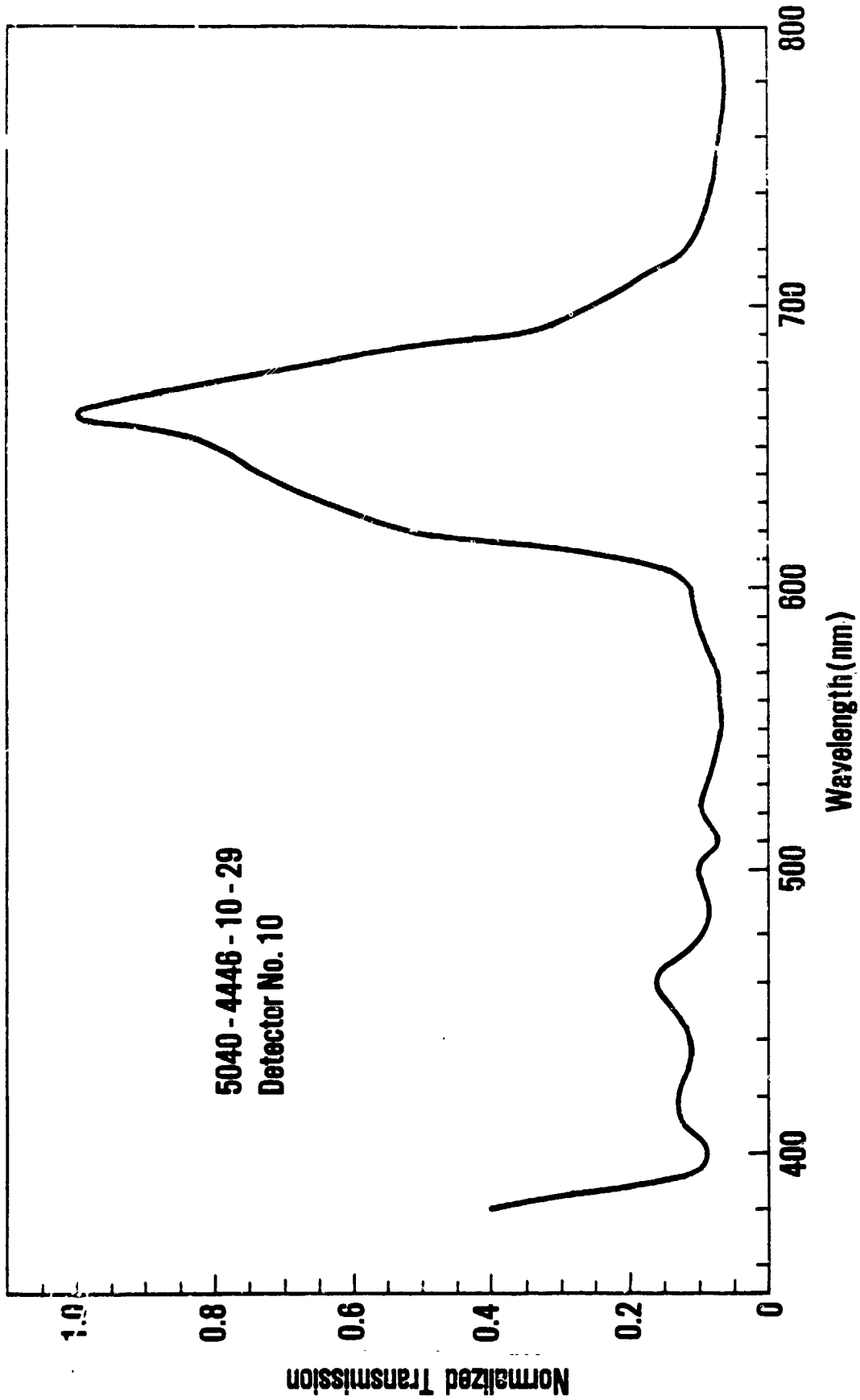


Figure 5.2 - 2. Transmission of Band 3

Figures 5.2-3 and 5.2-4 show the relationship between the filter transmission as calculated by section 4.2-3 and the inverted reflectance as measured by the Nanometrics. The Nanometrics reflectance measurements were taken on the same physical device as the transmission acquisition.

5.3 SPREAD FUNCTION

Chip 4996-15-9 was chosen for spread function acquisition. This device had the dual filter barrier to stray light as described in Section 4.2-3 and had reasonably good transfer efficiency. The 8 micrometer wide slit was optically focused and centered in the illuminated detector at a wavelength of 600nm. No additional focusing was performed as the various wavelengths were acquired.

The spread function plotted in Figure 5.3-1 shows the amount of signal captured by the four neighboring detectors as a percentage of the response of the illuminated detector. Two hundred and fifty-six (256) samples of each detector were acquired. The scale for the four graphs represents the center-to-center distance from the neighboring detector to the illuminated detector.

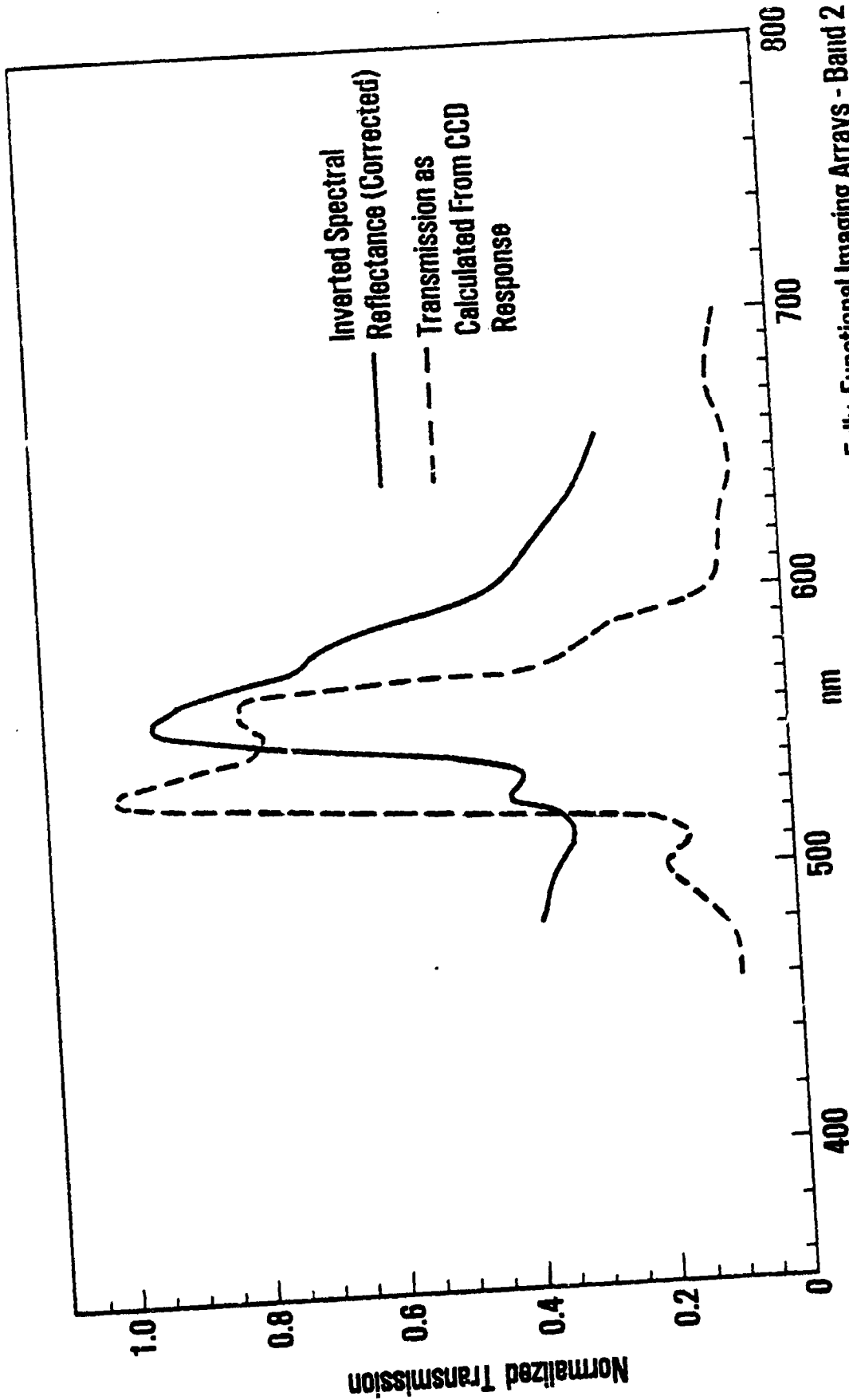


Figure 5.2-3. Comparison of Spectral Reflectance and Transmission on Fully Functional Imaging Arrays - Band 2

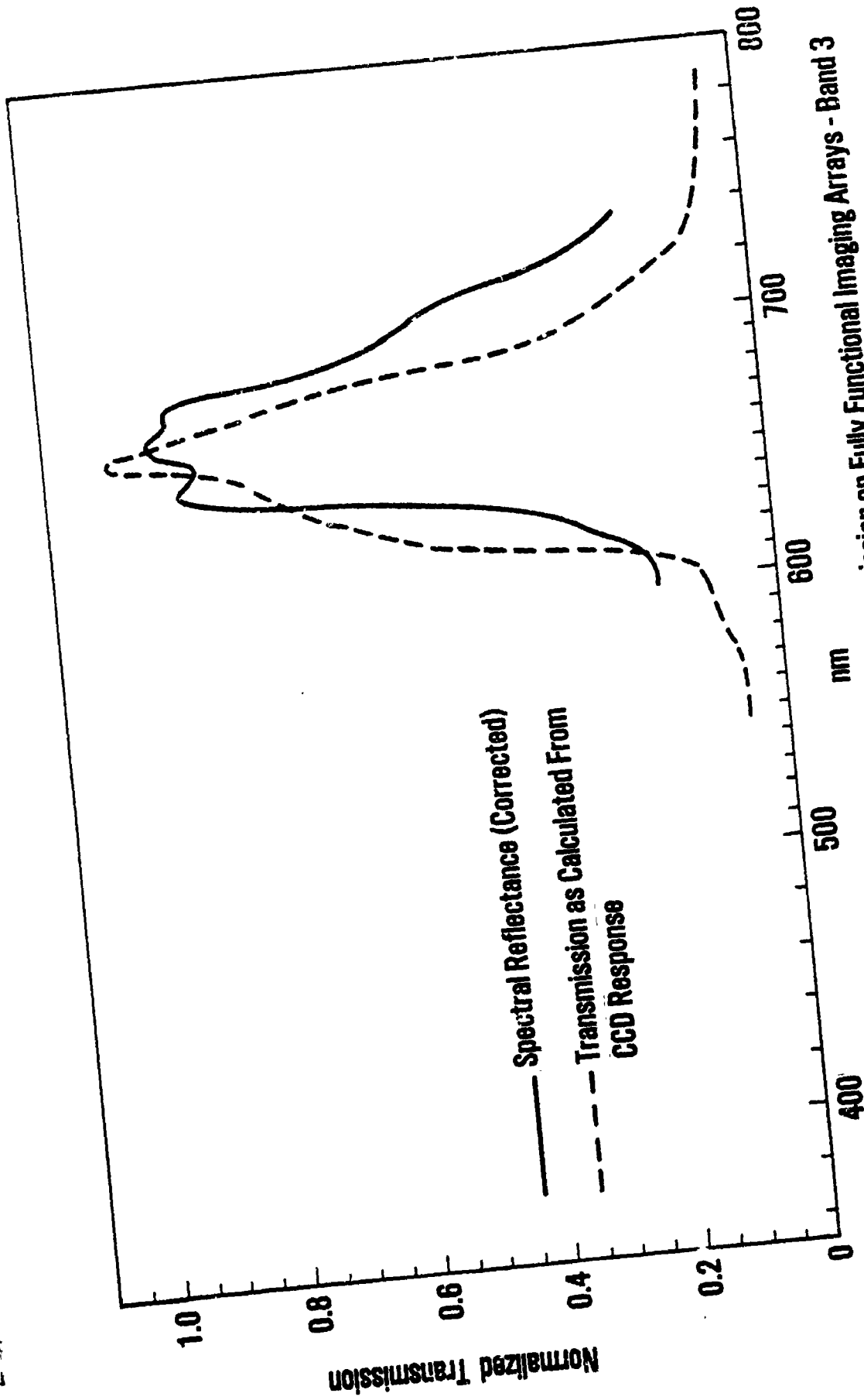


Figure 5.2-4. Comparison of Spectral Reflectance and Transmission on Fully Functional Imaging Arrays - Band 3

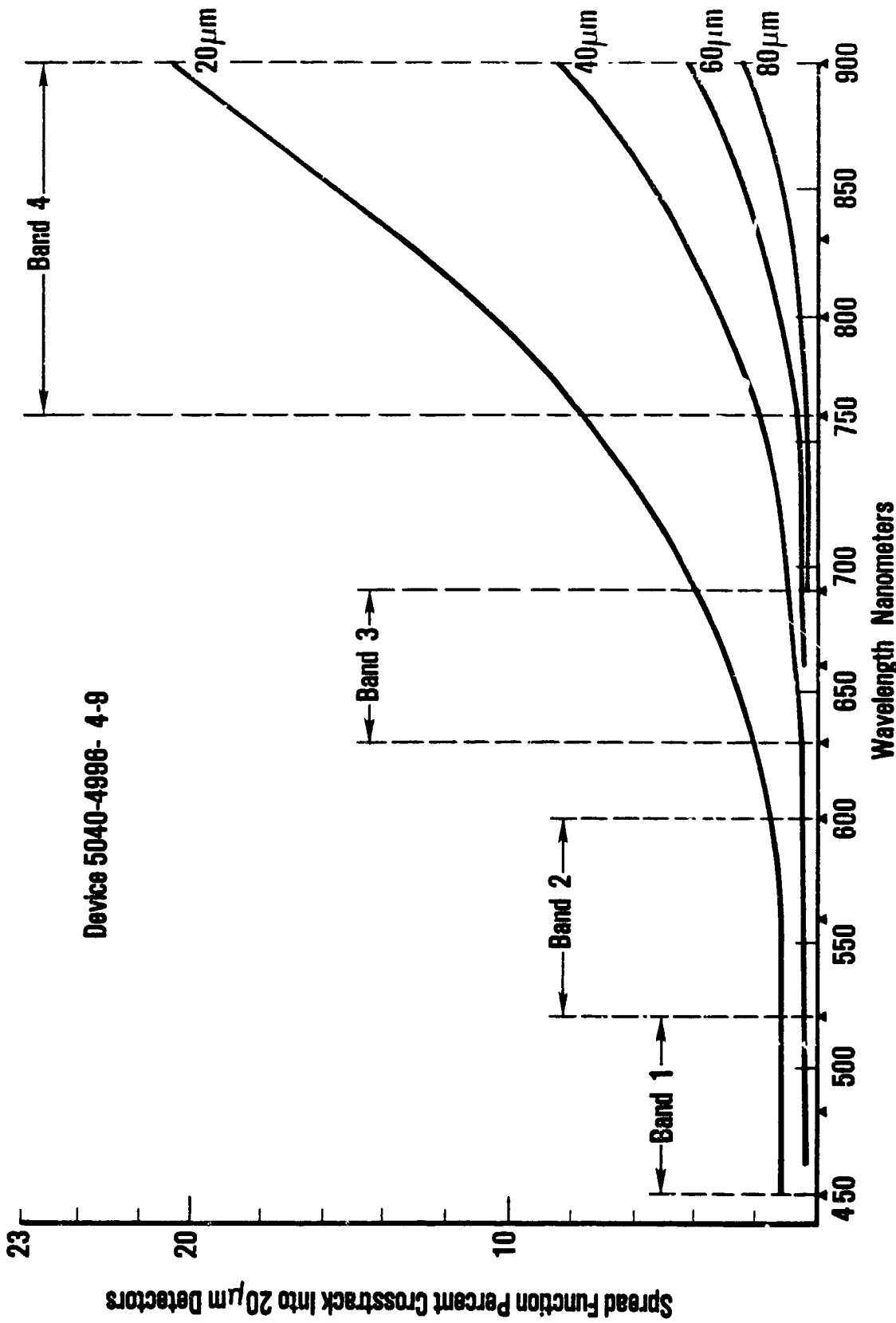


Figure 5.3-1. Slit Width - 8 μm Center-to-Center Spacing Between Detectors - 20 μm

6.0 PROBLEMS ENCOUNTERED IN FABRICATION

6.1 MECHANICAL DIFFICULTIES

Alignment problems were encountered with the first two sets of functional wafers sent to Optoline for filter deposition. The filter deposition photomasks were misaligned to the channel stops on the first set of wafers (4421-8 and 4421-9). This along with an incomplete rework of the photoresist resulted in gaps between filters, channel stop overlap and regions with double deposition.

The second group of wafers (4446-10, 3553-7 and 3553-9) were properly aligned nicely to the channel stops, however the green filter mask was shifted by four pixels ($\approx 80\mu\text{m}$). This resulted in clear areas and areas with double filter deposition. It should be noted that this alignment difficulty is a result of having to align the photomask to the wafer through very small clear areas on a largely opaque mask. Furthermore, the channel stops are very difficult to see under several levels of dielectric and gate structure. However, there were no alignment problems with the last two shipments of functional wafers which were photoengraved at Westinghouse, then shipped to Optoline for filter deposition. It is felt that alignment difficulties will be easily overcome with a revised mask design and use of modern equipment.

A liftoff process was used to remove the filter material from undesired regions. The filter resist material on the first two shipments of functional wafers processed by Optoline did not properly lift off. The resist under the filter dissolved, however patches of filter still remained. This excess

filter material was easily removed by light mechanical action as the resist prevented adhesion to the underlying silox. Also in some regions where the filter material did lift off there were ragged edges where the break occurred. These liftoff problems were minimal with wafers photoengraved by Westinghouse before shipment to Optoline for the filter deposition.

Two lots of CCD arrays were processed as backup for wafers on hand at the beginning of this program. One lot (4997) was placed on hold after completing two thirds of the processing. Lot 4996 was completed and used for filter deposition. An incorrect metal mask was used on this lot. This resulted in an aluminum stripe covering 50% of each imaging pixel. Only two pixels at the end of the array were not covered by this aluminum line. This line acts as a light shield, thus reducing the active imaging area by 50%. This in itself is no problem except that light may be scattered from the edges of the aluminum making spread function measurements questionable.

An important aspect of the filter deposition was uncovered during this study. The filter material becomes tightly bonded to the glass coating of the wafers. This makes rework of the filter material difficult. A rework procedure is an important aspect for future work.

6.2 TRANSFER EFFICIENCY DEGRADATION

The initial shipment of functional wafers processed by Optoline resulted

in line arrays whose transfer efficiency was significantly degraded when tested in package form. Table 6.2.1 summarizes the extent of this degradation. The second shipment of functional wafers processed by Optoline were tested at the wafer level before packaging to determine if the degradation was a result of the filter deposition or the packaging process. The transfer efficiency of the line arrays was degraded before packaging.

At this point several experiments were initiated to determine the cause of the degradation. One experiment evaluated the effect of "fat zero" on transfer efficiency. Fat zero consists of partially filling the transfer register with charge. This excess charge fills charge trapping sites which should improve transfer efficiency. This is normally unnecessary for buried channel devices. All of the functional arrays used in this program were buried channel. The transfer efficiency was measured using the optical illumination of a single pixel method illustrated in Figure 4.1.1. Using chip 4446-10-29 we found only a slight increase in transfer efficiency when fat zero was used. The measured transfer efficiency with fat zero was .9877.

Other experiments were conducted by Optoline using similar type CCDs. One wafer (3849-10) was subjected to a glow discharge clean and thermal cycling without actually having filter deposited. One wafer (3451-12) was put through a simulated photoengraving cycle with no filter deposition. Another wafer (3875-5) received filter deposition on surrounding arrays, but no filter on the arrays which were measured. The transfer efficiency of arrays on these three wafers was not degraded.

Once again using 5040 line arrays two additional experiments were performed by Optoline. The glow discharge plus thermal cycling experiment was repeated using wafer 4996-9. A second wafer (4996-15) was patterned with photoresist to protect the bonding pads only and band 2 filter was deposited across the entire wafer. The resist was then removed from the bonding pads leaving the pads clean for probing. Once again there was no degradation of transfer efficiency to arrays on either wafer.

Finally the band 2 filter mask was modified to allow a clear region near the output end of the array. Six wafers from lot 4996 which were photoengraved with the modified band 2 mask were sent to Optoline for filter deposition. Two wafers received the band 2 filter deposition, two wafers the band 3 filter and two wafers band 2 and band 3. It should be noted that all arrays tested from this lot required "fat zero" regardless of being processed by Optoline or not.

Samples from the three sets of wafers were evaluated for transfer efficiency after packaging. Results can be seen in Table 6.2.2. Fat zero was used and transfer efficiency was evaluated by the electrical injection and the single pixel illumination technique. The results obtained were the same for both measurement techniques. Preliminary transfer efficiency measurements were not performed on most arrays, however, post filter deposition results were good. Wafer 5 did not yield any arrays capable of being properly tested primarily due to open contacts. Three arrays on wafer 6 (also band 3) were tested at the wafer level using the electrical injection method. Results were also good.

Two possible explanations of the discrepancy between transfer efficiency results of the first two sets of functional wafers processed by Optoline and results obtained during later experiments are: 1) while being processed at Optoline the first two sets of functional wafers underwent some treatment which resulted in transfer efficiency degradation which Westinghouse has not been able to identify, or 2) the wafers used in the initial filter depositions were manufactured in a way which make them vulnerable to one of the Optoline processes. However, more recently manufactured arrays are not susceptible.

7.0 OPERATIONAL ENVIRONMENT

Due to the difficulties mentioned earlier with transfer efficiency degradation and photo definition of the filter material, fully functional arrays were obtained too late in the program to allow array evaluation after exposure to space environments.

Individual test wafers and some packaged chips (poor transfer efficiency) were tested for exposure to radiation vacuum and temperature stress. Also some simple tests were done to check mechanical film adhesion.

7.1 ADHESION

Thorium Fluoride was chosen by Optoline as the first layer material because of its excellent adhesion to silicon dioxide. Even if the Thorium Fluoride is not the first optical layer in the filter design, a 100A layer is deposited for adhesion purposes. To test adhesion, we subjected a finished non-functional wafer with both filter levels present to a high pressure TCE (trichloroethylene) spray and nitrogen blow dry. Visual inspection before and after showed no cracking or chipping at the filter edges. The next test was a simple one designed to check adhesion of deposited aluminum films. It consists of applying standard Scotch tape to the wafer surface, rubbing it firmly down into contact with the surface and then ripping it off. This technique also showed no visual damage to the filter material. In another attempt to clean up debris from a sample with incomplete lift-off, we soaked a wafer in acetone for twenty-four hours and then for another half-hour in an ultrasonic acetone bath. This also had no effect. The only thing we found short of direct physical force for removing the filter material

was a prolonged immersion for several hours in an ultrasonic acetone bath. Although this did result in damaging some of the defined regions, it did not remove enough of the filter material to be considered as a reasonable rework technique for improper filter deposition. We did not investigate the use of acid etches or ion mill techniques for filter removal, as the parts we were working with had exposed aluminum bonding pads. With a change in process and an additional mask level it should be possible to develop a filter rework technique if the need developed.

7.2 TEMPERATURE STRESS

Two packaged chips with both levels of filter present were submitted to a 100°C bake for a period of 15 hours in a nitrogen environment.

The spectral reflectance measurements taken with the Nanometrics Instrument before and after this anneal cycle are shown in Figure 7.2-1 and 7.2-2 for bands 2 and 3 respectively. Both filters show decreased reflection (increased transmission) out of band, but practically no change in structure or bandwidth. However, in all of the Nanometrics spectral reflectance-to-transmission comparisons done in this program, there has been relatively poor agreement for the out of band characteristics. This is particularly evident in Section 5.2, where spectral reflectance is compared to actual transmission through the filter. The Optoline transmission measurements on glass slides and the transmission calculated from the RSR of functional chips tend to agree much better in the out of band regions than the measured spectral reflectance

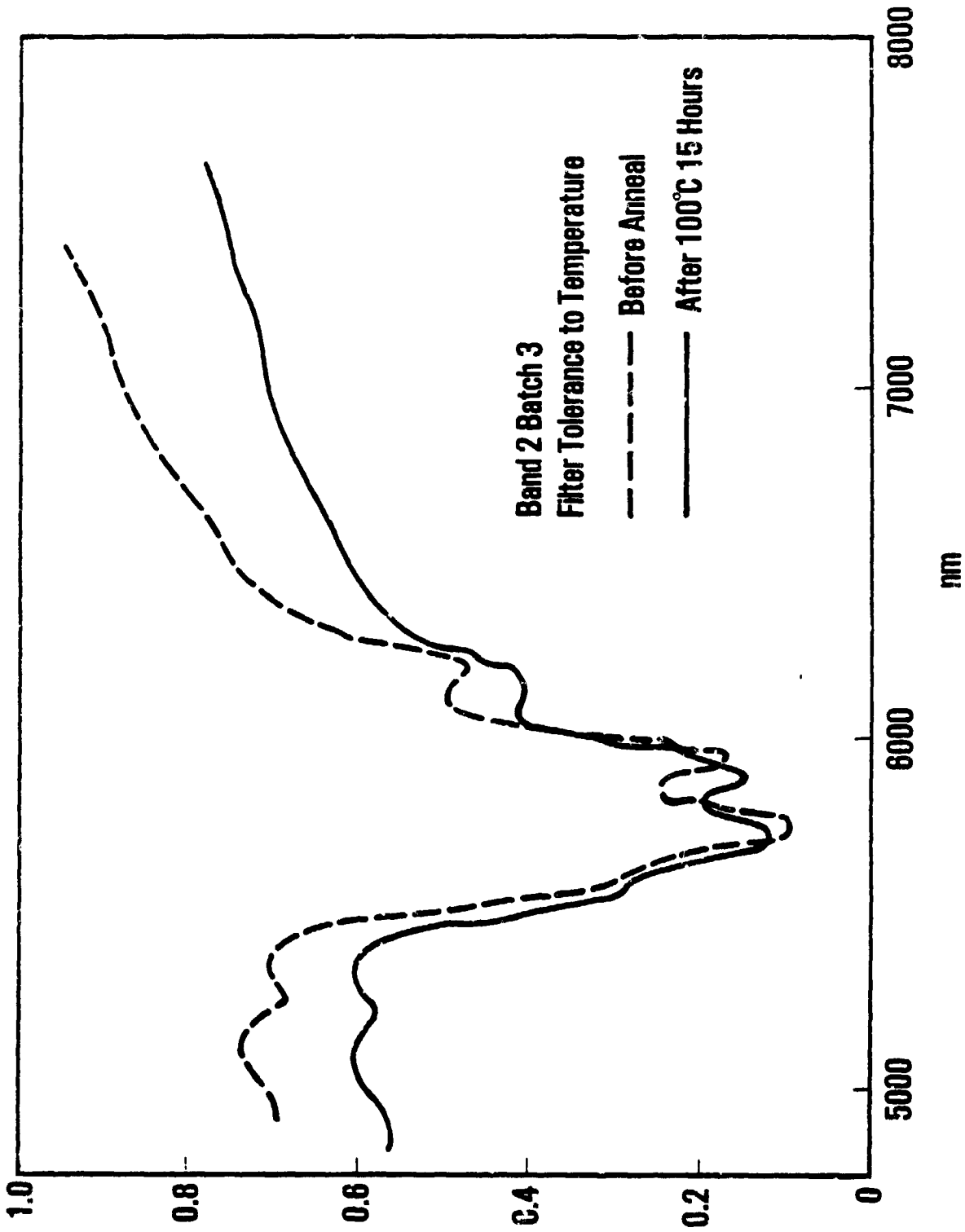


Figure 7.2-1. Filter Tolerance to Temperature

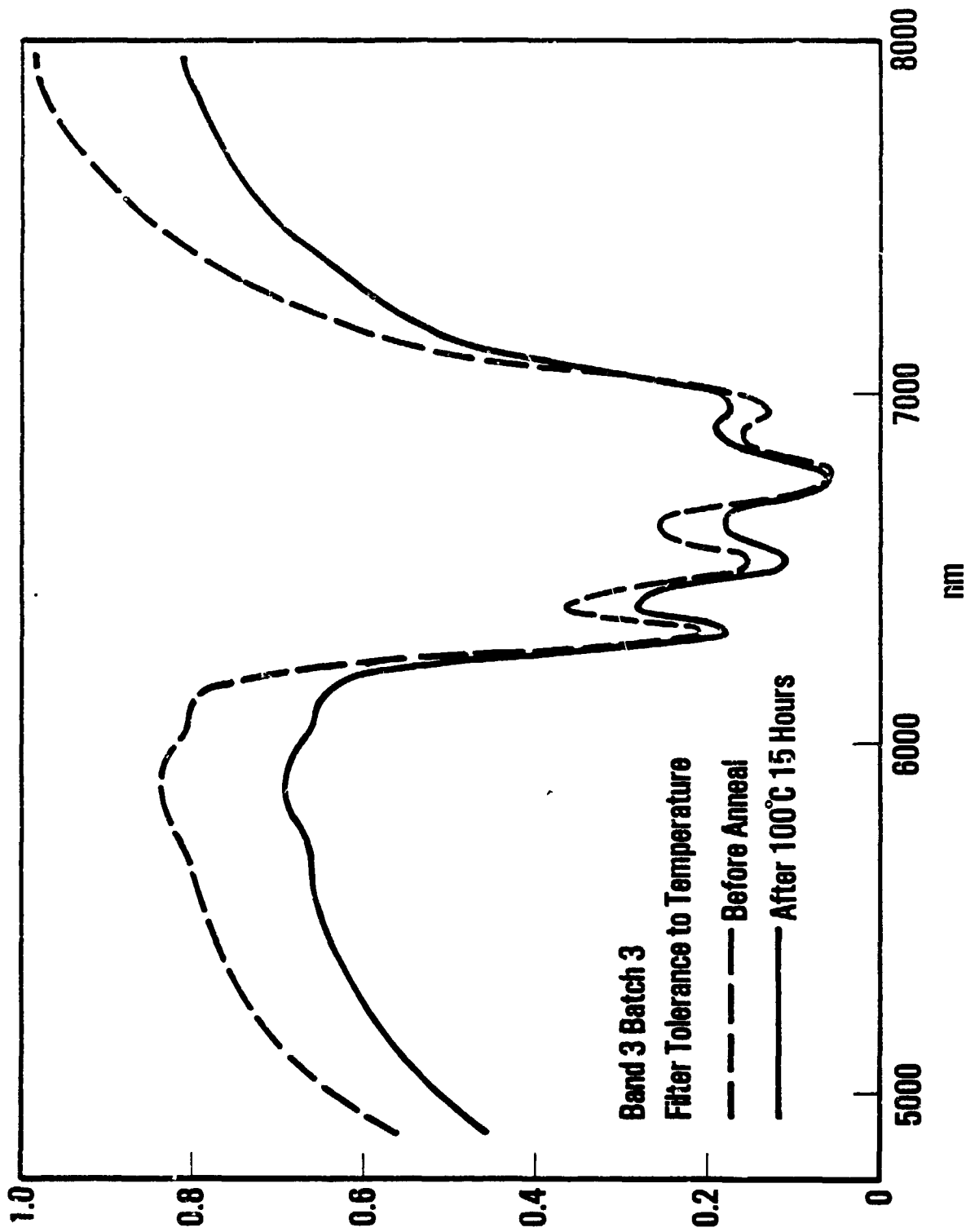


Figure 7.2-2. Filter Tolerance to Temperature

measurements from the Nanometrics Instrument. It may well be that the measurement system in use for spectral reflectance is particularly sensitive to surface conditions or granularity of the sample being evaluated. In order to determine the actual out-of-band transmission it will be necessary to temperature-stress a functional chip. The spectral reflectance measurements indicate that there may be an increase in out-of-band transmission but there is no catastrophic shift in bandpass or in-band attenuation.

7.3 RADIATION STRESS

One of the early test bulk wafers with filter material above a silox substructure was exposed to total dose irradiation from a Co60 source. Spectral response was measured at 100K rads, 500K rads and one megarad. This particular sample had no defined photopattern and a lot of substructure. In Figure 7.3-1 a comparison is shown of "before" and "after" radiation spectral reflectance. Essentially the only variation which occurs is in the location of the fine structure. Samples taken across the wafer indicate this much variation can be expected from just spatial variation and would not be significant in a design where the fine structure is eliminated. These results were consistent to 1 megarad, which is beyond the point where conventional CCD devices operate.

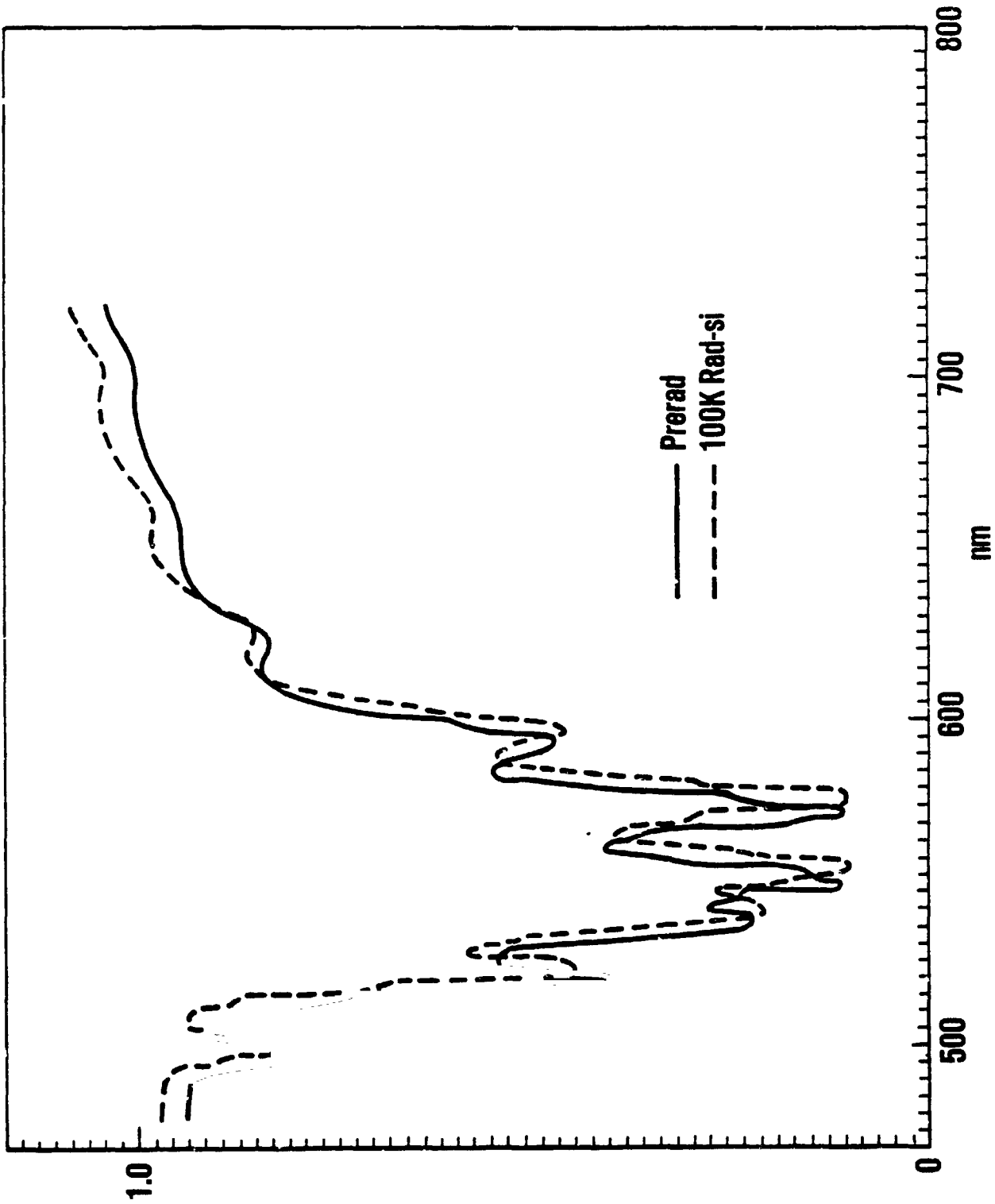


Figure 7.3-1 . Filter Tolerance to Total Dose Irradiation

7.4 VACUUM EXPOSURE

As the filter material is deposited in a vacuum and known not to be hygroscopic, little change in filter characteristics was expected due to vacuum exposure. Samples evaluated in an SEM vacuum environment showed no signs of outgassing or deterioration.

As a separate test, samples were submitted to a 56-hour, 10^{-7} Torr vacuum environment. Two samples for each band of completely processed filter/CCD combination were measured for spectral reflectance. Absolutely no variation in bandwidth or fine structure could be detected.

8.0 CONCLUSIONS

This program resulted in a positive recommendation. It is practical and apparently worthwhile, to form interference filters photolithographically directly on silicon CCD sensor chips to form a Multispectral Line Array for a pushbroom scanning instrument for Earth Resources sensing or similar applications. As shown below, all specific work statement questions appear to have been answered positively. The principal remaining concern is that the first two groups of wafers with operating CCDs which were processed by Optoline with photolithography performed at Hanscom AFB resulted in CCDs with very poor transfer efficiency despite good performance before Optoline processing. All wafers since then have been processed entirely at Westinghouse, with only the filter deposition itself performed at Optoline. None of these CCD chips showed any degradation in transfer efficiency or in any other characteristic. We believe, therefore, that when correctly processed, the addition of an integral color filter set should have no adverse effects on CCD yield. Further, the filter yield appears potentially high, although with some fine tuning of the process yet to be accomplished. Thus the overall integral filter concept appears a practical one for production and a leading candidate for a future MLA instrument.

Specific conclusions include:

1. Spectral separation - Specially filtered sensing arrays for NASA Landsat bands 1 through 4 can be built on a single silicon chip by placing them as suggested in Figure 1-1, with light shielded strips between successive arrays. Color signal separation should be adequate for the MLA application.

- (4)
2. Filter transmission - Computed spectral filter transmission into the silicon for an optimized band 2 filter was greater than 70%, about equal to the measured performance of typical chips without filters. Thus, at least for this case, the filter introduced no significant in-band loss. Measured reflectance data on an experimental wafer with this filter showed average reflectance over the passband of about 15%, indicating transmission into the silicon greater than 30%. Measurements on non-optimized filters on chips showed mid-band reflectance less than 10%, indicating peak transmission into the silicon greater than 90%. Computer out-of-band transmission for the optimized filter was about 5% at 440nm, and was much smaller at other out-of-band wavelengths. RSR data on chips with non-optimized filters showed out-of-band response ranging from 5 to 7% for a band 3 filter. The band 2 filter from the original Optoline recipe had measured response as high as 15 to 20%. Obviously, this filter would require redesign. Reflectance measurements taken at the Westinghouse R & D Center confirmed these results. Note that this program was intended to determine results when an existing Optoline filter design was applied to an existing CCD sensor chip, not to attempt to optimize either.

 3. Filter stability was checked by measuring spectral transmission before and after exposure of vacuum, before and after temperature cycling to 100°C for 15 hours and before and after total dose

irradiation to levels in excess of CCD operational limits. None of these conditions showed a change in bandwidth or in-band transmission other than that accountable to measurement variability due to non-uniformity of silox layers under the filter. These layers would be eliminated with the optimal filter design described in Section 3.5.

4. Filter deposition and photodefinition techniques have been developed which are compatible with conventional CCD fabrication techniques. Scanning electron microscopy evaluation of the deposited filter material has shown excellent resolution, surface planarity, conformal coverage and tenacious adhesion of underlying layers. Wafer dicing, chip mounting and packaging operations have been shown not to have a detrimental effect on filter characteristics indicating the feasibility of focal plane array fabrication.

5. Filter uniformity across individual arrays and wafers has been shown to be excellent. Filter repeatability from run to run varies significantly over long time periods, but tests indicate an almost acceptable variation over short periods. This means that with the use of test runs to characterize and set up the equipment and only slight improvement in deposition control a repeatable process would already exist. Also several options exist for improved process control which have not yet been considered.